The cooperation of the tumor suppressor gene Dlc1 and the oncogene Kras in tumorigenesis

By Cordula Buse

A Thesis submitted to the Faculty of Graduate Studies of

The University of Manitoba

in partial fulfilment of the requirements of the degree of

MASTER OF SCIENCE

Department of Biochemistry and Medical Genetics

University of Manitoba

Winnipeg

Date of Defense: October 9, 2012

Abstract

This thesis investigated the cooperation of the Kras2 oncogene with the tumor suppressor gene Dlc1 in lung tumor development. Dlc1 is a negative regulator of RhoGTPase proteins, which are mainly involved in the regulation of the actin cytoskeleton and cell migration. We hypothesized that loss of Dlc1 expression leads to more aggressive tumors, which should also result in increased incidence of metastasis.

All experiments were performed in mice containing a heterozygous oncogenic Kras allele and a heterozygous gene trapped Dlc1 allele (KD) and in mice only carrying the oncogenic Kras allele (K+). Throughout all experiments we have consistently found no significant differences between the two groups in terms of tumor burden (tumor numbers, sizes and areas), metastases or methylation patterns.

These results suggest that heterozygous downregulation of Dlc1 is not enough to increase tumor formation and metastasis development in the Kras lung tumors.

Acknowledgements

I would like to thank each and everyone who has supported me throughout the last few years and helped make the completion of my program a success!

First of all, I would like to thank my supervisor, Dr. Mowat, for taking me as a graduate student and for providing me with guidance in this challenging project. I would also like to acknowledge my advisory committee members, Dr. Mai, Dr. Merz and Dr. Halayko, for their encouragement and valuable suggestions. My lab members, past and present, have been a pleasure to work and "live" with in the lab. Special thanks to Golam Sabbir for his assistance and technical advice and to Heather Leslie for her help with the mouse work. Thanks to the department of Biochemistry and Medical Genetics especially to Tuntun Sarkar and Jan Middleton for their moral support and never ending patience. Thanks to Andrea Fristensky and Sandra Troup from the Manitoba Tumor Bank, Susan Pylypas from Oral Pathology and Michelle from the HSC Pathology for their providing me with resources in everything tissue related. Great thanks to Gerald Stelmack for his assistance with the Laser Scanning Cytometry and Dr. Qing for his expertise on lung tumor pathology. I would also like to thank Cancer Care Manitoba, University of Manitoba, Manitoba Health Research Council and Canadian Institutes of Health Research for funding this project.

And lastly I would like to thank my family and my closest friends, without whom this endeavour would not have been possible. Due to space constraints I cannot mention you all but you know who you are and I appreciate you very much!

Table of Contents

List of Tables

List of Figures

List of Abbreviations used

µg	microgram (weight)
µl	microliter (volume)
µM	micromolar (concentration)
aa	amino acid
Adeno-Cre	Cre expressing adenovirus
ANOVA	analysis of variance
APS	ammonium persulfate
BCA	bicinchoninic acid
bp	base pairs
BSA	bovine serum albumin
$CaCl_2$	calcium chloride
CaPi	calcium phosphate precipitate
CC10	Clara cell antigen 10
CDK	cyclin dependent kinase
cDNA	complementary DNA, copy DNA
CIN	chromosomal instability
CO_2	carbon dioxide
CpG	methylation site (cytosine and guanosine separated by phosphate)
$CuSO_4$	copper sulphate
DAB	3,3'-Diaminobenzidine
DAPI	4',6-diamidino-2-phenylindole
ddH_2O	double distilled water
DEAE	diethylaminoethyl (cellulose)
Dlc1	deleted in liver cancer 1
DMEM	Dulbecco's modified eagle medium
DNA	deoxyribonucleic acid
dNTP	deoxyribonucleotide

dpc	days post coitum
E	embryonic day
E.coli	Escherischia coli
ECL	enhanced chemiluminescence
EDTA	ethylenediaminetetraacetic acid
EGTA	ethylene glycol tetraacetic acid
ERK	extracellular signal-regulated kinase
FBS	fetal bovine serum
FISH	fluorescence *in situ* hybridization
FITC	fluorescein isothiocyanate
g force	gravitational force
G12D	oncogenic Kras mutation in codon 12
GAP	GTPase activation protein
GAPDH	glyceraldehyde 3-phosphate dehydrogenase
GDI	guanosine dissociation inhibitor
GDP	guanosine diphosphate
GEF	guanosine exchange factor
Gln	glutamine
Gly	glycine
GST	glutathione S-transferase
GTP	guanosine triphosphate
H&E	haematoxylin & eosin staining
HAc	acetic acid
HCl	hydrochloric acid
HNC	histidine tagged-Nuclear Localization Sequence-Cre protein
HRP	horse radish peroxidase
IF	immunofluorescence
IHC	immunohistochemistry
IN	intranasal
IP	intraperitoneal
IPTG	isopropyl β-D-1-thiogalactopyranosid

JNK	c-Jun N-terminal kinase
K+	mice with heterozygous floxed Kras allele and wild type Dlc1
KD	mice heterozygous for floxed Kras and heterozygous gene trapped Dlc1 alleles
$K_3Fe(CN)_6$	potassium ferricyanide
$K_4Fe(CN)_6$	potassium ferrocyanide
kb	kilo bases
KCl	potassium chloride
kDa	kilodalton
KH_2PO_4	monopotassium phosphate
KOAc	potassium acetate
Kras	Kirsten sarcoma virus homolog
L	liter (volume)
LacZ	part of the Lac operon
LB	Luria-Bertani medium
LoxP	locus of crossing over of phage 1
LSC	laser scanning cytometry
LSL	lox-stop-lox
MAP	mitogen activated protein kinase
m-banding	multicolor banding
MEF	mouse embryonic fibroblasts
MEK	mitogen activated protein kinase kinase
$MgAc_2$	magnesium acetate
$MgCl_2$	magnesium chloride
MgSO4	magnesium sulphate
ml	milliliter (volume)
mM	millimolar (concentration)
mRNA	messenger RNA
MTS	mitochondrial targeting signal
N_2	nitrogen
Na_2HPO_4	disodium hydrogen phosphate

NaCl	sodium chloride
$NaHCO_2$	sodium bicarbonate
NaOH	sodium hydroxide
NF-κB	nuclear factor kappa light chain enhancer of activated B-cells
$NiSO_4$	nickel sulphate
NLS	nuclear localization signal
nm	nanometer (length)
nM	nanomolar (concentration)
NP-40	nonyl phenoxypolyethoxylethanol
NSCLC	non-small cell lung cancer
OCT	optimal cutting temperature compound
OD	optical density
$p21^{Waf1/Cip1}$	cyclin-dependent kinase inhibitor 1
PA	polyadenylation site
PBS	phosphate buffered saline
PCR	polymerase chain reaction
PFU	plaque forming units
pH	measure of acidity of a solution
PI3K	phosphatidylinositol 3 kinase
PVDF	polyvinylidin fluoride
Ras	rat sarcoma
Rho	ras homologue
RIPA	radioimmunoprecipitation assay buffer
RNA	ribonucleic acid
ROCK	Rho associated kinase
ROSA26	floxed LacZ expression locus
rpm	revolutions per minute
RT	room temperature
RT-PCR	reverse transcriptase polymerase chain reaction
SA	splice acceptor site
SAM	sterile alpha motif

SCLC	small cell lung cancer
SDS	sodium dodecyl sulphate
SKY	spectral karyotyping
SOC	super optimal Broth with catabolite suppression
SP-C	surface protein C
START	steroidogenic acute regulatory lipid transfer domain
TAE	tris/acetate/EDTA buffer
Taq	Taq polymerase
TBE	tris/borate/EDTA buffer
TE	tris/EDTA buffer
TEMED	tetramethylethylenediamine
Tet-ON	tetracycline inducible conditional allele
Tris	tris(hydroxymethyl)aminomethane
Tris-Ac	tris acetate
TTBS	tris buffered saline with Tween-20
TTF-1	thyroid transcription factor 1
UV	ultraviolet
V	volt
WB	western blot
WT	wild type
X-Gal	5-bromo-4-chloro-3-indolyl-beta-D-galacto-pyranoside
αMEM	minimum essential medium alpha modification
β-gal	β-galactosidase enzyme

Chapter 1: Introduction

1.1 Introduction

The work in this thesis investigates the possible cooperation of the oncogene Kras2 and the tumor suppressor gene Dlc1 in tumor formation. A mouse model in which Dlc1 was downregulated and Kras could be conditionally activated was created to study tumor formation and metastasis development.

1.2 Oncogenes and tumor suppressor genes

An oncogene is "any gene that encodes a protein able to transform cells in culture or to induce cancer in animals", whereas tumor suppressor genes "generally encode proteins that in one way or another inhibit cell proliferation" (*Lodish et al. 2000*).

Most oncogenes are derived from genes that are normally involved in cell growth, also called proto-oncogenes. In these genes a mutation, mostly a gain of function change, renders them either constitutively active or increases the expression or stability of the corresponding protein. Tumor suppressor genes on the other hand are mostly involved in cell cycle regulation and a loss of function mutation will abolish their ability to inhibit tumor formation (*Lee & Muller 2010, Lodish et al. 2000*). In some instances a mutation can also create proteins with novel functions (*Freed-Pastor & Prives 2012*). The tumor suppressor protein p53 for example can exhibit oncogenic properties on top of the loss of tumor suppressor function in some cases (*Olivier et al. 2010*).

In general changes to one allele of a proto-oncogene are often enough to induce tumorigenesis whereas the inactivation of a tumor suppressor gene is mostly recessive and both alleles need to be inactivated on the way to cancer development (*Lodish et al. 2000*).

1.3 The Ras superfamily of small G proteins

The Ras-like small GTP binding proteins (G-proteins) are small monomeric proteins with a size of 20 to 40 kDa. They have a conserved primary structure and based on their structural similarity they have been classified into 5 groups: Ras, Rho, Rab, Sar1/Arf, Ran (*Bishop & Hall 2000, Takai et al. 2001, Wennerberg et al. 2005*). The first *ras* genes were identified as homologues to the cancer causing sarcoma viruses in rats, as reflected in their name (Rat sarcoma) (*Barbacid 1987, Chang et al. 1982*).

All members of the Ras superfamily act as molecular switches to turn on downstream effectors and exist in two interconvertible forms. Their activity is regulated by the binding and hydrolysis of GTP to GDP. These processes are tightly controlled by three classes of enzymes: the guanine nucleotide exchange factors the GTPase activating proteins and the guanine dissociation inhibitors.

In their inactive form G-proteins are bound to GDP. Upon stimulation by upstream signals, the GDP dissociates from the protein and is subsequently replaced by GTP. The dissociation of GDP from the inactive form is intrinsically very slow and is therefore facilitated by the guanine nucleotide exchange factors (GEF). The active, GTP bound form is then able to bind to downstream effectors and stimulate various signalling pathways. The intrinsic GTPase activity converts the GTP into GDP, which renders the protein inactive and releases any bound effectors. Because the intrinsic GTPase activity is

very low as well, the GTPase activating proteins (GAPs) are needed to catalyze the process. In their inactive states, the G-proteins are stabilized by Guanosine dissociation inhibitors (GDI), which maintain the G-proteins in their GDP bound form by inhibiting the GEF stimulated dissociation of GDP (*Takai et al. 2001*).

A variety of posttranslational modifications, such as methylation, proteolysis or the addition of lipid moieties such as farnesyl, geranylgeranyl or palmitoyl, at the C-terminal end are required for proper localization to the membrane and for binding to regulators as well as downstream effectors (*Takai et al. 2001*).

1.3.1 The oncogene Kras

The Ras (Ras sarcoma) proteins are the founding members of the Ras superfamily (*Wennerberg et al. 2005*). There are three known members: Hras, Kras and Nras. Hras and Kras were first identified as analogous to the oncogenes of the Harvey and Kristen sarcoma viruses, whereas Nras was first isolated from neuroblastoma (*Chang et al. 1982, Friday & Adjei 2005, Takai et al. 2001*). The three proteins are highly similar and have an approximate molecular weight of 21 kDa (*Bos 1989*).

Initially there were two isoforms of Kras, namely Kras1 and Kras2. However, Kras1 has since been identified to be a pseudogene (*McGrath et al. 1983*). The Kras2 gene can be spliced alternatively between the last two coding exons and therefore produces two more isoforms, K4A and K4B, which only differ in their C-terminal (*Wang & You 2001*). In the name of simplicity from here on forward all mentioning of Kras is related to Kras2.

The proteins of the Ras family are involved in the regulation of cell growth, differentiation and gene expression (*Friday & Adjei 2005*). They are localized at the

cytoplasmic side of the plasma membrane, which is mediated by posttranslational lipid-modifications (*Takai et al. 2001*). Those modifications are necessary to convert the small and hydrophilic Ras proteins into a more hydrophobic state that allows the binding to the lipid-rich membrane (*Friday & Adjei 2005*).

Mutated Ras genes have been found in 30 % of all human cancers, with Kras being the most frequently mutated and Hras the most rare (*Ellis & Clark 2000, Friday & Adjei 2005*). Point mutations, most commonly in codon 12 (Gly) or 61 (Gln) make the protein insensitive to the GTPase activating effects of the GAP proteins and therefore it remains in the active state (*Jackson et al. 2001, Karnoub et al. 2006*). The constitutively active protein then leads to excessive and inappropriate signalling, which plays a major role in transformation (*Ellis & Clark 2000*).

Mutated Kras genes have been found in several tumors types, but are most common in cancers of the pancreas (~70-90 %) , colon (~50) and lung (~25-50 %) (*Johnson et al. 2001, Ray et al. 2011*).

1.3.2 RhoGTPases

The Rho (Ras homologous) proteins are highly conserved members of the Ras super family of small GTP-binding proteins and share about 30 % sequence homology with Ras proteins (*Khosravi-Far & Der 1994, Wennerberg et al. 2005*).

To date more than 20 family members have been identified, which share about 50 % sequence homology with each other (*Khosravi-Far & Der 1994*). The Rho proteins are further divided on the basis of their functional and biochemical properties and their sequence: Rho, Rac, Cdc42, Rnd, RhoBTB and Miro. The three proteins RhoD, Rif and TTF/RhoH do not fall into any of those categories due to the lack of similarities in

sequence and/or function (*Gomez del Pulgar et al. 2005, Wennerberg & Der 2004*). The most studied members of this family remain RhoA, Rac1 and Cdc42, which are mainly involved in the regulation of the actin cytoskeleton and regulate different aspects in the motility and migration of cells. RhoA is involved in the regulation of contractile filaments such as the formation of stress fibers and focal adhesions. Rac1 on the other hand is mainly involved in the formation of lamellipodia and actin polymerization, whereas Cdc42 induces actin filament assembly and filopodia formation (*Etienne-Manneville & Hall 2002, Hall 1998, Hall 2005, Kozma et al. 1995, Nobes & Hall 1995*).

Although the main function of the Rho family of GTPases is the regulation of the actin cytoskeleton, they are also involved in a variety of other cellular processes, such as gene transcription, cell cycle progression and transformation. Activation of members of the ROCK (Rho associated kinase) family by RhoA is mostly involved in the maintenance of the actin cytoskeleton and stress fiber formation. Regulation of cyclin D1 and CDK inhibitors by RhoA leads to changes in the cell cycle. Stimulation of JNK (c-Jun N-terminal kinase) leads to apoptosis and together with NF-κB (nuclear factor kappa-light-chain-enhancer of activated B cells) is involved in cell survival, proliferation and inflammatory responses. Both cascades can be activated by all three Rho proteins, RhoA, Rac1 and Cdc42 (*Aznar et al. 2004, Benitah et al. 2004, Jaffe & Hall 2005, Pruitt & Der 2001*). Together all these modifications can lead to direct or indirect changes in cell shape, motility (migration) proliferation and cell survival (*Bishop & Hall 2000, Hall 2005*).

As all members of the Ras superfamily, the Rho proteins also act as molecular switches and their activity is regulated through the binding and hydrolysis of GTP and

GDP as described above (Figure 1.1). In the active state the Rho proteins are membrane bound and loaded with GTP. Similar to the Ras proteins, the Rho proteins are posttranslationally modified to facilitate the membrane association (*Wennerberg & Der 2004*). Inactivation of the protein occurs through the activation of the intrinsic GTPase activity by the RhoGAP proteins and therefore hydrolysis of GTP to GDP. The inactive Rho proteins are bound by GDIs, which also allow translocation to the cytoplasm and terminate signal transduction. They also inhibit spontaneous GTP exchange activity. The GEFs again exchange GDP for GTP, thus re-activating Rho (*Bishop & Hall 2000, Buchsbaum 2007*).

Only GTP bound active Rho can interact with a variety of effectors, such as kinases and scaffold proteins, which then lead to the discussed changes in cell behaviour (*Bishop & Hall 2000, Sahai & Marshall 2002*).

Through their involvement in the regulation of the cytoskeleton and the cell morphology Rho proteins seem to be a likely target for deregulation in tumors. And many studies have shown that Rho levels are elevated in many tumors, such as breast, colon, lung, bladder, pancreatic and testicular cancer (*Fritz et al. 2002, Fritz et al. 1999, Gomez del Pulgar et al. 2005, Kamai et al. 2001, Suwa et al. 1998*). However, only RhoH has been reported to actually be mutated in cancers (*Preudhomme et al. 2000*). This suggests that the elevated Rho levels are rather due to defects in the Rho controlling enzymes, such as GEFs and GAPs (*Ellenbroek & Collard 2007*). Due to their roles in the Rho cycle mutations in GEFs have an activating phenotype, whereas mutations in GAPs are inactivating (*Ridley 2004*).

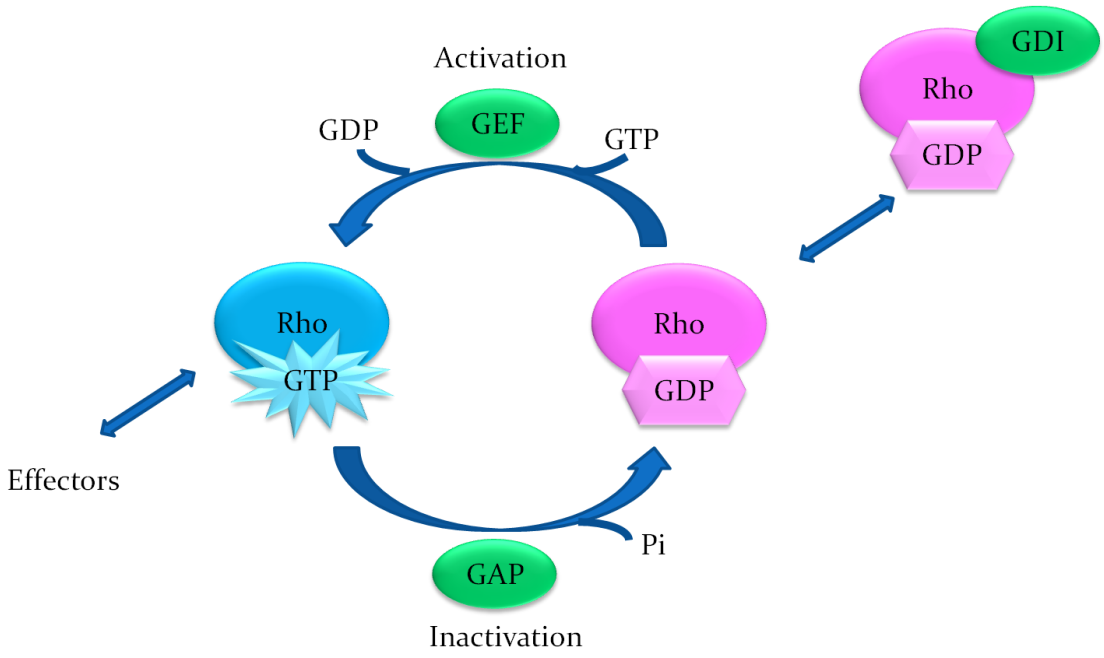

Figure 1.1: The RhoGTPase cycle

In its active state Rho is bound to GTP and able to interact with its downstream effectors. The RhoGTPase activating protein (GAP) increases the intrinsic GTPase activity, leading to the hydrolysis of GTP to GDP and therefore inactivation of the protein. In its inactive state Rho is bound by Guanosine dissociation inhibitors (GDIs) which stabilize the protein and allow for translocation to the cytoplasm to terminate signal transduction. The Guanosine exchange factors (GEFs) exchange GDP for GTP and therefore re-activate the Rho protein again.

This figure was adapted with permission from Macmillan Publishers Ltd (Nature Reviews Cancer): "Sahai, E., and Marshall, C. J. (2002) RHO-GTPases and cancer, Nat Rev Cancer 2, 133-142", copyright (2002)

Overactive RhoGTPase proteins can lead to changes in the morphology of the cells and increased cell motility and tissue invasion, due to the important role of Rho proteins in the regulation of the actin cytoskeleton. On the other hand, inhibition of different Rho proteins can inhibit the metastatic potential of invasive cells (*Clark et al. 2000, Jaffe & Hall 2002*). Experiments with a RhoC deficient mouse model have shown, that the protein is essential in metastases development and that the absence of RhoC can prevent metastases formation (*Hakem et al. 2005*). In contrast, deficiency in p190 RhoGAP delays tumor onset and inhibits progression (*Heckman-Stoddard et al. 2009*). Additionally, Cdc42 deficient mouse models have revealed a role in cell cycle progression and migration in haematopoiesis (*Yang et al. 2007*), which has yet to be confirmed for cancer.

Downregulation of RhoGTPase activity in tumors is therefore a potential target in anti-cancer therapy and to prevent metastasis (*Aznar et al. 2004, Wang et al. 2008*).

1.3.3 RhoGAP proteins

As mentioned above the RhoGTPase activating proteins (GAPs) are involved in regulating the activation state of the Rho proteins. All RhoGAPs share a conserved RhoGAP domain, which is about 170 amino acids long and specific for members of the Rho family of GTPases (*Bernards 2003, Ligeti & Settleman 2006, Peck et al. 2002*). The arginine residue of this domain interacts with the GTP binding core of the RhoGTPase, stabilizes it and therefore facilitates hydrolysis of the GTP molecule (*Bos et al. 2007, Gamblin & Smerdon 1998, Moon & Zheng 2003*).

With more than 80 proteins functioning as GAPs, they outnumber their substrates by far. This suggests an elaborate pattern of temporal and spatial regulation. GAPs can be

tissue specific or they only act on specific GTPases. They can exhibit selective regulatory capacity for a signalling pathway or the GAP domain may be a recognition module (*Kim et al. 2008, Moon & Zheng 2003, Tcherkezian & Lamarche-Vane 2007*).

RhoGAPs are regulated through many mechanisms such as phosphorylation, lipid-binding, protein-protein interaction and proteolytic degradation (*Ligeti & Settleman 2006, Moon & Zheng 2003*).

1.3.4 The tumor suppressor Dlc1

Dlc1 (Deleted in liver cancer 1) is a RhoGTPase activating protein, that is specific for RhoA and to a lower extent to Cdc42 (*Wong et al. 2003*). It is also known as ARHGAP7 or STARD12 (*Liao & Lo 2008*). The gene was first discovered in the rat as p122RhoGAP (*Homma & Emori 1995*). The human homologue was then cloned and mapped on the chromosome 8p22, a region which is frequently lost in hepatocellular carcinoma and other solid tumors (*Yuan et al. 1998*). The 14 exons of Dlc1 express three different isoforms, which are transcribed from two different promoters (*Durkin et al. 2007, Ko et al. 2010*). Recently a group from Singapore has found a fourth human isoform, which is transcribed from an additional promoter (*Low et al. 2011*). In the mouse there are similar four isoforms present which are differentially expressed in all tissues examined. Isoform 2 is the most prominent form and is generally higher expressed when compared to isoform 3 and isoform 1 as real time PCR experiments revealed (*Sabbir et al. 2010*). Human and mouse Dlc1 share 92 % sequence homology and a similar exon/intron structure (*Durkin et al. 2007*).

The structure of the Dlc1 protein is shared among all members of the Dlc family, namely Dlc1, Dlc2 and Dlc3. The N-terminal SAM (sterile alpha motif) binding domain

is responsible for protein-protein interaction and is known to interact with tensin and vinculin which localize Dlc1 to the focal adhesions (*Durkin et al. 2007*). It has also been shown that the SAM domain has an auto-inhibitory function on the RhoGAP domain (*Healy et al. 2008, Kim et al. 2008*). The C-terminal START (steroidogenic acute regulatory lipid transfer) domain is believed to be involved in lipid binding and metabolism (*Kim et al. 2009*). The ~150 amino acid long RhoGAP domain is the most highly conserved domain within the Dlc1 family with approximately 70% sequence similarity (*Durkin et al. 2007*). Between the SAM and the RhoGAP domains resides a serine rich unstructured middle region, which contains several potential phosphorylation sites as well as potential recognition sites for other signalling proteins (*Durkin et al. 2007*) (Figure 1.2).

In a variety of tumors, such as liver, lung and breast cancer, Dlc1 is expressed at a lower rate than in normal tissue (*Ng et al. 2000, Ullmannova & Popescu 2006*). And similar to the RhoGTPases, mutations in the Dlc1 gene are rare (*Wong et al. 2003*). Although rare, some mutations have been described in tumor sequencing studies, but most of them have only low impact and do not lead to major changes in the cell environment (*Cerami et al. 2012*). Only one study has found mutations that might be able to decrease the tumor suppressor function of Dlc1 (*Liao et al. 2008*).

In concordance with its name, the Dlc1 locus has frequently been found to be deleted in liver tumors and other tumours (*Ng et al. 2000, Wong et al. 2003*). As well Dlc1 expression can be abolished through epigenetic silencing. In this case hypermethylation of the CpG islands within the Dlc1 promoter prevents expression of the gene (*Wong et al. 2003, Yuan et al. 2003*). Downregulation of the Dlc1 protein then leads

Figure 1.2: Structure of Dlc1

The protein structure is very conserved among members of the Dlc family. The Dlc1 protein contains a N-terminal SAM (sterile alpha motif) domain, a C-terminal START (steroidogenic acute regulatory lipid transfer) domain, a RhoGAP (Rho GTPase activating protein) domain and a serine-rich unstructured middle region.

This figure was reproduced from „Kim, T. Y., Healy, K. D., Der, C. J., Sciaky, N., Bang, Y. J., and Juliano, R. L. (2008): Effects of structure of Rho GTPase-activating protein DLC-1 on cell morphology and migration, J Biol Chem 283, 32762-32770.“ with permission of the American Society for Biochemistry and Molecular Biology

to an abundance of active Rho protein, which in turn leads to the previously discussed changes in cell morphology.

Since this provides a starting point for anti-cancer therapy, various groups have studied if restoration of Dlc1 expression could reverse those changes. Indeed, re-expression of functioning Dlc1 can inhibit cell migration and proliferation and also induce apoptosis (*Ullmannova-Benson et al. 2008, Wu et al. 2009, Yuan et al. 2004, Yuan et al. 2003, Zhou et al. 2004*). It is widely believed that these effects are due to the impact on Rho protein activity (*Durkin et al. 2007, Wu et al. 2009, Zhou et al. 2004*). With Rho being implicated in tumor formation before and with Dlc1 being able to repress tumor formation through downregulation of Rho it makes a strong case for Dlc1 being a tumor suppressor gene (*Xue et al. 2008*).

1.3.5 Interaction between Kras and Dlc1

The activation of Ras triggers the activation of the MAP kinase pathway through the binding of Raf1 and a downstream cascade of serine/threonine kinases that stimulate changes in the expression of genes involved in the control of cell proliferation (*Khosravi-Far & Der 1994, Molina & Adjei 2006*). The activation of the MAP kinase pathway leads to two different outcomes. On one hand it stimulates cell proliferation, which has been implicated in transformation (*Dhillon et al. 2007, Khosravi-Far & Der 1994*). On the other hand activation of Ras also upregulates expression of the cell cycle inhibitor protein $p21^{Waf1/Cip1}$ thereby slowing down cell cycle progression (*Jaffe & Hall 2002, Mitomi et al. 2007*). As studies have shown, in Ras transformed cells the levels of $p21^{Waf1/Cip1}$ are elevated, which can be further increased when Rho is inhibited simultaneously (*Sahai et al. 2001*).

It has long been suggested that Ras transformation is partly Rho dependent. Mutated Ras, which can no longer bind to Raf1 can still transform cells, suggesting that there is a second, Raf1-independent pathway (*White et al. 1995*). Changes in cell morphology seen during transformation mimic those resulting from Rho protein activation (*Ridley & Hall 1992, Ridley et al. 1992*). Dominant negative mutants of RhoA and Rac1 are able to inhibit Ras induced transformation (*Khosravi-Far et al. 1995*). Together these results suggest that the Raf/MAPK pathway as well as the Rho activated pathway is necessary for full Ras induced transformation (*Jaffe & Hall 2002, Khosravi-Far et al. 1995*).

Contrary to Ras, RhoA has been found to inhibit $p21^{Waf1/Cip1}$ expression at the transcriptional level and therefore increase cell cycle progression (*Jaffe & Hall 2002*). It has been suggested that in Ras induced transformation, Rho is downregulating the excess $p21^{Waf1/Cip1}$ and therefore overcomes the Ras induced growth arrest. Experiments have confirmed, that in Ras transformed cells, levels of Rho are elevated (*Chen et al. 2003, Karnoub et al. 2006*). It has also been shown that when Rho is inhibited, constitutive Ras activation leads to a block of the cell cycle in the DNA synthesis phase. Concurrently Rho signalling is required for Ras transformation (*Olson et al. 1998, Sahai et al. 2001*). It has also been confirmed, that Rho's primary function is the suppression of $p21^{Waf1/Cip1}$, since cells lacking $p21^{Waf1/Cip1}$ do not require the activity of Rho to continue in the cell cycle (*Olson et al. 1998*). Inhibiting the downstream pathways of Ras, such as Raf/MEK/ERK and PI3K had no effect on the Rho levels, suggesting that Ras and Rho are interacting through different means (*Sahai et al. 2001*). It has been proposed, that in cells with the Ras oncogene activated selection for increased Rho takes place, which

enables downregulation of $p21^{Waf1/Cip1}$, allowing increased proliferation to overcome the Ras induced growth arrest (*Olson et al. 1998, Sahai et al. 2001*) (Figure 1.3). Since it is already known that increased Rho activity is not due to changes in Rho itself, but rather due to changes in the controlling enzymes such as Dlc1, it seems logical, that this selection process also favors the loss of Dlc1 in tumors.

1.4 Lung Cancer

In 2011 lung cancer was the leading cause of cancer related deaths in the US and Canada (*American Cancer Society 2011, Canadian Cancer Society 2011*). It was also second on the list of newly diagnosed cancers per year, being after prostate and breast cancer in males and females respectively (*American Cancer Society 2011, Canadian Cancer Society 2011*).

Based on its histological features, lung cancer can be divided into two main groups: small cell lung cancer (SCLC) and non-small cell lung cancer (NSCLC). SCLC is a neuroendocrine tumor with small, oval shaped cells, whereas the more frequent NSCLC is categorized as epithelial tumor and can be further divided into three subtypes: squamous cell carcinoma that is characterized by keratinization; large cell lung carcinoma, which is defined as undifferentiated and adenocarcinoma that can be of acinar, papillary, bronchioalveolar or solid type. But most adenocarcinomas are heterogeneous and cannot be classified under a single type (*Beasley et al. 2005*).

The biggest risk factor for lung cancer remains smoking, but exposure to occupational and environmental factors is also a contributor (*Ellis 2012*). Although survival rates have been improving, the high mortality rate among lung cancer patients is

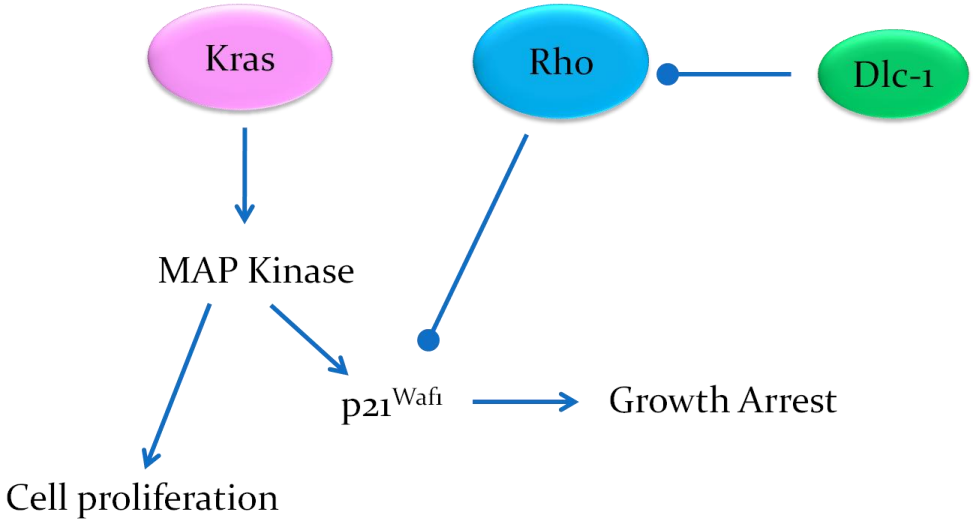

Figure 1.3: Interaction of Ras and Rho

The activation of Ras triggers the activation of the MAP kinase pathway which can lead to two different outcomes. On one hand the pathway stimulates cell proliferation, but on the other hand it also up regulates the expression of the cell cycle inhibitor protein $p21^{Waf1}$ and therefore slows down cell cycle progression. Since Rho is able to down regulate $p21^{Waf1}$ expression, it was proposed that in Ras transformed cells higher Rho levels are selected to overcome the Ras induced growth arrest. And since levels of Rho are controlled by Dlc1 we hypothesize, that Dlc1 and Kras cooperate through the Rho signalling pathway.

This figure was adapted with permission from EMBO Journal: "Sahai, E., Olson, M. F., and Marshall, C. J. (2001) "Cross-talk between Ras and Rho signalling pathways in transformation favours proliferation and increased motility", EMBO J 20, 755-766."

due both to the heterogeneity of the disease and the frequently late diagnosis (Borczuk et al. 2009, Ellis 2012).

Around 30 % of all human lung adenocarcinomas show activating Kras mutations (*Jackson et al. 2005*). Studies have also shown that Dlc1 expression is reduced in 95 % of NSCLC primary tumors (*Healy et al. 2008, Yuan et al. 2004*). These studies have also found that Dlc1 in these tumors is mainly silenced through promoter methylation instead of deletion (*Yuan et al. 2004*).

1.5 Mouse models

Throughout the years a variety of mouse models for lung cancer have been developed. Since mutations in Kras are prominent in lung cancer, a great number of the mouse models depend on the involvement of Kras in tumor initiation (*Kim et al. 2005*). In 2001 Tyler Jacks and his team published the development of a mouse model with a latent oncogenic Kras allele ($Kras^{LA}$). Spontaneous recombination in the mouse then leads to the activation of the allele and in turn to a variety of tumors, but predominantly non small cell lung cancer (*Johnson et al. 2001*). They also developed a model with a conditional oncogenic Kras allele (LSL-$Kras2^{G12D}$). Recombination with Cre recombinase removes the transcriptional control element which activates the oncogene (*Jackson et al. 2001*). A team from the Netherlands used a similar strategy but with a different Kras mutation (*Meuwissen et al. 2001*). In mice in which the oncogenic Kras is under the control of a doxycyclin-inducible ccsp (clara cell secretory protein) promoter specific for type II alveolar epithelial cells the oncogenic Kras is required for both the tumor initiation as well as the ongoing development (*Fisher et al. 2001, Tichelaar et al. 2000*). All these conditional mouse models have the advantage that the activation of Kras

can be controlled in a spatial and temporal manner, which enables researchers to study even early cancer onset (*Kim et al. 2005*).

To study the cooperation of the Kras oncogene and Dlc1 we made use of two mouse models. The first contained a gene trapped Dlc1 gene developed in our lab (*Sabbir et al. 2010*) whereas the second contained the conditional oncogenic Kras allele first described by Tyler Jacks (*Jackson et al. 2001*).

1.5.1 Dlc1 gene trapped mouse

To study the role of the Dlc1 gene in tumorigenesis, our laboratory has previously developed a knockdown mouse model for Dlc1. These mice were made by using embryonic stem cells from the 129 strain (XE082 from Bay Genomics) in which the Dlc1 isoform 2 gene was disrupted by a gene trapping cassette between exon 1 and exon 2 (*Sabbir et al. 2010*). The gene trapping cassette contains a splice acceptor site followed by a LacZ reporter gene, a neomycin resistance gene for selection and a polyadenylation site (Figure 1.4). Expression of the gene trapped allele then results in a prematurely truncated protein fused to the β-Gal reporter (*Stanford et al. 2001*). In 2005 Durkin and his group first reported that homozygous elimination of the Dlc1 gene leads to an embryonic lethal phenotype after 10.5 dpc in C57BL/6 mice (*Durkin et al. 2005*). Further experiments in our lab confirmed developmental defects such as open neuronal tubes and absence of blood vessels in the yolk sac and placental labyrinth (*Sabbir et al. 2010*). It was therefore only possible to establish a heterozygous mouse model.

Heterozygous gene trapped mice that were as old as 2 years did not show any spontaneous tumor formation (*Sabbir et al. 2010*). This supports the idea that loss of Dlc1 needs a cooperating oncogene for tumor formation.

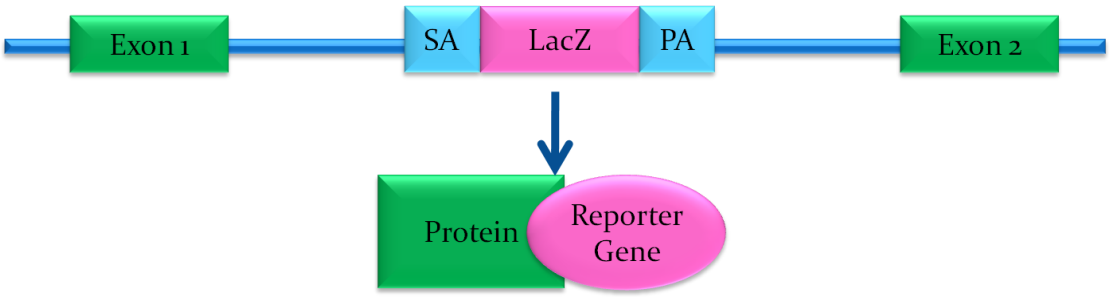

Figure 1.4: Gene trapped allele of Dlc1

The Dlc1 gene is disrupted by a gene trapping cassette between exon 1 and exon 2. The gene trapping cassette contains a splice acceptor site (SA), a LacZ reporter gene together with a neomycin selection gene and a polyadenylation site (PA). Expression of the allele results in a prematurely truncated protein fused to the β-Gal reporter.

1.5.2 Kras conditional mouse

The LSL-Kras2^{G12D} transgenic mouse strain carries a conditional oncogenic Kras allele that can be activated by Cre recombinase and was obtained from the National Cancer Institute Mouse Repository. A point mutation in exon 1 of the oncogenic Kras gene results in an amino acid substitution in codon 12 from glycine to aspartic acid (G12D) which upon expression will lead to constitutively active Kras protein. The oncogenic Kras allele is negatively controlled by an upstream transcriptional control element (Stop cassette). The stop cassette is flanked by two LoxP sites (floxed), which are recognized by the Cre recombinase. Hence the name "LSL"(Lox-Stop-Lox). Expression of Cre protein will result in site-specific excision of the negative control element, which in turn leads to the activation of the oncogenic Kras^{G12D} allele (*Jackson et al. 2001, Tuveson et al. 2004*) (Figure 1.5).

Similar to Dlc1, a homozygous Kras knockout is embryonic lethal at around E 12.5 and results in heart abnormalities and neuronal cell death (*Johnson et al. 1997, Koera et al. 1997*). Therefore, it is only possible to establish a heterozygous model.

In addition to the oncogenic point mutation, the Kras^{G12D} allele also carries a silent point mutation in the same exon, which introduces a HindIII digestion site (Figure 1.5). This is a useful tool to determine the activation status of the mutated allele and distinguish it from the wild type through RT-PCR experiments (see Chapter 2: Materials & Methods).

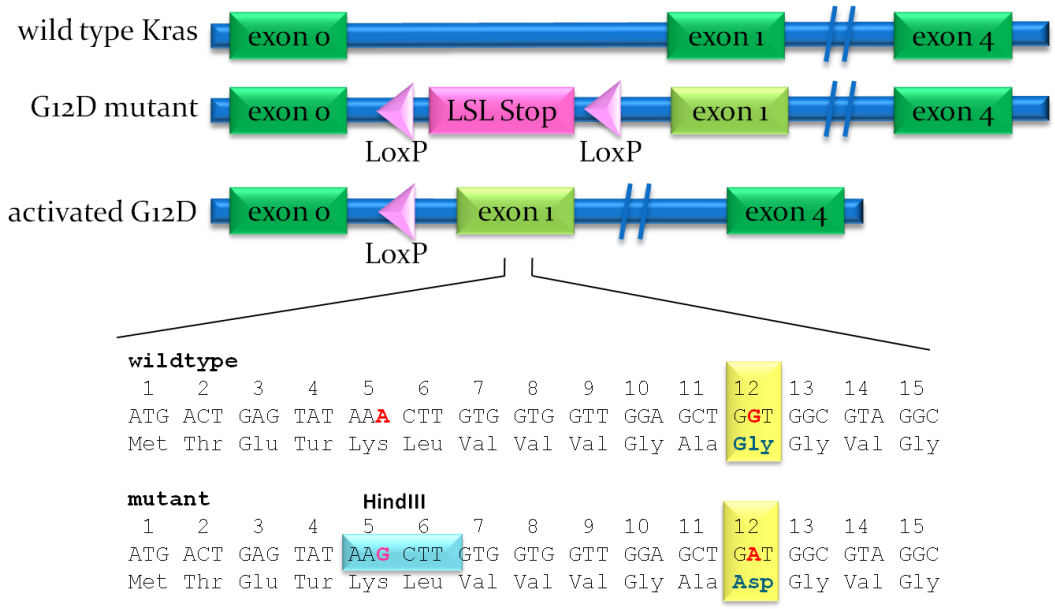

Figure 1.5: Wild type and Kras^{G12D} alleles

Schematic of the wild type and mutant Kras allele. The mutant allele (G12D mutant) contains a floxed stop cassette (LSL Stop) between the first two exons, which can be excised by site specific recombination through Cre recombinase. Removal of the stop cassette then allows for expression of the oncogenic allele.

Below the alleles their sequences are shown. The mutant allele contains two point mutations within exon 1: the oncogenic G12D mutation (yellow box) and the silent mutation introducing a HindIII restriction site (blue box). The mutated nucleotides are shown in red.

1.5.3 Dlc1 and Kras mouse model

Dlc1 gene trapped mice alone do not show any spontaneous tumor formation (*Sabbir et al. 2010*). We believe that the cooperation of an oncogene is required for Dlc1 suppression to have an impact. We therefore combined the LSL-$Kras^{G12D}$ mouse model with our gene trapped Dlc1 mice. It is to note that the genetic background of both models is C57BL/6.

Crossing the heterozygous gene trapped Dlc1 mice with the heterozygous floxed LSL-$Kras^{G12D}$ mice resulted in mice that were either heterozygous for both the oncogenic Kras and gene trapped for Dlc1 ($Kras^{LSL/+}$/$Dlc1^{gt/+}$ = KD) or were heterozygous floxed for Kras only ($Kras^{LSL/+}$/$Dlc1^{+/+}$ = K+). A schematic of the breeding scheme can be found in Chapter 2. In both the KD and the K+ mice the Kras allele was then activated by Cre recombination, using technologies described in the next section.

1.6 Kras activation by Cre recombinase

The 38 kDa Cre recombinase (causes recombination) is a protein originally produced by bacteriophage P1 and recognizes two 34 bp LoxP sites (Locus of crossing over (X) of P1) (*Hoess et al. 1990, Hoess et al. 1982, Sternberg & Hamilton 1981*). Depending on the orientation of the LoxP sites one can either delete the sequence between (LoxP sites in the same direction) or invert it (LoxP sites in opposite direction) (*Abremski & Hoess 1984, Feil 2007*).

There are various ways of introducing the Cre recombinase into a conditional mouse model system. The simplest method is to cross floxed target-expressing mice to Cre expressing transgenic mice. Expression can then be controlled through a time and/or

tissue specific promoter or be ligand-activated such as the Tet-ON system. However, the requirement for tight spatial and temporal control is an issue and this can be compromised by leaky and mosaic expression (*Feil 2007*). Another method of Cre delivery is the injection of viral expression vectors, such as adenovirus or lentivirus. Although they seem to target cells very efficiently, there can be issues with toxicity of the delivered protein, and local inflammatory responses to the virus (*Ahmed et al. 2004, Akagi et al. 1997, Pfeifer et al. 2001*). It has also been reported that native Cre is able to cross the cell membrane without modification (*Will et al. 2002*). On this basis Ruley and his group performed a study using cell permeable Cre protein with different tags attached to increase efficiency and reduce toxicity (*Jo et al. 2001, Lin et al. 2004*).

The two methods we used for the work in this thesis were injection of the Cre recombinase using adenoviral vectors and cell permeable Cre protein.

1.6.1 Kras activation by cell permeable HNC

As mentioned, Dr. Ruley and his team from Vanderbuilt University have tested a variety of cell permeable Cre proteins for their ability to cross the cell membrane, recombination rate and cell toxicity (*Jo et al. 2001, Lin et al. 2004*). All tested proteins contained the Cre protein tagged with a variety of different signal peptides, such as NLS (Nuclear Localization Signal), MTS (Mitochondrial Targeting Signal) and others. They found that the Cre protein uptake can be greatly enhanced by a preceding NLS from the SV40 large T-antigen. This is most likely due to its better targeting to the nucleus, where it performs DNA recombination. A His6 tag at the N-terminal not only facilitates the purification of the protein through nickel affinity chromatography, but also increases cell uptake (*Lin et al. 2004*). *In vivo* studies with ROSA26 mice have shown that the cell

permeable Cre protein is distributed throughout the whole body upon intraperitoneal injections. Staining with X-Gal showed that recombination takes place in almost all organs, although the highest expression can be observed surrounding the blood vessels. Additionally no adverse effects to the Cre protein were reported (*Jo et al. 2001*).

1.6.2 Kras activation through Cre-expressing adenovirus

Previous work in our laboratory has made use of a Cre expressing adenovirus (Adeno-Cre). When injected through the tail vain, the K+ and KD mice developed predominantly thymomas but tumors have also been observed in the lung, ovary and testes (*Sabbir et al. 2012*).

In 1998 Fasbender and colleagues reported that cellular uptake of Cre expressing adenovirus, especially in airway epithelia, can be greatly increased when injected as a precipitate intranasally (*Fasbender et al. 1998*). The group was studying cystic fibrosis and methods of gene delivery. They argued that normally the adenovirus interacts with the cell through adenovirus fibers that bind to cell surface receptors, but that airways lack that receptor activity and therefore gene transfer by adenovirus is decreased. Another drawback is the protective abilities of the airway epithelia against the environment. In their paper, however, they report that adenovirus injected as a $CaPO_4$ precipitate (CaPi) enhances the cellular uptake through fiber-independent binding of the virus. Their method is simple and inexpensive and targets the airways directly. Also, through the higher cellular uptake, lower doses of adenovirus are required to achieve the same results and little cell toxicity was observed.

Intranasal injection of CaPi precipitated Adeno-Cre leads exclusively to lung tumors in mice (*Jackson et al. 2001*). The multiplicity as well as the timing of the tumor

formation can easily be controlled through the amount of Adeno-Cre injected. Those experiments also showed that expression of $Kras^{G12D}$ is sufficient to induce the formation of hyperplasic lesions.

1.7 Hypothesis & Aims

The purpose of this project was to determine if there is cooperation between the tumor suppressor gene Dlc1 and the oncogene Kras in lung tumor formation.

1.7.1 Hypothesis

Our hypothesis is that loss of Dlc1 expression cooperates with the Kras oncogene to enhance tumor formation. Additionally we hypothesized that tumors coupled with Dlc1 loss are more aggressive, which should manifest as increased incidence of metastasis.

1.7.2 Aims

In order to test our hypothesis and investigate the cooperation of Kras and Dlc1 five specific aims were identified, all linked to Cre induction using either intraperitoneal or intranasal injections.

1. Determine if Cre recombinase is able to activate the Kras in target organs and if that activation is related to the tumor formation. In concordance with the literature we expected intraperitoneal injection of Cre to activate Kras throughout the body, whereas the intranasal injection of Adeno-Cre would activate Kras in the lungs (*Jackson et al. 2001*, *Jo et al. 2001*).

2. Determine how levels of Dlc1 expression in tumors compare to levels of expression in normal cells. We expected that in tumors arising from KD mice, Dlc1 expression may be reduced compared to wild type and K+ tumors, since one allele is gene trapped and the other allele may be turned off or deleted.
3. To examine the methylation status of the Dlc1 promoter in tumors and determine if there is a difference between mice with and without a gene trapped Dlc1 allele. We expected that in tumors the methylation status of the Dlc1 would be greater compared to non-tumorigenic and wild type tissues.
4. To determine if there is a difference in tumor formation between mice carrying both the conditional Kras as well as the Dlc1 gene trapped allele compared to mice carrying only the conditional Kras allele. According to our hypothesis we expected that mice with both alleles would form tumors more quickly than mice with only the conditional Kras allele and therefore would also have a higher amount of overall tumor burden. To determine tumor formation we looked at tumor number, tumor sizes and overall tumor area.
5. Assess the development of metastasis in other organs. Again we hypothesized that mice with both the oncogenic $Kras^{G12D}$ allele and the Dlc1 gene trapped allele would form more aggressive tumors than mice with only the $Kras^{G12D}$ allele, which would result in an increased rate of metastasis.

Chapter 2: Materials & Methods

2.1 HNC protein approach

2.1.1 The HNC plasmid

The HNC, (His6-NLS-Cre) plasmid was a generous gift from Dr. Earl Ruley from Vanderbilt University. A map of the HNC protein expressing plasmid was constructed using the freely available program "ApE - A plasmid Editor" (*Editor*) (Figure 2.1). The required information about the plasmid, such as the vector backbone as well as available restriction sites were taken from (*Jo et al. 2001, Lin et al. 2004*). Briefly explained, the HNC sequence is integrated into a pET28-a (+) plasmid backbone. The total size of the plasmid is 6370 bp. It contains the Cre recombinase, preceded by an NLS (Nuclear Localization Signal) which allows the protein to be transported into the nucleus to perform its actions. Also attached to the NLS-Cre is a His6-Tag, which facilitates the purification of the protein via nickel-affinity chromatography under non-denaturing conditions (*Lin et al. 2004*). Just before the HNC sequence the vector contains a LacOperon, which can be activated by IPTG to induce protein production. Also included in the vector backbone is a kanamycin resistance gene, that allows for selection of the HNC expressing bacteria. The F1, M13 and ColE1 origins of replication allow for the replication of this plasmid in different cells.

2.1.2 HNC plasmid transformation

The HNC plasmid was transformed into competent E. coli BL21 cells (Invitrogen) using a heat shock protocol (*Sambrook & Russell 2001*). First, 2 µl TE buffer (10 mM

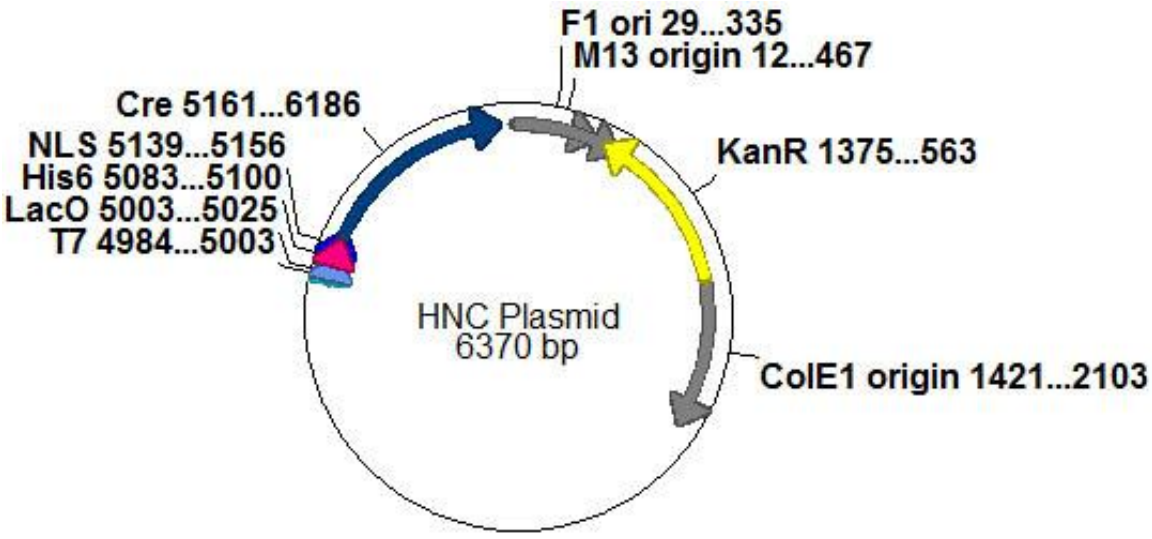

Figure 2.1: HNC Plasmid Map

This figure shows the plasmid map designed using "Ape - A Plasmid Editor".

The HNC sequence is integrated into a pET28-a (+) plasmid backbone. The total size of the plasmid is 6370 bp. It contains the Cre recombinase, preceded by an NLS which allows the protein to be transported into the nucleus to perform its actions. Also attached to the NLS-Cre is a His6-Tag, which facilitates the purification of the protein via nickel-affinity. Just in front of the HNC sequence the vector contains a LacOperon, which can be activated by IPTG to induce protein production. Also included in the vector backbone is a kanamycin resistance gene, that allows for selection of the HNC expressing bacteria. The F1, M13 and ColE1 origins of replication allow for the replication of this plasmid in different cells.

Tris, 1 mM EDTA, pH 8.0) were added to the plasmid to increase the work volume. Of this plasmid solution 0.5 µl were combined with 50 µl competent BL21 cells and flicked gently to mix. The cells were then incubated on ice for 20 minutes, followed by 2 minute incubation at 8°C immediately followed by 50 seconds at 42°C using the PTC-200 Peltiere Thermal Cycler (MJ Research) to allow the plasmid to enter the cells. Cells were then immediately placed on ice for another 2 minutes. After 300 µl SOC (Super Optimal Broth with Catabolite suppression) medium (2 % tryptone, 0.5 % yeast extract, 0.05 % NaCl, 2.5 mM KCl, 10 nM $MgSO_4$, 50 nM NaOH, 20 mM glucose) was added the transformed cells were incubated for 2 hours on a shaker at 37°C. Approximately 50 µl of the transformed cell solution were then plated on agar plates (1 % tryptone, 0.5 % yeast extract, 1 % NaCl, pH 7.0, 1.5 % agar) supplemented with 30 µg/ml kanamycin and incubated at 37°C over night. The following day colonies were picked and grown in 3 ml LB (Luria-Bertani) medium (1 % tryptone, 0.5 % yeast extract, 1 % NaCl, pH 7.0) supplemented with 30 µg/ml kanamycin over night at 37°C.

2.1.3 Plasmid miniprep

Plasmid minipreps were performed as described previously (*Birnboim & Doly 1979*). All steps were executed on ice unless otherwise noted. Briefly, 1.5 ml of bacterial culture was pelleted by centrifugation for 5 minutes at 10000 rpm (Micro 20, Hettich Centrifuges). The pellet was then resuspended in 120 µl of 50 mM Tris-HCl, pH 8.0 by vortexing. Treatment with 16 µl lysozyme solution (20 µg/µl lysozyme freshly prepared in 50 mM Tris) for 10 minutes allowed the cell walls to weaken. This was followed by incubation with 16 µl of 250 mM EDTA, pH 8.0, for 10 minutes to inhibit the DNases. Remaining RNA was removed by adding 5 µl RNase A (10 mg/ml) and incubating for

10 minutes. To allow for denaturation of the plasmid DNA 340 µl of 0.2 M NaOH / 1 % SDS (freshly prepared) were added slowly and mixed gently, followed by incubation for 10 minutes. Finally 255 µl of 3 M KOAc / 2 M HAc were added as neutralization and mixed by shaking on a horizontal platform. The *E.coli* DNA was then pelleted by centrifugation for 10 minutes at 14,000 rpm. All following centrifugation steps were performed at 14,000 rpm for 5 minutes. The supernatant was transferred to a new tube and the plasmid DNA was extracted once with 500 µl of a 25:24:1 phenol/chloroform/isoamylalcohol mixture, followed by centrifugation. The upper aqueous phase was removed and the DNA was precipitated with 0.7 volumes of isopropanol at room temperature for 10 minutes and pelleted. The pellet was then washed with 70 % ethanol and dried for about 5 minutes before being dissolved in TE buffer for storage.

2.1.4 Plasmid Digestion

The plasmid obtained from the miniprep was entered used in different digestions to confirm the size and correct composition. The first 20 µl digestion sample combined 2 µl DNA with 1 µl EcoRV in 2 µl NE3 buffer supplemented with 1 µl BSA, which resulted in 2 fragments of 4457 bp and 1913 bp. The second 20 µl digestion sample combined 2 µl DNA with 1 µl PvuII in 2 µl NE2 buffer to obtain 3 fragments of 5278 bp, 999 bp at 93 bp.

An undigested sample, as well as the two digested samples were then separated on a 1 % agarose gel (in TAE buffer: 40 mM Tris, 20 mM acetic acid, 1 mM EDTA) supplemented with 0.4 µg/ml ethidium bromide at 70 V (BioRad agarose gel-electrophoresis system) and visualized under UV light.

2.1.5 Bacterial stocks

Glycerol stocks of the transformed bacteria were prepared by mixing glycerol and bacterial culture in a relation of 1:1. Glycerol stocks were then frozen and stored at -80°C.

2.1.6 HNC protein production

After the integrity of the plasmid as well as the transformed bacteria was ensured, the protein was produced at a higher scale.

Two starter cultures of 5 ml each of LB medium supplemented with 30 µg/ml kanamycin (= LB-Kana) plus 25 µl glycerol stock of bacteria were grown over night on a shaker at 37°C. This 10 ml culture were then expanded into 250 ml and grown again over night on a shaker at 37°C. The following day, 2 L of LB-Kana were inoculated with the 250 ml of overnight culture and grown for approximately 2-4 hours on a shaker at 37°C. Once the OD reached 0.6-1.0 at 600 nm, 1 M IPTG was added to a final concentration of 0.4 mM to induce protein production. From this time point cells were grown for additional 4 hours before cell lysis.

2.1.7 Lysis of HNC producing E.coli cells

Cells were harvested by centrifugation for 15 minutes (4°C) at 2000 rpm (Beckman J2-MC centrifuge, JA10 Rotor). Cells were washed once with 1x PBS (Phosphate Buffered Saline: 137 mM NaCl, 2.7 mM KCl, 10 mM Na_2HPO_4, 1.76 mM KH_2PO_4, pH 7.4) on ice and centrifuged again for 15 minutes (4°C) at 2000 rpm. In the last step all PBS was aspirated carefully and 40 ml lysis buffer (50 mM Tris, 50 mM sodium phosphate, 300 mM NaCl) supplemented with 1x Protease Inhibitor Cocktail (1 tablet from Sigma per 100 ml buffer) were added. Cells were resuspended and transferred

into two 50 ml tubes. To rupture the cell structure, cells were first sonnicated 6x for 15 seconds and then incubated for 15 minutes at 4°C on a rocking platform. Cell debris was then pelleted for 15 minutes (4°C) at 7000 rpm (IECDPR-6000 centrifuge, Fisher Scientific, 269 Rotor). After transferring the supernatant to a new 50 ml tube the remaining debris was pelleted again for 15 minutes (4°C) at 9000 rpm. The cleared supernatant was filtered through a 0.45 µm syringe filter (Pall Life Sciences) and aliquoted in 15 ml tubes for storage at -20°C.

2.1.8 HNC protein purification by affinity chromatography

The HNC protein was purified using a His-Trap HP column (GE Healthcare). The high performance nickel-sepharose beads were pre-packed to perform metal-ion affinity chromatography. Because the pores would clog very quickly, and usage became very labour intensive, the beads from inside the column were emptied into a 50 ml tube. For every step the required buffers were added, the beads incubated by gently shaking the tube and then centrifuging for 3 minutes at 3000 rpm (IECDPR-6000 centrifuge, Fisher Scientific, 269 Rotor) to collect the beads.

In the first step the beads were washed with 25 ml of ddH_2O followed by 25 ml of freshly prepared elution buffer (20 mM sodium phosphate, 0.5 M NaCl, 500 mM imidazole, pH 7.4). The beads were then equilibrated with 50 ml of freshly prepared binding buffer (20 mM sodium phosphate, 0.5 M NaCl, 30 mM imidazole, pH 7.4). The sample was pre-treated with 30 mM imidazole and applied to the beads. After binding of the proteins to the beads, they were washed with 50 ml binding buffer and eluted with 25 ml elution buffer using a one-step gradient.

In the final step the beads were stripped with 25 ml stripping buffer (20 mM sodium phosphate, 0.5 M NaCl, 50 mM EDTA), 25 ml binding buffer and 25 ml ddH_2O and then recharged with 2.5 ml of 0.1 M $NiSO_4$, followed by 25 ml ddH_2O and 25 ml binding buffer. The beads were then stored in 20 % ethanol at 4°C.

2.1.9 Protein concentration and dialysis

Because the concentration of the protein after column purification was very low, a 20 ml Vivaspin concentration column (VivaScience) with a cut-off weight of 30 kDa was used to obtain smaller volumes. The protein solution was applied onto the column and then centrifuged according to the manufacturer's instructions at 5000xg several times until the final volume was around 1ml.

To remove the salts and make the solution safer for injection into animals, the concentrated sample was dialyzed using Slide-A-Lyzer Dialysis cassettes (Pierce Thermo Scientific) cassettes with a cut-off weight of 10 kDa. The dialysis medium consisted of DMEM medium (including antibiotics but without FBS) supplemented with 300 mM NaCl to avoid protein precipitation. Dialysis took place stirring overnight at 4°C.

2.1.10 BCA Assay

To determine the concentration of the final protein solution, BCA (Bicinchoninic Acid) protein assays were performed according to the manufacturer instructions (Sigma Aldrich). Briefly, 25 µl of sample (double determination) or standard (single determination) were pipetted into a 96 well plate and 200 µl of BCA working solution were added to each well. The plate was then covered with parafilm (Pechiney Plastic Packaging Company, Chicago) and incubated for 30 minutes at 37°C, 15 minutes at 65°C or 2 hours at RT. Absorption at 562 nm was then measured using a Spectramax 190

Spectrometer (Molecular Devices) and the final protein concentration calculated using MS Excel.

Serial dilutions (undiluted, 1:10 and 1:20) of the proteins samples were made in DMEM supplemented with 300 ml NaCl to avoid protein precipitation. BSA-standards covered a range from 0, 200, 400, 600, 800 and 1000 µg/ml.

2.1.11 Western blot analysis of HNC protein

To ensure the integrity of the HNC protein western blot analysis was performed. The bacterial cultures were grown and protein production was induced as described above. After lysis and determination of the protein concentration western blot analysis was performed as described further below. Briefly, 10 µg protein were loaded onto a SDS-polyacrylamide gel and separated at 100 V. After transferring the protein to a PVDF (Polyvinylidin fluoride) membrane (Millipore), the size of the HNC protein was confirmed with the His6 antibody (Invitrogen).

2.1.12 HNC protein test by X-Gal staining

Each batch of HNC protein solution was tested on ROSA26 MEF cells (mouse embryonic fibroblasts) for integrity and activation potential. The ROSA26 cells, which were a generous gift from Dr. Hao Ding (University of Manitoba), carry a β-galactosidase (β-gal) gene, which contains an upstream floxed stop cassette, similar to the conditional Kras allele. Introduction of the Cre protein results in the excision of the stop signal and allows the expression of the β-galactosidase (*Mao et al. 1999*). The expression of the β-gal and therefore the rate of recombination can then be visualized through X-Gal staining and by counting the blue cells.

2.1.12.1 Seeding of ROSA26 cells

The ROSA26 cells were cultured in αMEM on 10 cm culture dishes, washed 1x with PBS and trypsinized with 0.5 x Trypsin/EDTA for 3 minutes. After stopping the trypsinization with culture medium, cells were harvested into 15 ml tubes and centrifuged for 2 minutes at 2000 rpm in (IEC DPR-6000 centrifuge, Fisher Scientific, 269 Rotor). After resuspending the pellet in 1-2 ml medium, cells were counted using a haemocytometer or Coulter Counter (Coulter Z2).

For the haemocytometer an aliquot of 100 µl was diluted with 100 µl eosin yellow (Fisher Scientific), mixed and added drop wise onto the haemocytometer. In 5 large squares (area of 1 mm^2 each) the cells were counted, including cells that were touching the right and upper lines, but excluding cells that touched the left and bottom lines. The cell number per ml was calculated by determining the average number of cells per square and multiplying that number with the dilution (50) and 10^{-4} (conversion from surface area to ml). For the Coulter Counter an aliquot of 100 µl was added to 10 ml of Coulter Counter Solution and counted according to the manufacturer's instructions.

Considering the counting results, cells were seeded into 96 well plates, with a concentration of 1000 cells per well in 100-200 µl medium. The plates were then incubated over night at 37°C for protein treatment the next day.

2.1.12.2 Application of HNC protein solution on ROSA26 cells

Serial dilutions of the HNC-protein (1:2, 1:10, 1:20 and 1:100) were prepared in culture medium. After aspiration of the medium in the 96 well plate 75 µl of the dilutions were added to each well, including one medium-only control and incubated for 24 hours

at 37°C. Wells were then filled up to 200 µl with culture medium and incubated for another 24 hours at 37°C until staining.

2.1.12.3 X-Gal staining of HNC treated ROSA26 cells

X-Gal staining is a special method to visualize β-gal expression. It uses the organic compound X-Gal (5-bromo-4-chloro-3-indolyl-beta-D-galacto-pyranoside) as a substrate for the β-galactosidase enzyme. Following a specific staining protocol (*Wellcome 2004*) the β-gal expression is visible through blue colored cells, which can then be counted and used for determination of the efficiency of the Cre recombination through the HNC protein.

Cells were washed 3x with 200 µl PBS, then fixed in 100 µl of 4 % paraformaldehyde for 15 minutes at RT. After removal of the paraformaldehyde cells were washed 3x with 200 µl PBS, with the second wash incubating for 10 minutes at RT. The PBS was aspirated and 50 µl X-Gal staining buffer (1 mg/ml X-gal, 5 mM $K_3Fe(CN)_6$ (potassium ferricyanide), 5 mM $K_4Fe(CN)_6$ (potassium ferrocyanide), 2 mM $MgCl_2$, in PBS) were added and cells were incubated over night at 32°C to minimize the endogenous β-gal expression. The next day, the X-Gal staining buffer was removed, cells were washed 1x with 200 µl PBS and 200 µl PBS was added before cells staining could be examined under the microscope.

As estimation of the recombination activity blue cells were counted in different dilutions at the same magnification. Only protein that has been tested this way and yielded in activation in more than 50 % of cells was used for mouse injections.

2.1.13 *In vitro* test of Kras activation by HNC

To test the recombination abilities of the HNC protein *in vitro* mouse embryonic fibroblasts (MEFs) were used. In those cells the Kras allele was either in the wild type, heterozygous or homozygous state. The cells were treated with different concentrations of HNC protein and harvested at different time points. The Kras activation was then analyzed by RT-PCR followed by restriction digestion as described below.

MEFs were grown on 10 cm plates in DMEM supplemented with 10 % FBS until about 70 % confluent. For the experiment 150 µg of HNC protein was added to the cells in 5 ml of medium and cells were incubated for 24 hours. After filling up the medium to 10 ml the cells were incubated for 2 weeks, before the cells were harvested for RNA preparation. The RNA was prepared using the RNeasy Mini Kit from Qiagen according to the manufacturer's instructions. From this RNA the activation status of the $Kras^{G12D}$ gene was determined using RT-PCR and restriction digestion as described below.

2.2 Adenovirus Approach

Another method of introducing Cre recombinase is through a Cre-expressing adenovirus (Adeno-Cre) vector, which was injected as a calcium phosphate precipitate (CaPi) (*Fasbender et al. 1998*).

The adenovirus original stock solution ($7.5x10^{10}$ PFU/ml) was diluted with αMEM to obtain aliquots containing $5x10^{8}$ PFU/60µl or $5x10^{7}$ PFU/60µl respectively. These new stock solutions were stored in 450 µl aliquots at -80°C until further use. On the day of injections, $CaCl_2$ was freshly added from a 2 M stock solution to obtain a final Ca^{2+} concentration of 12 mM. The αMEM medium already contained the required 1 mM

of phosphate. Incubation for 30 minutes at room temperature allowed for the precipitate to form. After this period the virus precipitate was kept on ice until injection.

2.3 Mouse work

2.3.1 Mouse breeding scheme

The mice used for our experiments contained a floxed $Kras^{G12D}$ allele as well as a gene trapped Dlc1 allele on a C57BL/6 background (*Jackson et al. 2001*, *Sabbir et al. 2010*). To obtain those mice heterozygous Dlc1 gene trapped mice were crossed with heterozygous Kras floxed mice (Figure 2.2). In the offspring the tumor development was compared in $Kras^{LSL/+}/Dlc1^{gt/+}$ (KD) versus $Kras^{LSL/+}/Dlc1^{+/+}$ (K+) after Cre injection to determine if there were any differences.

2.3.2 Genotyping

All mice were genotyped for Kras and Dlc1 genes at around 3 weeks of age by Heather Leslie, the technician in our lab. DNA for the genotyping was obtained by incubating a tail sample in DNA buffer (500 mM KCl, 100 mM Tris-HCl, 0.45 % NP-40, 0.45 % Tween-20, 0.1 mg/ml gelatine) with 1 µg/µl of Proteinase K over night in a 55°C water bath. The next day the sample was boiled for 10 minutes and then centrifuged for 5 minutes at full speed (Micro 20, Hettich Centrifuges).

2.3.2.1 Genotyping of the $Kras^{G12D}$ allele

The $Kras^{G12D}$ gene was amplified from the tail DNA using the Taq HS system from TaKaRa according to the Mouse Repository's instructions (*Repository*). The total volume of 30 µl contained 1x PCR buffer, 2 mM $MgCl_2$, 200 µM dNTP mix, 0.75 U Taq HS polymerase, 1.5 µl DNA and 60 nM of K004 or K005 forward together with

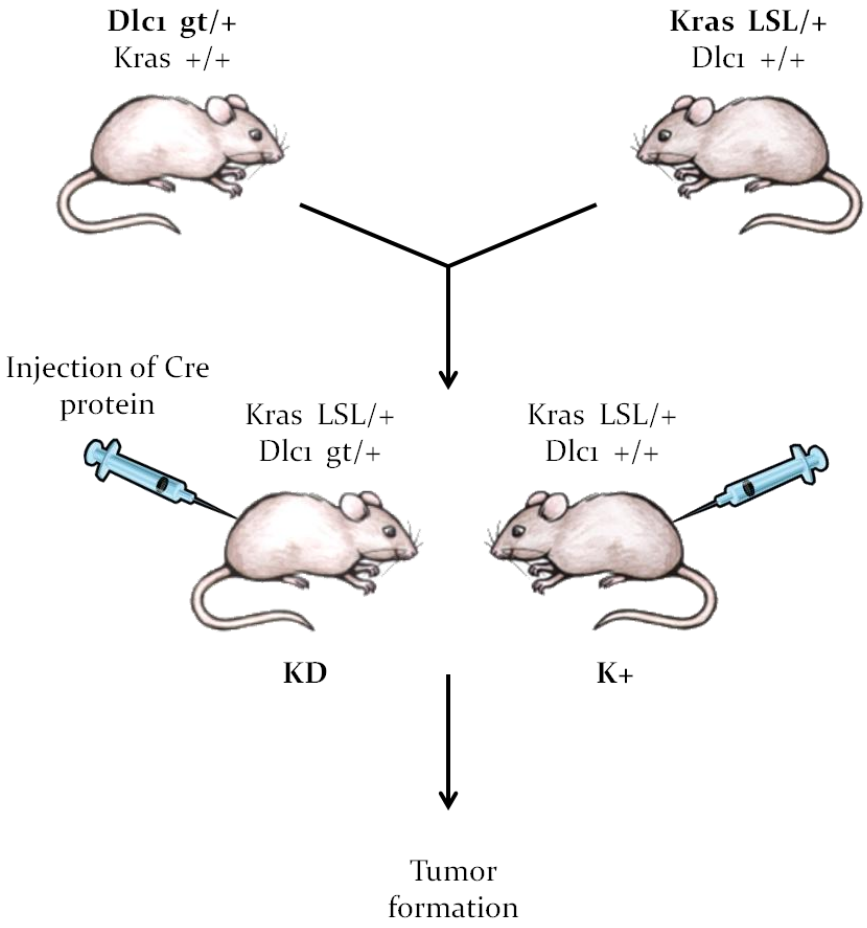

Figure 2.2: Breeding scheme for Kras activation

Heterozygous Dlc1 gene trapped mice ($Dlc1^{gt/+}$) were crossed with heterozygous LSL-$Kras^{G12D}$ mice ($Kras^{LSL/+}$). From the offspring only mice that were either heterozygous gene trapped for Dlc1 as well as heterozygous floxed for $Kras^{G12D}$ ($Kras^{LSL/+}/Dlc1^{gt/+}$ = KD) or only heterozygous floxed for $Kras^{G12D}$ ($Kras^{LSL/+}/Dlc1^{+/+}$ = K+) were used for further studies. KD and K+ mice were then injected with Cre protein (IP with HNC or IN with Adeno-Cre) and tumor development was studied.

The mouse image was taken from www.wildbritart.com with the permission of Elee Kirk for educational purposes.

60 nM of K006 reverse primer (Table 2.1). The conditions for the PCR were as follows: denaturation at 94°C for 3 minutes, followed by 35 cycles of denaturation at 94°C for 1 minute, annealing at 60°C for 2 minutes, extension at 72°C for 1 minute, and a final extension step at 72°C for 3 minutes before holding it at 4°C.

For visualization, 17 µl of the PCR product were mixed with 3 µl of 6x loading dye (10 mM Tris, 0.03 % bromphenol blue, 0.3 % xylene cyanol FF, 60 % glycerol, 60 mM EDTA) and all 20 µl were loaded onto a 1.5 % agarose gel (in TAE buffer) supplemented with 0.5 mg/ml ethidium bromide and separated at 100 V.

Another 5 µl of the PCR product were entered into a digestion over night at 37°C. The digestion mix contained 10 µl PCR product, 1x NE2 buffer2 and 1 µl HindIII (both from NE Biolabs) in a total volume of 20 µl. A sample without any enzyme, but PCR product was treated as negative control. The next day the 20 µl digestion were mixed with 4 µl of 6x loading dye and all 24 µl were loaded onto a 1.5 % agarose gel (in TAE buffer) supplemented with 0.5 mg/ml ethidium bromide and separated at 100 V.

2.3.2.2 Genotyping of the Dlc1 allele

The Dlc1 gene trapped allele was also amplified from the DNA using the Taq HS system from TaKaRa according to (*Sabbir et al. 2010*). The total volume of 25 µl contained 1x PCR buffer, 200 µM dNTP mix, 1.5 U Taq HS polymerase, 2 µl DNA and 240 nM of Genotype-F forward and Genotype-R reverse primer as well as 160 nM of Neo-F forward primer (Table 2.1).

The conditions for the PCR were as follows: denaturation at 94°C for 1 minute, followed by 40 cycles of denaturation at 94°C for 15 seconds, annealing at 63°C for 30 seconds, extension at 72°C for 45 seconds and a final extension step at 72°C for

	Primer Sequence (in 5' to 3')
Genotyping Kras	
Forward K004 (F)	GTCGACAAGCTCATGCGGGTG
Forward K005 (F)	CCTTTACAAGCGCACGCAGACTGTAGA
Reverse K006 (R)	AGCTAGCCACCATGGCTTGAGTAAGTCTGCA
Genotyping Dlc1	
Forward Geno- F	TCCTGCTGGTGTGTGTAAACAGAC
Forward Neo-F	GATTCCACCGCCGCCTTCTATG
Reverse Geno-R	CCAAAGGAGGAGGCAAACTTACAC
RT-PCR Kras	
Forward Kras -	GCCATTTCGGACCCGGAGCGA
Reverse Kras-R	CCTACCAGGACCATAGGCACATC
Pyrosequencing Kras	
Forward Pyro-Kras-F	GCCATTTCGGACCCGGAGCGA
Reverse Pyro-Kras-R-bio	Biotin-CCTACCAGGACCATAGGCACATC
Sequencing Pyro-Kras-seq	TGCTGAAAATGACTGAG
Methylation sensitive PCR	
Forward MSP-F	AAATATATTGGATAGAGTTGCGTACGC
Reverse MSP-R	AAAAAACTTACGCGAAATACGAAAATTA
Forward NMSP-F	TAGAAATATATTGGATAGAGTTGTGTATGT
Reverse NMSP-R	ACAAAAAAACTTACACAAAATACAAAAATTA
Pyrosequencing Dlc1	
Forward Pyro-Iso2-F	Biotin-GTAAGAAAAGGTAGAGGGGAAATTGAGTA
Reverse Pyro-Iso2-R	CTCCTTCCCCCTTTCCTAAAATAT
Sequencing Pyro-Iso2-seq	TTTTCCCAAAATCTACACT
Isoform PCR	
Forward Iso2-F (6.1kb)	CTTCTGGCAGCCTCGACGTTC
Forward Iso3-F (6.2kb)	CATCAGAGACTCCACCGCCAG
Reverser Iso23-R	TGCATACTGGGGGAAACCAGTC
Forward GAPDH-F	TTCCGTGTTCCTACCCCCAATGTGT
Reverse GAPDH-R	GGAGTTGCTGTTGAAGTCGCAGGAG

Table 2.1: PCR Primers used

This table shows a list of all the primers used in the various PCR experiments throughout this thesis.

8 minutes before holding it at 4°C.

For visualization, 17 µl PCR product were mixed with 3 µl of 6x loading dye and all 20 µl were loaded onto a 1.5 % agarose gel (in TAE buffer) supplemented with 0.5 mg/ml ethidium bromide and separated at 100 V.

2.3.3 Intraperitoneal injection of HNC Protein

The cell permeable HNC protein was injected intraperitoneally into 10-15 day old mice. The concentration of injected HNC protein was 25 µg per gram bodyweight of the mouse on three consecutive days (*Jo et al. 2001*). Young mice were injected to allow for more cell divisions as we expected tumor formation to be more frequent due to increased cell turnover in cells with a mutant $Kras^{G12D}$ allele.

2.3.4 Intranasal injections of Adeno-Cre

Adult K+ and KD mice were anesthetized using a combination of 1 mg ketamine and 0.1 mg xylazine per 10 g body weight. The CaPi precipitate of the Adeno-Cre adenovirus was then injected intranasally. $5x10^8$ PFU/mouse or $5x10^7$ PFU/mouse were prepared for a total volume of 60 µl (see above). The solution was injected in three rounds of 20 µl, with 5 minutes break in between to allow the mice to breathe in the liquid and recuperate. After injections mice were kept in quarantine for 72 hours and then returned to their colonies. In addition two wild type mice were injected with $5x10^7$ PFU/mouse as negative controls.

2.3.5 Mouse care

Breeding and animal husbandry was provided by the staff in the Cancer Care Animal Facility and followed the regulations of the University of Manitoba Animal

Protocol Management and Review Committee. Additionally, the mouse weight was recorded by me on a weekly basis. In combination with their appearance it was used as indicators of sickness. If a mouse appeared to be sick (hunching behaviour, fur conditions, breathing rhythm) or lost 10 % bodyweight it was sacrificed by cervical dislocation, as specified in the animal protocol.

2.4 Primary organ follow up

The dissections of all mice were performed in a biosafety cabinet in a semi-sterile environment. Upon dissection a variety of organs were removed (brain, thymus, heart, lung, liver, spleen, kidney, uterus or prostate/testis) and incubated in RNAlater solution (Ambion) over night at 4°C to allow for proper diffusion of the solution into the inner core of the tissues. The next day, the organs were further dissected and divided for DNA, RNA and histology analysis.

2.4.1 Histology

For histological analysis the organs were incubated in 10 % formalin solution over night at room temperature and then transferred into 70 % ethanol. The paraffin embedding as well as the H&E staining of these sections was performed by either Susan Pylypas (Department of Dental Diagnosis and Surgical Sciences) or Andrea Fristensky and Sandra Troup (Manitoba Breast Tumor Bank). Essentially, the sections were deparaffinised with 2 changes of xylene for 2 minutes each. They were then hydrated with decreasing ethanol grades for 2 minutes each (2x absolute ethanol, 95 %, and 70 %). After a 5 minute wash with tap water the sections were stained for 4 minutes with filtered Harris haematoxylin solution. Another wash with tap water was followed by differentiation in 5-7 dips of 1 % acid alcohol (glacial acid in ethanol). Two washes in tap

water alternated with a 2 minute wash in Scott's tab water (200 ml ddH_2O, 5 drops of Mallinckrodt Ammonia Strong Solution 27 %) to blue the sections. The sections were then incubated for 2 minutes in 95 % ethanol, followed by 2 minutes in 0.2 % eosin and then destained by 10 dips in 70 % ethanol and 15 dips in 95 % ethanol. Dehydration was achieved through 2 changes of absolute ethanol for 2 minutes each. In the last step the sections were cleared in 2 changes of xylene for 2 minutes each and then mounted with Permount mounting media (Fisher Scientific).

The slides were then analysed using a Olympus BX51 microscope with the according software, courtesy of Dr. Eisenstat's lab. Slides were first screened for primary tumors and metastases in other organs. The tumor burden in K+ mice was also compared with burden in KD mice.

2.5 Studying the $Kras^{G12D}$ allele

2.5.1 RNA preparation

As mentioned earlier, the organs were submerged in RNAlater immediately after dissection. The next day tissues were transferred to -20°C for storage until use. The total RNA was extracted from the different tissues using either the RNeasy Mini Kit (Qiagen) or the TRIZOL® protocol (Invitrogen) according to the manufacturer's instructions. For the TRIZOL® treatment, approximately 50 mg of tissue were crushed in liquid nitrogen and resuspended in 1 ml of TRIZOL® Reagent on ice. Samples were then homogenized by passing through a 1 ml syringe with a 28 gauge needle. After incubation for 5 minutes at room temperature to allow the complete dissociation of the nucleoprotein complexes, 0.2 ml of chloroform was added and the tubes were shaken vigorously by hand for

15 seconds. Incubation for 10 minutes at room temperature was followed by centrifugation for 15 minutes at 13,000 rpm at 4°C (Micro 20, Hettich Centrifuges).

The upper aqueous phase was then transferred to a fresh tube and the RNA was precipitated with 0.5 ml isopropanol for 10 minutes at RT. After centrifugation for 10 minutes at 13,000 rpm at 4°C the supernatant was decanted and the pellet was washed with 1 ml of 75 % ethanol in nuclease-free water through vortexing. The pellet was then centrifuged for 5 minutes at 10,000 rpm at 4°C and briefly allowed to dry. RNA was dissolved in 50 µl nuclease-free water and incubated for 10 minutes at 65°C to linearize the nucleic acids.

To measure the concentration, RNA was diluted 1:50 in nuclease-free water and the absorption at 260 nm was measured using an Ultraspec 3000 Spectrometer (Pharmacia Biotech). The RNA concentration (in µg/ml) was then calculated by multiplying the OD (at 260 nm) with the OD unit for RNA (40 µg/ml) and the dilution (50).

2.5.2 cDNA preparation

The complementary DNA (cDNA) was synthesized using the RevertAid M-Mulu reverse transcriptase system from Fermentas and the PTC-200 Peltier Thermal Cycler (MJ Research). Briefly, 2 µg RNA were combined with 0.4 µg random hexamer primer in a total volume of 12.5 µl. Samples were incubated for 4 minutes at 65°C and then immediately chilled on ice. A master mix containing 1x cDNA synthesis buffer, 1 mM dNTP mix and 60 U RevertAid M-Mulu reverse transcriptase was added to the primer/RNA mix to a final volume of 20 µl. Samples were then incubated for 10 minutes

at 25°C, 60 minutes at 37°C and 10 minutes 70°C. The cDNA sample was then immediately entered into a PCR reaction or stored at -20°C until further use.

2.5.3 PCR for the Kras^{G12D}

The Kras gene was amplified from the cDNA sample using the Taq HS system from TaKaRa on the PTC-200 Peltier Thermal Cycler (MJ Research). The total volume of 25 µl contained 1x PCR buffer, 200 µM dNTP mix, 1 U Taq HS polymerase, 2 µl cDNA and 240 nM of Kras-F forward and Kras-R reverse primer (Table 2.1). The conditions for the PCR were as follows: denaturation at 95°C for 1 minute, followed by 40 cycles of denaturation at 95°C for 15 seconds, annealing at 62°C for 30 seconds and extension at 72°C for 35 seconds, and a final extension step at 72°C for 10 minutes, before holding at 4°C.

For visualization 10 µl PCR product were supplemented with 2 µl of 6x loading dye and 10 µl of this mixture were loaded onto a 1.8 % agarose gel (in TAE buffer) and separated at 100 V. The remaining 10 µl were entered into a digestion over night at 37°C. The digestion mix contained 10 µl PCR product, 1x NE2 buffer and 1 µl HindIII (both from NE Biolabs) in a total volume of 20 µl. The next day the enzyme was inactivated for 20 minutes at 65°C. The digestion mix was supplemented with 5 µl of 6x loading dye and 20 µl of this mixture were loaded onto a 1.8 % agarose gel (in TAE buffer) and separated at 80 V.

2.5.4 Pyrosequencing for mutation analysis

To determine the exact percentage of activated Kras, pyrosequencing analysis was performed as described before (*Sabbir et al. 2010*). Figure 2.3 shows the principle of the pyrosequencing technique used for mutation analysis as well as methylation analysis.

2.5.4.1 Pyro PCR

The Kras allele was amplified using the Taq HS system from TaKaRa on the PTC-200 Peltier Thermal Cycler (MJ Research). The total volume of 25 µl contained 1x PCR buffer, 200 µM dNTP mix, 1 U Taq HS polymerase, 2 µl cDNA and 240 nM of Pyro-Kras-F forward and Pyro-Kras-R-biotin reverse primer (Table 2.1). The conditions for the PCR were as follows: denaturation at 95°C for 1 minute, followed by 40 cycles of denaturation at 95°C for 15 seconds, annealing at 62°C for 30 seconds and extension at 72°C for 30 seconds, and a final extension step at 72°C for 10 minutes.

An aliquot of 4 µl PCR product was supplemented with 2 µl of 6x loading dye and loaded onto a 1.5 % agarose gel (in TAE buffer) and separated at 90 V.

2.5.4.2 Preparation of the samples for pyrosequencing

After amplification of the allele through PCR the samples were pyrosequenced using the PyroMark Q96 MD sequencing machine (Biotage) and the protocol Kras v2.0 (Qiagen).

In the first step, the PCR products were immobilized onto streptavidin sepharose HP beads (GE Healthcare). The immobilization solution contained 40 µl binding buffer (10 mM Tris, 2 M NaCl, 1 mM EDTA, 0.1 % Tween-20, pH 7.6), 2 µl beads and 10 µl PCR product in a total volume of 80 µl nuclease-free water. After adding the solution to a PCR plate, the samples were incubated on a shaker at 140 rpm for 15 minutes at RT.

During the incubation of the samples the annealing solution was prepared. In a total volume of 15 µl annealing buffer (20 mM Tris, 2 mM $MgAc_2$, pH 7.6) 10 µM

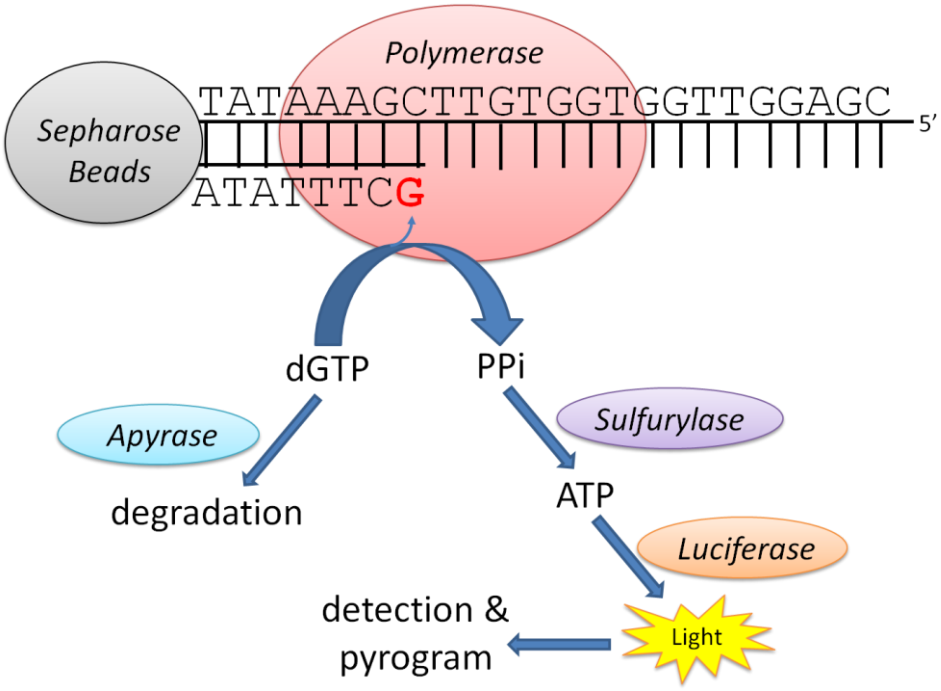

Figure 2.3: Pyrosequencing Technique

The DNA to be analyzed is amplified by PCR and immobilized onto sepharose beads through a biotin-residue introduced by one of the primers. The machine will then dispense nucleotides in the order of the reference sequence. Each time a nucleotide gets incorporated, a phosphate is released, that will then be metabolized by Sulfurylase and Luciferase to produce light emission, which can be detected. Before the next nucleotide is dispensed the residual ones are degraded by Apyrase. In the case of the mutation site (mutation analysis) or the CpG islands (methylation analysis), one doesn‘t know which nucleotide to dispense depending on the status of that site. The machine will therefore dispense both nucleotides (for both possible states) in two steps after each other. Depending on the peak height in the resulting pyrogram one can then determine the percentage for each stage.

sequencing primer (Table 2.1) was diluted to a final concentration of 0.3 µM and added to a thermo stable plate.

Immediately after the incubation finished, the samples were treated and washed using the PyroMark-Q96 Vacuum Workstation (Biotage). Through the application of the vacuum, the beads were attached to the filter probes of the vacuum workstation. Subsequent 5 second washes in 70 % ethanol, denaturation buffer (0.2 M NaOH), wash buffer (10 mM Tris-Ac, pH 7.6) and ddH_2O prepared the samples for release into the annealing solution. After release of the beads the final samples (now containing the beads with immobilized PCR product and the sequencing primer) were then sealed and incubated at 92°C for 2 minutes before being allowed to cool down for at least 10 minutes to RT.

2.5.4.3 Pyrosequencing run

The pyrosequencing itself was then performed in the PyroMark Q96 MD sequencer (Biotage). The reference sequence for the run was "TAT AAA/G CTT GTG GTG GTT GGA GCT GG/AT GGC" (with the possible mutations underlined). This resulted in a dispensation order of "G TAT AGA CT GT GT GT GA GCT GAGT". The amounts of enzyme, substrate and nucleotides (Qiagen) depend on the sequence and the sample number, but are available through the PyroMark Q96 MD software after the new run is set up.

2.5.4.4 Analysis of the pyrosequencing results

The analysis of the results was performed using the PyroMark Q96 MD software (Biotage). After the run finished, the software displays the results in a pyrogram, showing the incorporation (or non-incorporation) of the dispensed nucleotides. At the locations of

the mutations (the silent mutation and the oncogenic mutation) the program dispensed the nucleotides for both possibilities after each other. For example in the case of the oncogenic mutation that would be the G for the wild type allele and A for the mutated allele, hence the dispensation order of G followed by A. Depending on the incorporation of the mutated nucleotide or the non-mutated nucleotide a peak can be seen. By dividing the peak height of each peak through the height of both peaks combined one can then calculate the percentage of the mutated allele versus the wild type allele.

2.6 Studying the Dlc1 allele

2.6.1 Antibody Validation Dlc1

In our lab there were two polyclonal antibodies for Dlc1 available, one from Santa Cruz and one from BioSource. Both the rabbit antibody from Santa Cruz (sc-32931) as well as the goat antibody from BioSource, (MBS421454) were raised against the N-terminal of the human Dlc1 protein. Since they were to be used in immunohistochemistry experiments to study the expression of Dlc1 these antibodies needed to be validated first. To do so immunohistochemistry and immunofluorescence experiments were performed on Dlc1 expressing and non-expressing cell lines. These cells were derived from murine breast cancer. Rachelle Dillon in our lab had previously shown by western blot experiments that these cells either express Dlc1 normally or at a very low level (data not shown).

2.6.1.1 Immunohistochemistry

Immunohistochemistry experiments were performed by the staff in the Manitoba Breast Tumor Bank.

The Dlc1 expressing or non-expressing breast cancer cells were grown in 10 cm plates until almost confluent. They were washed with PBS and trypsinized with 0.5 x Trypsin/EDTA. The trypsinized cells were transferred into a 15 ml tube and centrifuged for 5 minutes at 2000 rpm (Micro 20, Hettich Centrifuges). After aspiration of the media, the pellet was gently resolved in 10 ml of 10 % formalin and incubated over night at RT. The next day the cells were again pelleted for 5 minutes at 2000 rpm and the formalin was replaced with 70 % ethanol. When ready to process the cells were quickly pelleted again and resuspended in 500 µl 1 % agarose. Vortexing the agarose/cell solution created a slight gradient in the block. When solidified, the pellet was cut in half and processed as normal for paraffin embedding.

The agarose cell pellets were sliced into 5 µm sections and washed twice in xylene for 5 minutes, then for 2 minutes each in 2x 100 %, 95 % and 70 % ethanol, followed by 5 minutes in PBS. Cells were then quenched for 10 minutes at room temperature in 3 % H_2O_2 in PBS, followed by two 2 minute washes in PBS. Dlc1 antibodies were then blocked for 1 hour at room temperature with 10 % normal serum in PBS (rabbit serum for the antibody from Biosource, goat serum for the antibody from Santa Cruz). The primary antibodies (dilutions of 1:50 and 1:400) were incubated in blocking solution (PBS with serum) over night at 4°C. After two 2 minute washes in PBS the secondary antibodies were incubated for 1 hour at room temperature in PBS (dilution 1:400). Slides were then washed 2 times for 2 minutes in PBS, 2 minutes in ddH_2O, followed by 2-3 minutes in 3,3'-Diaminobenzidine, followed by 2 washes for 2 minutes in ddH_2O. A 5 minute wash in 1 % $CuSO_4$ was followed again by two 2 minute washes in ddH_2O. The last step consisted of Harris Hematoxylin staining (50:50 diluted in ddH_2O)

for 10 seconds. Alternate washes for 2 minutes in tap water and Scott's tap water were then followed by dehydration for 2 minutes each in 70 %, 95 % and 2x 100 % ethanol. After washing twice in xylene the coverslips were mounted with Permount mounting media (Fisher Scientific).

Primary antibodies were: Dlc1 (Rabbit, Santa Cruz, sc-32931), Dlc1 (Goat, BioSource, MBS421454). Secondary antibodies were HRP conjugated goat-anti-rabbit and rabbit-anti-goat antibodies from Jackson.

2.6.1.2 Immunofluorescence

As second part of the antibody validation immunofluorescence experiments were performed on the same Dlc1 expressing or non-expressing breast cancer cell lines as for the immunohistochemistry.

Cells from the same batch used in the immunohistochemistry experiments were grown on 10 cm plates until fully confluent and were then plated on coverslips in 6 well plates. The next day cells were about 80 % confluent and ready for immunostaining. After washing in PBS twice cells were fixed in 2 % paraformaldehyde in PBS for 10 minutes at RT. Three more washes in PBS were followed by permeabilization of the cells in 0.2 % Triton-X in PBS for 10 minutes at RT. After another 3 washes in PBS for 5 minutes each, cells were blocked in 5 % skimmed milk in PBS (PBS-milk) for 1 hour at RT. The primary antibody at different dilutions (1:50, 1:100, 1:250 and 1:500) was incubated in 1 % PBS-milk for 1 hour at RT. Three washes with PBS for 5 minutes each were followed by incubation with secondary antibody (anti-goat 1:1000, anti-rabbit 1:500) in 1 % PBS-milk for 1 hour at 37°C in the dark. After the final three washes in PBS for 5 minutes each the coverslips were mounted with 1 drop Vectormount mounting

media containing DAPI. Slides were then stored upright in the fridge until examination the next day.

Primary antibodies were: Dlc1 antibodies from Santa Cruz and BioSource (see "Immunohistochemistry section"). Secondary antibodies were Alexa Fluor 488 conjugated anti-goat (Invitrogen) and FITC conjugated anti-rabbit (Sigma Aldrich).

2.6.2 PCR for Dlc1 isoform expression

2.6.2.1 DNase treatment of RNA

Tumor RNA was prepared from either whole tissues or micro dissected lung tumors as described above. The RNA was then treated with RQ1 DNase (Promega) according to the manufacturer's instructions to eliminate any remaining traces of DNA. In a small tube 1 µl DNase per 1 µg RNA was mixed in 1x reaction buffer in a total volume of 5 µl. The sample was incubated at 37°C for 30 minutes. The enzyme was then inactivated by heating for 10 minutes at 65°C in the presence of 2 mM EGTA and the whole solution was then entered into cDNA synthesis.

2.6.2.2 DEAE treatment of Taq polymerase

Since using the Taq Polymerase straight out of the box would give unspecific bands in the negative control samples (water with Master Mix), the enzyme was pre-treated with DEAE (Diethylaminoethyl) cellulose as described previously (*Glushkov et al. 2009*). In essence, 0.6 ml of pre-swollen DEAE cellulose (Sigma Aldrich) was equilibrated with 1ml suspension buffer (5 mM Tris, 1 mM EDTA, 200 mM NaCl) at room temperature for 5 minutes. An aliquot of 200 µl from this mixture was centrifuged for 1 minute at 3000xg and the supernatant was carefully removed. Approximately the same amount of Taq was then added and gently mixed for 5 minutes at room temperature.

The mixture was then spun for 2 minutes at 15000xg and the supernatant (now clean Taq) carefully moved to a new tube, without disturbing the pellet.

2.6.2.3 PCR for Dlc1 isoforms

To investigate the expression of the Dlc1 isoforms in the different tumors, isoform-specific RT-PCR was performed as described previously (*Sabbir et al. 2012*). Two Dlc1 isoforms (6.1 kb isoform 2 and 6.2 kb isoform 3) as well as GAPDH were amplified from the cDNA sample using the Taq HS system from TaKaRa on the PTC-200 Peltier Thermal Cycler (MJ Research). The total volume of 25 µl contained 1x PCR buffer, 200 µM dNTP mix, 1.5 mM $MgCl_2$, 0.5 U DEAE cellulose treated Taq HS polymerase, 2 µl cDNA, 200 nM of Iso2-F or Iso3-F forward together with Iso23-R reverse primer or 20 nM of GAPDH forward and reverse primers (Table 2.1). The conditions for the PCR for the two Dlc1 isoforms were as follows: Denaturation at 95°C for 1 minute, followed by 35 cycles of denaturation at 95°C for 15 seconds, annealing at 66°C for 15 seconds and extension at 72°C for 15 seconds, and a final extension step at 72°C for 10 minutes. For the GAPDH amplification the annealing temperature was lowered to 64°C and the total number of cycles was 40.

The 25 µl PCR product were supplemented with 5 µl of 6x orange loading dye (Fermentas) and 20 µl of this mixture were loaded onto a 2 % agarose gel in 0.5x TBE buffer (45 mM Tris-Borate, 1 mM EDTA) and separated at 120 V.

2.6.3 DNA preparation from lung tumors

Micro dissection was performed on the lung tissue samples to obtain as pure as possible tumor tissue as pure as possible and avoid extensive contamination with normal cells.

2.6.3.1 Removing the RNA later solution from lung tissues

After dissection of the mouse, all organs were stored in RNAlater. However, RNAlater is not compatible with cryosectioning because it prevents solid freezing of the tissue. To remove the RNAlater solution, the lungs were washed two times in PBS for 5 minutes each at room temperature on a shaker. They were then incubated with freshly prepared 2 % paraformaldehyde in PBS for 1 hour at room temperature on the shaker. This was followed by washes in sucrose solutions of incremental percentages. First the lungs were incubated in 5 % sucrose in PBS at 4°C until they sank to the bottom of the tube, which is a sign that the sucrose has sufficiently penetrated the tissue. This was followed by incubation in 10 % sucrose under the same conditions. The tissues were then incubated in 20 % sucrose in PBS overnight and then next day the solution was changed twice. Another overnight incubation in 20 % Sucrose in PBS, supplemented 1:1 with OCT (Optimal cutting temperature compound) at room temperature was followed by embedding of the tissues in OCT alone and storing in -80°C until sectioning.

2.6.3.2 Cryosectioning & staining

The frozen tissues were sectioned at 20 µm on a Cryostat machine. One of the cryosections was then stained with H&E to locate the tumor and act as reference during the micro dissection process. Briefly, the frozen sections were stained with haematoxylin for 30 seconds, followed by 2 fast dips in acid alcohol (70 % ethanol with 1 % HCl) and 60 seconds in Scott's tap water, before and after each of these steps the slides were washed in tap water for 2 minutes. After incubation in 70 % ethanol and 95 % ethanol for 60 seconds each, slides were stained with eosin for 30 seconds followed by washing in

70 %, 95 % and 2x 100 % ethanol. After two washes in xylene for 2 minutes coverslips were mounted with Permount mounting media (Fisher Scientific).

2.6.3.3 Micro dissection from Cryosections

The cryosections were air-dried for about 10 minutes. Taking the H&E stained sections as reference, the tumors were then micro dissected with a scalpel blade under the Leica MZ6 dissection microscope.

2.6.3.4 DNA preparation

The dissected tumors from 4 sections were transferred to a 1.5 ml microcentrifuge tube and incubated with 40 µl DNA buffer (10 mM Tris, 100 mM NaCl, 10 mM EDTA, 0.5 % SDS) and 20 µg of Proteinase K for 2 hours in a 55°C water bath. The concentration of the DNA was determined through spectrometry and equal amounts of DNA were used for bisulfite treatment.

2.6.4 DNA from abdominal tumors

Because the tumor samples from the abdominal tumors were pure tumor tissue without surrounding normal tissue, no micro dissection was necessary. To extract the DNA 100-200mg of tumor tissue were crushed in liquid N_2, resuspended in 5 ml DNA lysis buffer (10 mM Tris, 100 mM NaCl, 10 mM EDTA, 0.5 % SDS) and heated for 10 minutes in a 65°C water bath. Proteinase K (200 µg) was added and the sample incubated over night at 56°C. The next day the sample extracted with phenol followed by phenol/chloroform/isoamylalcohol (25:24:1) and chloroform/isoamylalcohol (24:1) alone. In between steps the sample was mixed slowly on a horizontal shaker for 20 minutes and then centrifuged for 15 minutes at 3000 rpm (IEC DPR-6000 centrifuge,

Fisher Scientific, 269 Rotor). After the final step the upper supernatant was precipitated with isopropanol, washed with 70 % ethanol and dissolved in 200 µl TE buffer.

2.6.5 Bisulfite treatment of DNA

2.6.5.1 Bisulfite treatment of DNA from Intestinal tumors

The DNA was treated with bisulfite as previously described (*Ghoshal et al. 2002, Sabbir et al. 2010*). The bisulfite treatment converts all non-methylated cytosines into uracil residues, whereas the methylated ones remain cytosines. This can then later be used by the pyrosequencing to distinguish between the methylated and non-methylated residues. Briefly 5 µg DNA in 10 µl were supplemented with 300 mM NaOH and then incubated for 30 minutes at 37°C. After adding the bisulfite solution (2.63 M bisulfite, 45 mM hydroquinone) the sample was heated to 95°C for 2 minutes and then incubated at 50°C for 30 minutes to a total of 20 cycles in a thermal cycler (overnight). The DNA was then cleaned using the PCR Purification Kit from Qiagen according to the manufacturer's instructions. The DNA was eluted in 100 µl ddH_2O, supplemented with 0.3 M NaOH for desulphonation and incubated at 37°C for 30 minutes. The DNA was then precipitated with a combination of 1 µg glycogen, 1.4 M ammonium acetate and 3 volumes of ethanol at -80°C for 1-2hours. After washing with 70 % ethanol the DNA was dissolved in 20 µl TE buffer. From there 5 µl were used in the PCR.

2.6.5.2 Bisulfite treatment of DNA from Lung tumors

The DNA obtained from the micro dissection was treated with bisulfite following the same protocol as described above. But due to the small amounts of DNA present (1 µg), 10 µg of salmon sperm DNA (Invitrogen) was added to the sample prior to bisulfite treatment (*Tan & Dobrovic 2001*).

2.6.6 Methylation sensitive PCR

The methylated and unmethylated Dlc1 sequences were amplified through the Taq HS system from TaKaRa on the PTC-200 Peltier Thermal Cycler (MJ Research). The total volume of 25 µl contained 1x PCR buffer, 200 µM dNTP mix, 1 U Taq HS polymerase, 5 µl cDNA and 240 nM of both forward and reverse primers specific for the methylated (MSP-F/MSP-R) or non-methylated (NMSP-F/NMSP-R) sequence (Table 2.1). The conditions for the PCR were as follows: denaturation at 94°C for 1 minute, followed by 40 cycles of denaturation at 94°C for 30 seconds annealing at 57°C for 30 seconds, extension at 72°C for 20 seconds and a final extension step at 72°C for 10 minutes. Because the first round of PCR would not yield enough products to be seen on an agarose gel, a second round of PCR was performed with 2 µl of PCR product from the first round and 15x cycles, but otherwise under the same conditions.

For visualization, 17 µl PCR product were supplemented with 3 µl of 6x loading dye and 17 µl of this mixture were separated on a 2 % agarose gel (in TAE buffer) at 90 V alongside 5 µl of Generuler 1kb Ladder Plus (Fermentas).

2.6.7 Pyrosequencing for methylation studies

The pyrosequencing experiments for gene trapped Dlc1 isoform 2 were essentially performed as described for the Kras allele. The DNA for the pyrosequencing experiment was extracted and bisulfite treated as described above.

2.6.7.1 Pyro-PCR

The Dlc1 isoform 2 (6.1 kb) was amplified from bisulfite treated DNA samples using the Taq HS system from TaKaRa on the PTC-200 Peltier Thermal Cycler (MJ Research) as described previously (*Sabbir et al. 2010*).

The total volume of 25 µl contained 1x PCR buffer, 200 µM dNTP mix, 1.5 U Taq HS polymerase, 2 µl bisulfite treated DNA and 240 nM of Pyro-iso2-F forward and Pyro-iso2-R reverse primer (Table 2.1). The conditions for the PCR were as follows: Denaturation at 95°C for 1 minute, followed by 40 cycles of denaturation at 95°C for 15 seconds, annealing at 55°C for 15 seconds and extension at 72°C for 15 seconds, and a final extension step at 72°C for 10 minutes.

An aliquot of 4 µl PCR product was supplemented with 2 µl of 6x loading dye and loaded onto a 1.5 % agarose gel (in TAE buffer) and separated at 100 V.

2.6.7.2 Preparation of the samples for pyrosequencing

For details on sample preparation, please refer to the section "Pyrosequencing for mutation analysis".

2.6.7.3 Pyrosequencing run

The pyrosequencing run itself was then performed in the PyroMark Q96 MD sequencing machine. The reference sequence (after bisulfite treatment) for the run was "TTTACR(1)ACR(2)ACR(3)AAAAACR(4)CCTAAAAATCR(5)CCAACTACTAACC TCTAAAATAAAA" (with the positions for possible methylation underlined). This sequence resulted in the following dispensation order: "ESCTGATCAGATCAGATCAAGAATCGACTAGATACGACAC". The amounts of enzyme, substrate and nucleotides depend on the sequence and the sample number, but are available through the PyroMarkQ-CpG software after the new run is set up.

2.6.7.4 Analysis of the pyrosequencing results

The analysis of the results was performed using the PyroMarkQ-CpG software (Biotage) as described before.

2.6.8 Statistical analysis

Statistical analysis was performed using the Prism Software (GraphPad). One-way ANOVA was used to compare the total methylation (averaged from all five CpG islands per sample) of each tumor sample to the mean of two WT samples. To compare the methylation on each CpG island separately, two-way ANOVA determined any differences between the tumor samples and the mean of two WT samples.

2.7 Determination of tumor burden

To investigate any differences in tumor burden between K+ and KD mice a view through the whole lung was needed. Therefore the paraffin blocks of the whole lung were sectioned at 5 µm. Each 10^{th} section was stained with H&E as described above to allow for a three dimensional look through the organ. The sectioning and the H&E staining were performed by the staff at the Manitoba Breast Tumor Bank.

2.7.1 Counting procedure for tumor numbers

The H&E stained tumor sections were analyzed with the Olympus BX51 microscope at a 4x magnification. From each section overlapping pictures were taken using the Olympus DP70 camera. These pictures were then merged using Adobe Photoshop to obtain images of the whole section. The number of tumors was marked on each section and counted, taking into account that tumors could grow through more than one section and therefore needed to be only counted once. It was also assumed, that if

two tumors merged at some point that they originated from two separate transformation events, rather than one tumor projection.

2.7.2 Measurement of tumor sizes

For each mouse the two biggest tumors were determined by eye and for each the biggest section selected. The area of the two tumor sections was measured using Image J. The pixel values obtained were entered into Microsoft Excel to convert into mm^2 areas.

2.7.3 Measurement of tumor area

To obtain a better idea of the total area the tumors are occupying in the tissue Laser Scanning Cytometry (LSC) was performed using the Research Imaging Cytometer (CompuCyte) and the iCys 3.3 Software with the help of Gerald Stelmack from Dr. Halayko's Lab. In principle this method scans the H&E sections at 10x magnification with a blue laser (488 nm), which will then be absorbed or reflected by the tissue. Differences in absorption can be used to distinguish tumor areas (denser and therefore absorbing more light) from the normal surrounding tissue (less dense). The actual procedure consists of a two-step scanning method (Figure 2.4 F). In the first step the full slides were scanned with the laser at a lower resolution (X-step = 20 µm) to detect where the sections are located on the slide. In a second step the sections were defined as regions of interest and scanned again, this time at higher resolution (X-step = 4 µm). For each scan the gain and offset were manipulated to optimize signal to background ratio. The scanned image was inverted for easier visualization, so that dense regions (aka tumors) with a high absorption appeared white on a black background (Figure 2.4 A). To determine the area of tumors (as well as normal tissue) the scanned field was overlaid with a lattice network of phantoms (computer generated circles) with a radius of 20 µm

(Figure 2.4 B). Within each phantom the grey level values of each pixel (between 0 and 16383) were summed up and plotted in a histogram (Figure 2.4 E). The X-axis shows the sum of the grey level values, whereas the Y-axis shows the corresponding number of phantoms for each of those summed up grey level values. When regions corresponding to the tumor (yellow) as well as the normal tissue (red) were defined in the histogram the software colored the corresponding phantoms accordingly (Figure 2.4 C,D). The size of the phantoms was determined empirically to outline the tumor as detailed and smooth as possible but to not pick up too much background such as airway or vessel epithelia. After assigning the phantoms to a region (either tumor or normal tissue), the software then calculated the total number of phantoms in each region. Through the previously defined radius of the phantoms, the total area covered by each region (or the phantoms in that region) was calculated.

2.7.4 Statistical analysis

All tumor burden studies compared KD with K+ mice. Statistical analysis was performed using the Prism Software (GraphPad). A two-tailed Student t-Test and a Mann-Whitney statistical test compared the tumor numbers, tumor sizes and tumor areas of K+ and KD mice with each other in order to find any significant differences.

2.8 Cell culture

All MEFs (Kras and ROSA26) cells were cultured in αMEM (Gibco) supplemented with 60 mg/L penicillin G sodium salt, 2.2 g/L $NaHCO_2$, 100 mg/L streptomycin sulphate. After filter-sterilizing the medium through a 22 µm pore sized Stericap Plus Filter Unit (Millipore) 10 % fetal bovine serum (FBS, Sigma Aldrich) was added.

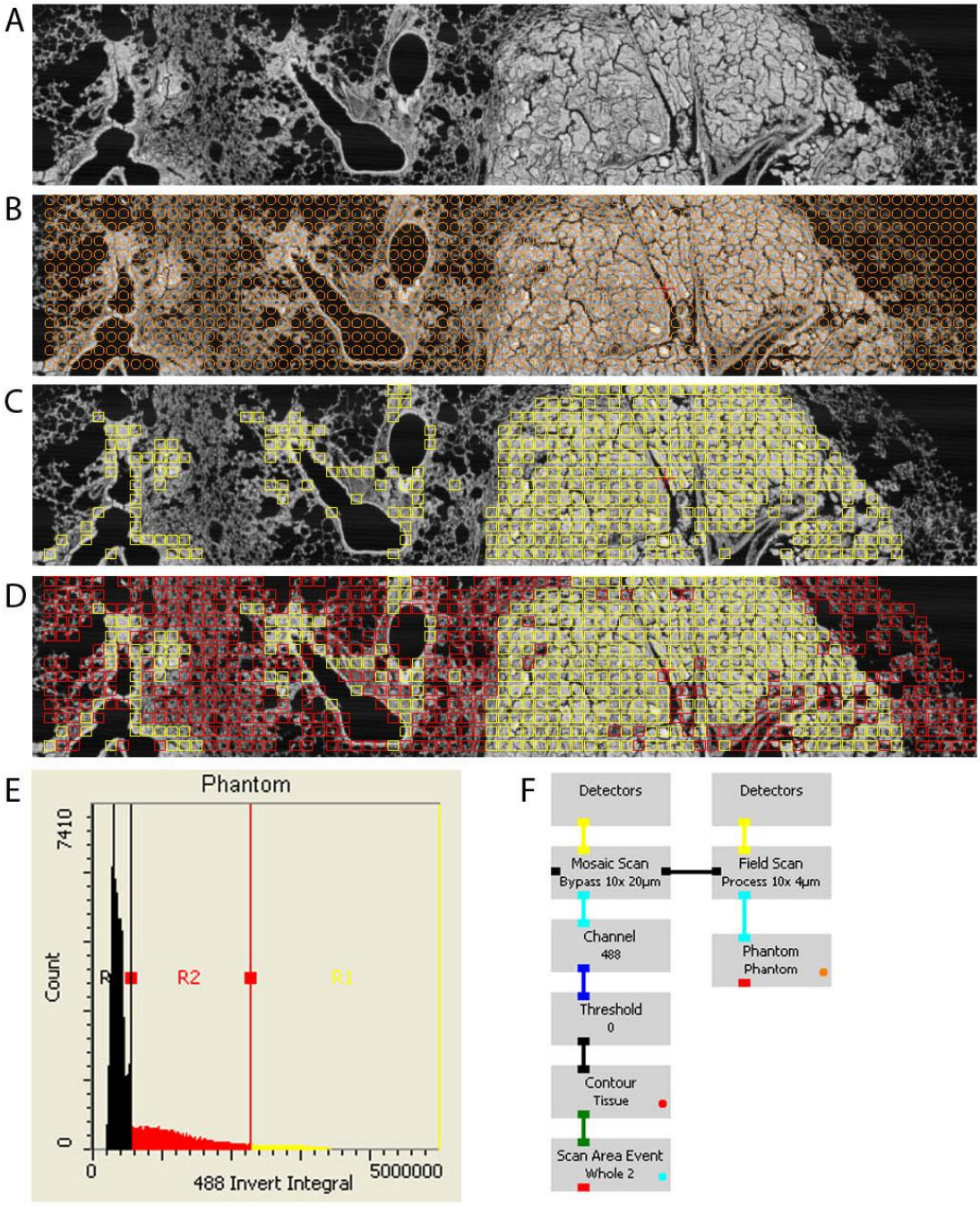

Figure 2.4: Laser Scanning Cytometry

The protocol of Laser Scanning Cytometry consists of a two-tailed scanning procedure (F). In the first step the whole slide is scanned at a lower resolution (X-step = 20 µm) to determine the location of the tissue on the slide. In a second step the regions of interest

are defined and scanned again, this time at a higher resolution (X-step = 4 µm). After scanning the image (A), a network of lattice phantoms (computer generated circles) with a radius of 20 µm were overlaid (B). The grey values of the pixels within each phantom are summed up and the integrated light intensity for each phantom is then plotted in a histogram (E). In the histogram, the X-axis shows the sum of grey level values, whereas the Y-axis shows the number of phantoms corresponding to those summed up grey level values. By defining regions in the histogram (R1 yellow = tumor tissue, R2 red = normal tissue), the phantoms corresponding to the determined intensities are then highlighted as tumors (yellow) or normal tissue (red) (C+D). The software determines the total number of phantoms in each region and with the know radius of those phantoms the total area they cover can be calculated.

The breast cancer cell lines were cultured in TM15 medium (DMEM (Gibco) supplemented with 1 µg/ml hydrocortisone, 5 µg/ml insulin, 5 ng/ml epidermal growth factor, 35 µg/ml bovine pituitary extract, 100 U/ml penicillin G, 0.1 mg/ml streptomycin sulphate, 10 % fetal bovine serum).

All cells were maintained in a humidified CO_2 incubator 610 (Fisher Scientific) at 5 % CO_2. Every 2-3 days when confluence reached around 80 % cells were split by washing with 1x PBS and trypsinization with 0.5 x Trypsin/EDTA.

2.9 Western Blotting

2.9.1 Sample preparation for western blot

Cell lines were grown on 10 cm culture dish in αMEM supplemented with 10 % FBS until almost confluent. They were then washed with PBS and harvested in 500 µl RIPA lysis buffer (20 mM Tris, 150 mM NaCl, 1 % NP-40, 1 mM EDTA, 1 % SDS) supplemented with Protease Inhibitor Cocktail (Sigma). The cells were scraped with a cell scraper and transferred into 1.5 ml tubes.

For samples obtained from animal tissues, approximately 30 mg of tissue were crushed in liquid N_2 and resuspended in 1 ml RIPA buffer. The solution was homogenized by passing through a syringe (18 gauge)

Both cells and tissue were then subjected to sonnication for 3x 15 seconds in a Sonifier Cell disruptor (Branson Sonic Power Co). The cell pellet debris was pelleted through centrifugation for 20 minutes at 13,000 rpm at 4°C (Micro 20, Hettich Centrifuges) and the supernatant transferred to a fresh tube. The protein concentration of all samples was determined using a BCA Assay as described above.

2.9.2 SDS-PAGE

SDS-PAGE was performed using the BioRad Mini-Protean Set. The hand cast system was used to make either 8 % or 12 % polyacrylamide separating gels (8 % or 12 % polyacrylamide, 3.5 mM SDS, 375 mM Tris, 0.05 % TEMED, 0.5 % APS), topped with a 4 % stacking gel (4 % polyacrylamide, 3.5 mM SDS, 125 mM Tris, 0.05 % TEMED, 0.5 % APS).

After determining the protein concentration of the samples, 30 µg of protein were supplemented with SDS sample buffer (0.08 M Tris, 2 % SDS, 10 % glycerol, 5.3 % β-mercaptoethanol, 20 % bromphenol blue) and loaded onto the SDS polyacrylamide gels. Additionally 5 µl of Pageruler Prestained Protein Ladder (Fermentas) were loaded as a marker. The samples were then separated in SDS running buffer (25 mM Tris, 192 mM glycine, 0.1 % SDS) through a current of 100 V until the marker band almost reached the lower glass corner.

2.9.3 Protein transfer to membrane

Proteins were transferred to a PVDF membrane using the wet transfer system from BioRad. Briefly, a PVDF membrane was activated in methanol, washed with ddH_2O and then layered into a "sandwich" with the SDS-gel, filter paper and sponges as described by BioRad. Briefly, from bottom to top a soaked sponge was followed by a filter paper, the gel, the activated membrane, another filter paper and another soaked sponge. The "sandwich" was incubated in methanol supplemented transfer buffer (25 mM Tris, 192 mM glycine, 20 % methanol) over night at 50 V and 4°C. The membrane was then dried for 2 hours at room temperature or for 30 minutes at 37°C.

2.9.4 Western Blotting

The western blot protocol was modified from (*Harlow & Lane 1999*). The PVDF membrane was re-activated with methanol, washed with ddH_2O and blocked with 5 % skimmed milk in TTBS (20 mM Tris, 1.37 mM NaCl, 0.1 % Tween-20) for 1-2 hours at RT, shaking. The membrane was then incubated with the primary antibody in TTBS-milk for 1 hour at room temperature or overnight at 4°C. After three washing steps for 10 minutes in TTBS, the membrane was incubated with the secondary antibody in TTBS-milk for 1 hour at RT, shaking. Another 3 washing steps of 10 minutes in TTBS preceded the ECL detection. The membrane was incubated with the ECL reagent (GE Healthcare) for 3-5 minutes, wrapped in saran wrap and scanned with the Storm scanner or exposed to film for 30 seconds and developed.

Primary antibodies were: Dlc1 (1:500, Rabbit, Santa Cruz Biotechnology); Actin (1:1000, Rabbit, Sigma Aldrich); $p21^{Waf1/Cip1}$ (1:500, Mouse, Dako); GAPDH (1:1000, Rabbit, Santa Cruz Biotechnolgy), HisG (1:500, Goat, Invitrogen). Secondary antibodies were anti-mouse anti-rabbit (Santa Cruz Biotechnology) and anti-goat (Upstate), which were diluted to 1:2000.

Chapter 3: Results

As mentioned in the introduction, my studies were aimed at investigating the cooperation of Kras and Dlc1 genes in tumor development. I based my hypothesis on literature reports that in Ras induced tumorigenesis increases Rho levels that are able to overcome the $p21^{Waf1/Cip1}$ induced growth arrest. Since Rho activity is controlled in part by Dlc1, I hypothesized that Kras and Dlc1 cooperate in tumor development.

3.1 Expression of Dlc1 and $p21^{Waf1/Cip1}$

3.1.1 Dlc1 expression in normal tissues

To first establish a baseline for the Dlc1 expression, in a previous study I assessed the expression profile of Dlc1 is in normal tissues Figure 3.1 (*Sabbir et al. 2010*). Samples were taken from different organs of wild type mice (brain, thymus, lung, heart, liver, kidney, spleen, testis, and placenta) and whole cell lysates were prepared. Approximately 30 µg of protein was separated by SDS-PAGE (12 % polyacrylamide) and western blot analysis was performed as described in Materials & Methods.

Figure 3.1 shows the Dlc1 expression in the different tissues. The upper panel of the figure shows the Dlc1 expression as determined with the Dlc1 antibody sc-32931 (Santa Cruz). The lower band is the Dlc1 isoform 2 with a size of 123 kDa (*Sabbir et al. 2010*). The upper band may be the Dlc1 isoform 3 with a size of 127 kDa. However, this is still undergoing further analysis through mass spectrometry (*Sabbir et al. 2012*).

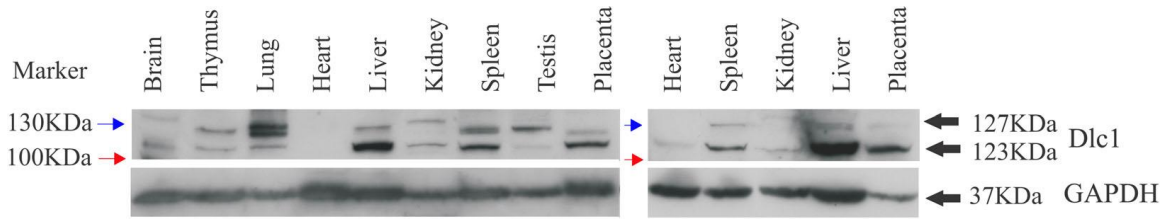

Figure 3.1: Dlc1 expression in normal tissues

Whole cell lysates were prepared from various tissues of wild type mice and analyzed by western blot. The upper panel shows that Dlc1 is differentially expressed in many tissues. The lower panel shows GAPDH expression as internal control and indicates equal. The multiple bands for Dlc1 may represent different splice variants.

This figure reproduced from „Sabbir, M. G., Wigle, N., Loewen, S., Gu, Y., Buse, C., Hicks, G. G., and Mowat, M. R. (2010) Identification and characterization of Dlc1 isoforms in the mouse and study of the biological function of a single gene trapped isoform, BMC Biol 8, 17." with permission of the original publisher, BioMed Central.

The lower panel shows GAPDH expression as accounts for differential loading between lanes. One can see that Dlc1 is expressed in all tissues tested but with varying intensities in the different isoforms. In the lung for example the expression of isoform 2 is lower than expression of isoform 3.

3.1.2 Dlc1 and p21$^{Waf1/Cip1}$ expression in cell lines

My work was based on the hypothesis that Kras and Dlc1 may cooperate in tumor development through the Rho signalling pathway. We believe that Rho is likely downregulating the cell cycle inhibitor p21$^{Waf1/Cip1}$ that has increased expression due to Ras transformation. To establish a correlation between Dlc1 and p21$^{Waf1/Cip1}$ expression, I previously performed western blot analysis on mouse embryonic fibroblast with different Dlc1 gene trapped status Figure 3.2 (*Sabbir et al. 2010*). Figure 3.2 shows the expression of Dlc1 as well as p21$^{Waf1/Cip1}$ in separate blots and as duplicates. Blotting with β-actin served as a loading control and confirmed equal loading of protein. In the upper panel one can see that Dlc1 expression in homozygous Dlc1$^{gt/gt}$ cell lines is greatly reduced in comparison to the wild type (Dlc1$^{+/+}$). Similarly in the lower panel it is shown that p21$^{Waf1/Cip1}$ expression is also reduced in the Dlc1$^{gt/gt}$ cell lines compared to the wild type and heterozygous Dlc1 gene trapped lines. Densitometry indicated, that this downregulation is statistically significant (*Sabbir et al. 2010*). Two distinct Dlc1 bands are seen and likely represent isoforms 2 (lower) and 3 (upper band), respectively.

These results are support our suggestion that downregulation of Dlc1 is coupled with the downregulation of p21$^{Waf1/Cip1}$ expression through the Rho signalling pathway.

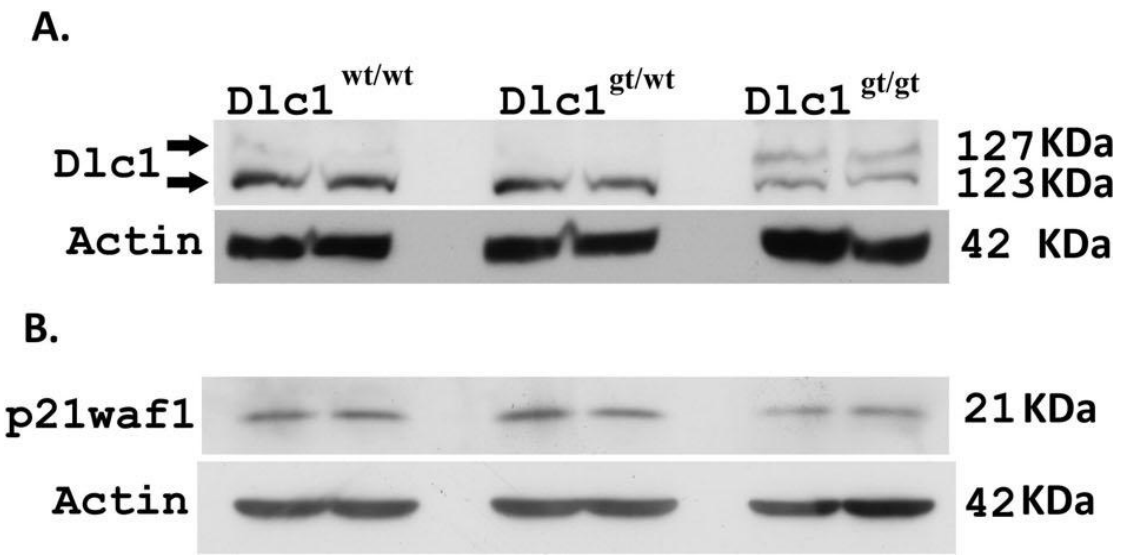

Figure 3.2: Dlc1 and p21$^{Waf1/Cip1}$ expression in cell lines

Western blots analysing Dlc1 and p21$^{Waf1/Cip1}$ expression in in Dlc1$^{wt/wt}$, Dlc1$^{wt/gt}$, and Dlc1$^{gt/gt}$ mouse embryonic fibroblasts. Samples were loaded as duplicates. A) shows the expression of Dlc1 cell lines where the upper panel indicates that levels of Dlc1 are reduced in the homozygous gene trapped cells in comparison to wild type and heterozygous gene trapped cell ines. B) shows the expression of p21$^{Waf1/Cip1}$ and the upper panel indicates similarly reduced p21$^{Waf1/Cip1}$ levels in the homozygous gene trapped cells. In both panels the actin-bands serve as loading control and indicate equal loading.

This figure reproduced from „Sabbir, M. G., Wigle, N., Loewen, S., Gu, Y., Buse, C., Hicks, G. G., and Mowat, M. R. (2010) Identification and characterization of Dlc1 isoforms in the mouse and study of the biological function of a single gene trapped isoform, BMC Biol 8, 17." with permission of the original publisher, BioMed Central.

3.2 Protein production HNC

3.2.1 Integrity of the plasmid and the protein

The HNC plasmid was transformed into E. coli BL21 cells for amplification. The integrity of the plasmid as well as the transformed bacteria was then confirmed through miniprep experiments followed by restriction digestions (data not shown). Digestion with EcoRV and PvuII resulted in the expected production of two and three specific fragments, respectively, confirming the composition of the plasmid.

After confirming the integrity of the plasmid, HNC protein was produced at a large scale. Bacterial cultures were treated with IPTG to induce protein production through the LacOperon. After cell lysis the protein was purified by nickel affinity chromatography. Preliminary western blot experiments performed on the purified HNC protein indicated that the concentration of the HNC protein was too low to be detected data not shown). Therefore the total volume of the HNC solution was reduced from 25 ml after purification to around 1 ml through concentration columns. Samples of each wash-flow-through during purification were kept and analyzed together with the final protein through western blot analysis. As can be seen in Figure 3.3 the purification of the HNC protein was very clean. The size of the protein correlates with the predicted size of 42 kDa and cannot be found in any other flow-through than the original input, which supports the integrity of the purification process.

3.2.2 *In vitro* testing of HNC protein on MEFs

The last test before moving on to live animals was testing the protein *in vitro* on MEFs containing the oncogenic Kras allele.

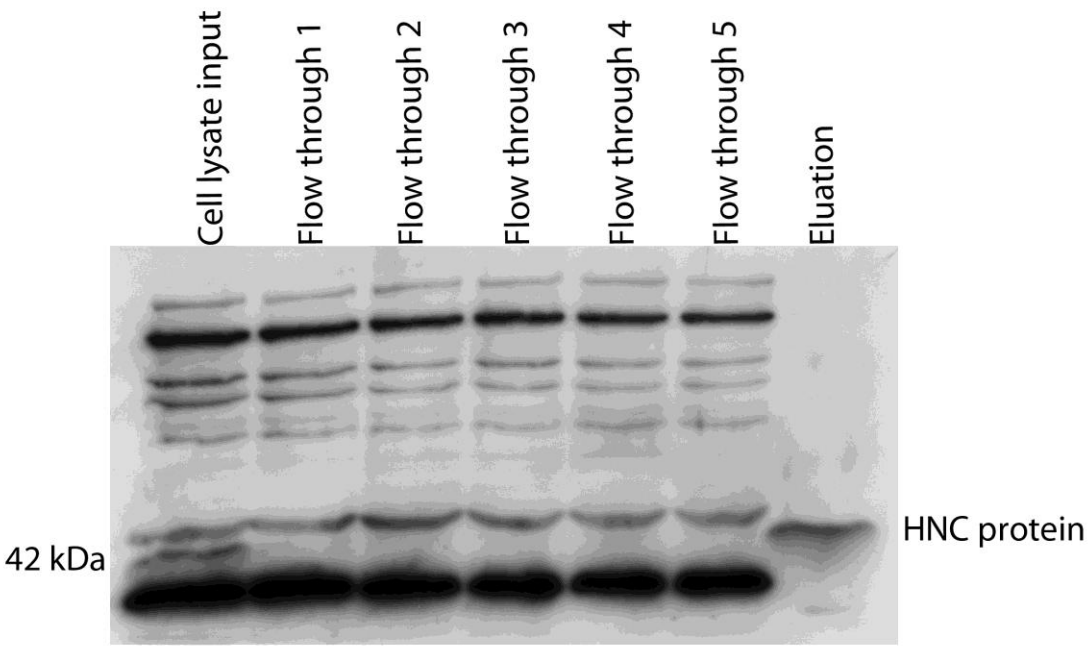

Figure 3.3: Integrity of the HNC protein

Cell lysates of E.coli expressing the HNC protein were purified through nickel affinity chromatograpy. At each step in the process samples were taken and subjected to western blot analysis with an anti-His_6 antibody, together with the cell lysate input and the eluatant. The band at 42 kDa confirms the correct expression whereas the lack of additional bands confirms the proper purification of the protein.

MEFs were treated with HNC protein and harvested after different passages and time points. Kras activation was assessed by RT-PCR followed by HindIII digestion as described above. In addition to the oncogenic point mutation the $Kras^{G12D}$ allele also contains a silent mutation introducing a HindIII restriction site. Digestion of the PCR product therefore results in cutting of the mutant allele but not the wild type allele. This can then be visualized by two distinct bands on an agarose gel.

Figure 3.4 shows the Kras activation *in vitro* at different time points. Again the upper band indicates the wild type band, whereas the lower band indicates the mutant. One can see that 5 days after the incubation with the HNC protein there is no visible Kras activation. Allowing the cells to grow for an additional week resulted in approximately 25 % activation. However, there is no difference in activation between the 12 days and 15 days samples, suggesting that maximum activation levels were reached by Day 12.

The last lane shows a tumor control sample. This thymic tumor was obtained through tail vein injection of Adeno-Cre. It shows almost the same band intensity for the wild type and the mutant band. Because the conditional Kras allele is heterozygous two equally intense bands would correspond to 100 % activation of the mutant allele.

3.3 IP injections of HNC

The clean, concentrated and tested HNC protein was then injected intraperitoneally into 10-15 days old mice. Young mice were selected to allow for higher cell turn over and therefore more chance for secondary events to occur for tumor formation. On three consecutive days the mice were injected with 25 µg HNC per gram bodyweight. Weekly weighing and observation of their appearance were used as indicators of health or sickness. Because of the young age of those mice the genotype was

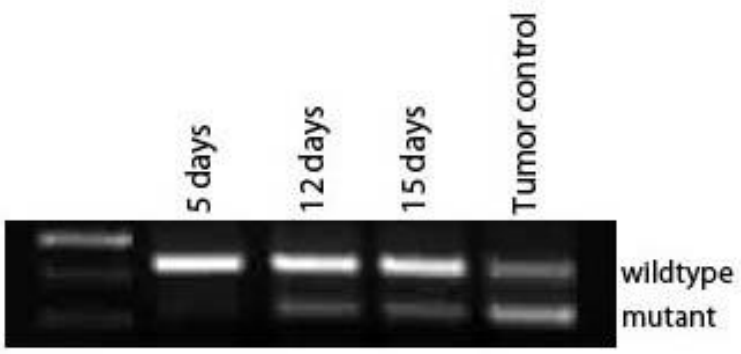

Figure 3.4: Kras activation *in vitro*

Heterozygous LSL-Kras^{G12D} embryonic fibroblasts were incubated with cell permeant Cre protein (HNC) for 24 hours, harvested at different time points and analysed by RT-PCR. The amplified fragments were digested with HindIII, which only cuts the mutant allele, but not the wild type, resulting in a two band pattern.The upper band represents the uncut wild type Kras allele expression, while the lower two bands shows the digested oncogenic Kras allele. It can be seen that 5 days after the incubation with the HNC protein there is no visible Kras activation. Allowing the cells to grow for an additional week resulted in acceptable activation. However, there is no difference in activation between the 12 days and 15 days samples. This is probably due to the fact that the time points were too close together for additional activation to show. Further cell growth might show different results. The last lane shows a tumor control sample. This thymic tumor was obtained through tail vein injection of Adeno-Cre. It shows almost the same band intensity for the wild type and the mutant band. Because the conditional Kras allele is heterozygous two equally intense bands would correspond to 100 % activation of the mutant allele.

unknown at the time of injection and therefore the whole litter had to be treated. For further studies only the KD and K+ mice were considered.

3.3.1 Development of abdominal tumors

Throughout the course of this experiment 17 K+ mice and 7 KD mice were injected. Additionally 2 wild type mice were examined as age control without being injected. Out of the 24 mice injected and taken for examination only 2 showed excisable tumors that could be used for further analysis. Both were 14 months old and became sick approximately 13 months after injection. Mouse #082-0 (K+) had a tumor wrapped around the upper intestines and mouse #097-0 (K+) had tumor nodules all through the intraperitoneal cavity. Both tumors seemed to arise from the surrounding tissue rather than from a specific organ. Figure 3.5 shows the tumors in these two mice after H&E staining at different magnification (macroscopic, 4x, 20x). Upon histological examination both tumors showed spindle shaped cells (arrows in Figure 3.5), which suggests that they are either spindle cell carcinomas or sarcomas. However, to confirm the exact nature of the tumors further immunostaining is necessary.

Of the 24 mice injected with the Cre protein 15 animals presented with tumor in liver, kidney or lung or in a combination of two organs. Liver tumors were found in 5 animals (3 K+, 2 KD), kidney tumors were found in 7 animals (4 K+, 3 KD) and lung tumors presented in 7 animals (4 K+, 3 KD). However, those lesions were too small to be excised and could therefore not be used for further analysis. Determined by the shape and growth pattern, these lesions were likely adenocarcinomas, although in different stages of differentiation (Figure 3.6). Tumors in the lung present as well differentiated adenocarcinoma, with the typical glandular structure (A) whereas lesions in the liver are

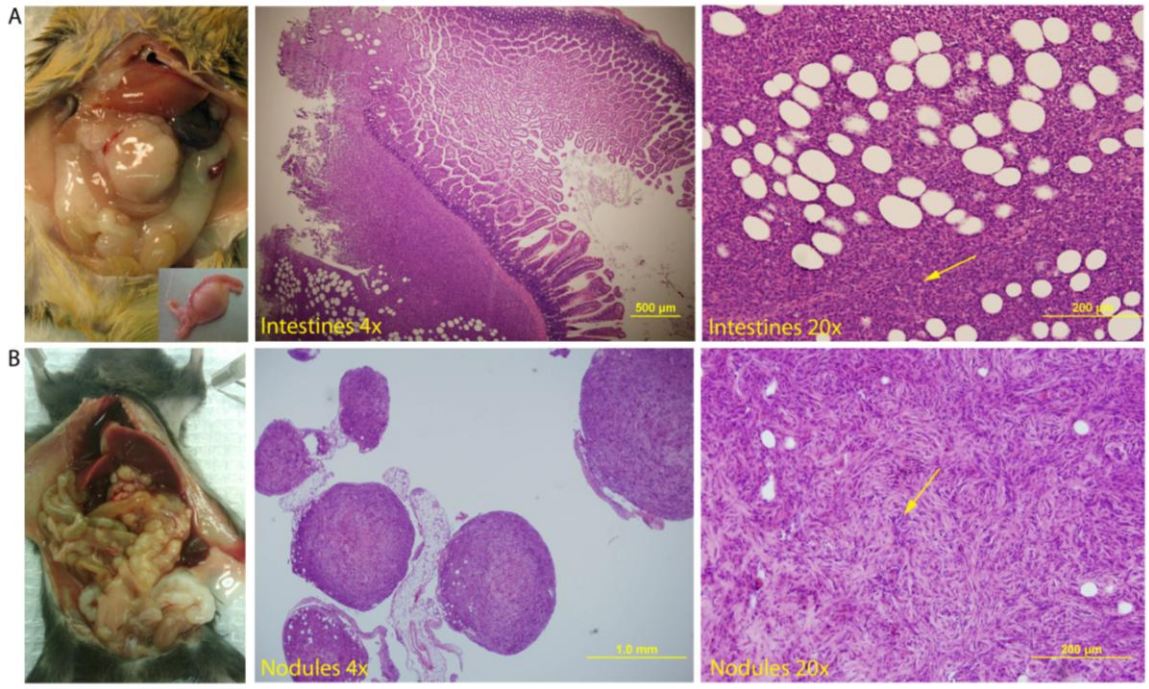

Figure 3.5: Abdominal tumors following IP injection of HNC protein

IP injection of HNC protein only resulted in excisable tumors in two animals of the cohort. Both mice were K+ and exhibited tumors in the abdominal cavity, that seemed to arise from the sourrounding tissue rather than a specific organ. The arrows indicate the spindle shaped cells. A) shows the macroscopic and H & E stained sections (4x and 20x) of the tumor nodules found throughout the whole cavity of the mouse #097-0. B) shows the tumor of the upper intestines of #082-0, again in the macroscopic and microscopic (4x, 20x) view.

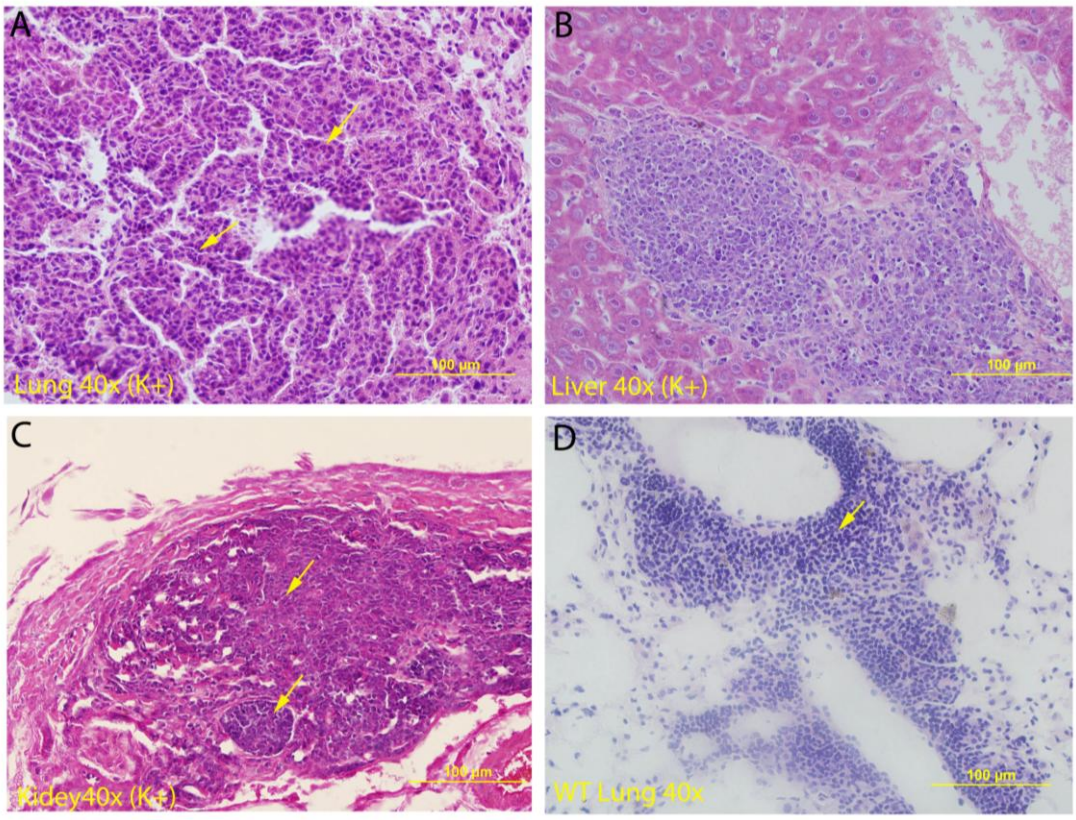

Figure 3.6: Tumors in IP injected mice

Most of the injected mice also showed lesions in liver, kidney and lung when histologically examined. Determined by the shape and growth pattern these lesions were adenocarcinomas, although in different stages of differentiation. Tumors in the lung (A) present as well differentiated adenocarcinoma, with the typical glandular structure indicated by the arrows, whereas lesions in the liver (B) are poorly differentiated. Lesions in the kidney (C) show signs of more poorly differentiation (upper arrow) and higher differentiation (lower arrow). In contrast in the wild type control (here lung, D) only aggregations of lymphocytes (arrow) indicative of inflammation were found.

poorly differentiated (B) and lesions in the kidney show signs of both (C). In contrast only inflammatory lesion were found in the wild type control (here lung) (D).

3.3.2 Test IP injections in 126 mice

Dr. Ruley's group had initially tested their Cre protein on ROSA26 mice and shown that the Cre protein is able to activate the β-galactosidase expression throughout the whole animal within three days (*Jo et al. 2001*). To investigate why our injections didn't result in more tumors and to determine the ability of our HNC to activate Kras, we repeated the experiment. Two K+ mice were injected with the HNC protein intraperitoneally in the same fashion as the regular test animals. After three days the mice were sacrificed and analysed for Kras activation with RT-PCR and HindIII digestion. As Figure 3.7 shows, the Kras allele is activated in almost all tissues after those three days, but mainly in organs of the intraperitoneal cavity, such as uterus and kidney.

3.4 Intranasal injections & metastases

Since it took so long for the tumors to develop after IP injections of HNC protein and there were not enough samples to compare in further studies. a new approach was taken.

This time the mutant $Kras^{G12D}$ allele was activated through intranasal injection of a Cre recombinase expressing adenovirus (Adeno-Cre). The virus was delivered as a calcium phosphate precipitate to increase the rate of infection and allow for the development of adenocarcinomas in the lung after relatively short time (*Fasbender et al. 1998, Jackson et al. 2001*). Different concentrations of virus were tested to allow for

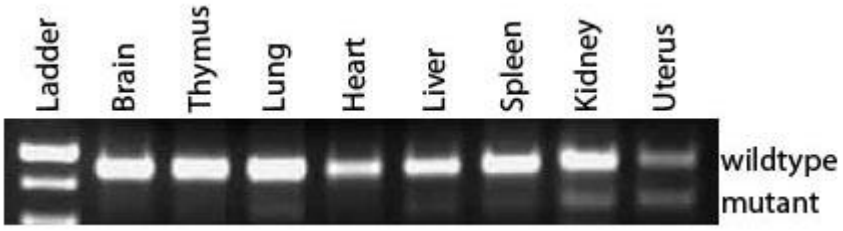

Figure 3.7: Kras activation after three days

Two mice were injected with the HNC protein following the regular protocol, then sacrificed after three days to assess Kras activation to confirm that the protocol is working. RT-PCR was followed by HindIII digestion to show the activation of the $Kras^{G12D}$ allele. The agarose gel shows high activation in the uterus and the kidney, but also lower activation in all organs of the abdominal cavity, such as the liver and the spleen.

tumor growth and metastasis development without killing the mouse through the primary disease.

In a pilot study 4 mice (all K+) were injected with 5x 10^8 PFU when they were 3 months old. Due to the high dose of the virus they became sick very quickly and had to be sacrificed after 2 months. Histological analysis of the lungs revealed a multitude of lung adenocarcinomas. There were no metastases observed, which is most likely due to the quick demise of the animals (data not shown).

Subsequent injections were therefore done with 5x 10^7 PFU when the mice were 2 months old. At 7 months after injection of the Adeno-Cre precipitate, 12 mice were sacrificed and dissected (6 KD and 6 K+). Three non-injected wild type mice were taken as age control. Additionally, 2 wild type mice were also injected with Adeno-Cre precipitate to control for adverse effects of the virus. Histological analysis of all tissues did not reveal any adverse effects of the injection.

Samples of all organs were taken for histological, DNA and RNA analysis.

Upon histological analysis the first four mice of the cohort (#108-2 to #114-2, equalling two K+ and two KD mice) were excluded from further studies, because their tumor burden in the lungs was very small to non-existent and would therefore offset any calculations based on tumor burden.

Figure 3.8 shows histological images of the lung tumors in mice injected IN with Adeno-Cre precipitate. The upper row shows a 4x magnification (A+B) whereas the lower row shows 20x (C) and 40x magnification (D) of the adenocarcinomas. The highly differentiated structure of the tumors, characterized by the glandular pattern, which can be seen in C and D, was used for further studies to identify the tumor lesions. Although

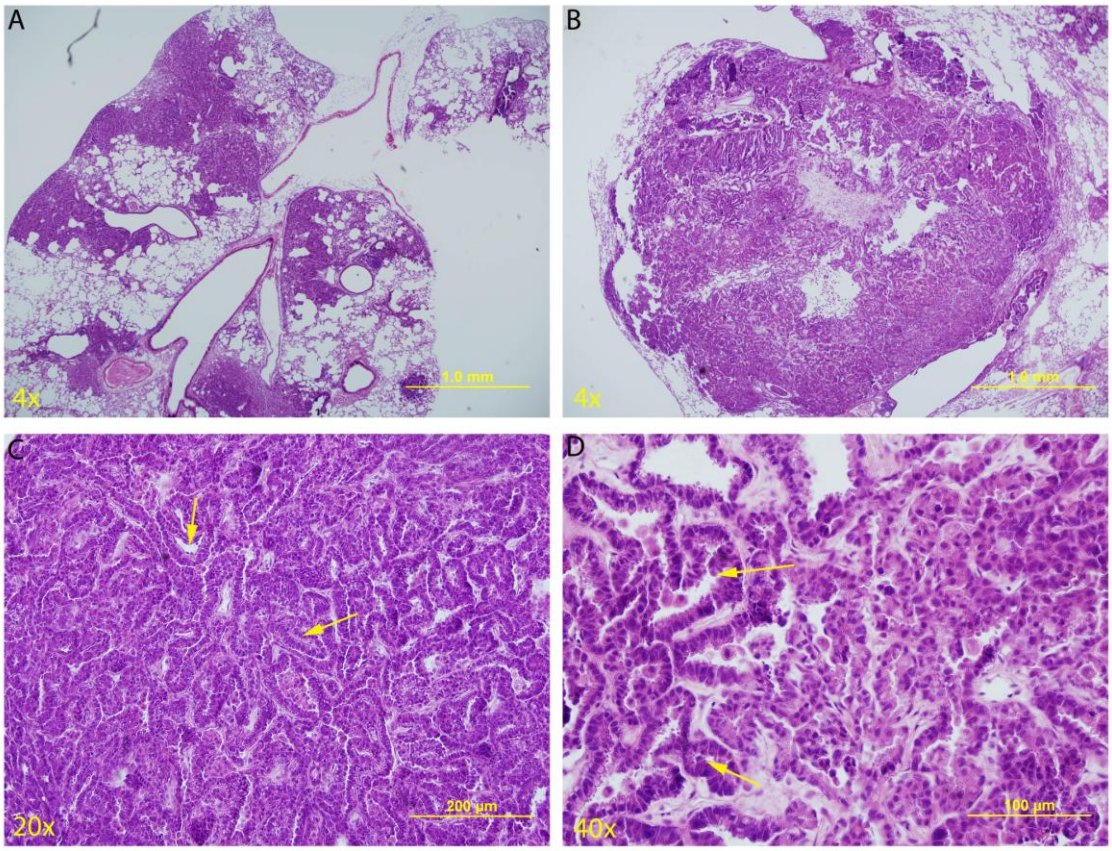

Figure 3.8: Histology of lung tumors following IN injection of Adeno-Cre

The upper row shows a 4x magnification (A+B) whereas the lower row shows 20x (C) and 40x magnification (D) of the adenocarcinomas. The highly differentiated glandular structure of the tumors, indicated in C and D by the arrows, was used in further studies to identify the tumor lesions. Although the bigger tumors exhibited a rounder and more compact shape (B) the smaller lesions showed a more invasive phenotype (A). Together with the cell shape aberrations, such as increased size of nucleus and membrane irregularities, and metastasis development these are characteristics of malignant tumors.

the bigger tumors exhibited a rounder and more compact shape (B) the smaller lesions showed a more invasive phenotype (A). Together with the cell shape aberrations, such as increased size of nucleus and membrane irregularities, and metastasis development these are characteristics of malignant tumors (*Baba & Catoi 2007*).

All organs of injected animals were histologically analyzed for metastases, including the mediastinal lymph nodes. Examination revealed abnormal growth in the liver (A), kidney (B) and lymph nodes (E) of animals with lung tumors (Figure 3.9). Compared to the mostly well differentiated adenocarcinomas in the lung, these lesions were more poorly differentiated. They did not exhibit the glandular structure observed in the lung, but they still showed abnormal nuclei, membrane irregularities and dense cell growth. The similarity in tumor type suggests that they were likely metastases from the lung cancer. Surprisingly similar lesions could be found in the non-injected wild type control animals. This suggests that the mice used in this study were prone to spontaneous tumor development. The injected wild type controls however only showed an increase in lymphocyte aggregation (D) but no adenocarcinoma, as determined by the smaller, more regular and rounder shape of the cells. And while this shows that four wild type control mice are not enough to normalize for spontaneous tumor development, the normal tissues from injected controls as well as the fact that especially liver tumors do rarely develop spontaneously suggests, that the lesions we found in multiple organs in mice with lung cancer are indeed metastases. To make a conclusive statement about the status of metastases however immunohistochemical staining with lung cancer specific makers needs to be done. Counting of the total number of metastases in each animal, followed by statistical analysis did reveal no significant difference between KD and K+ mice (F).

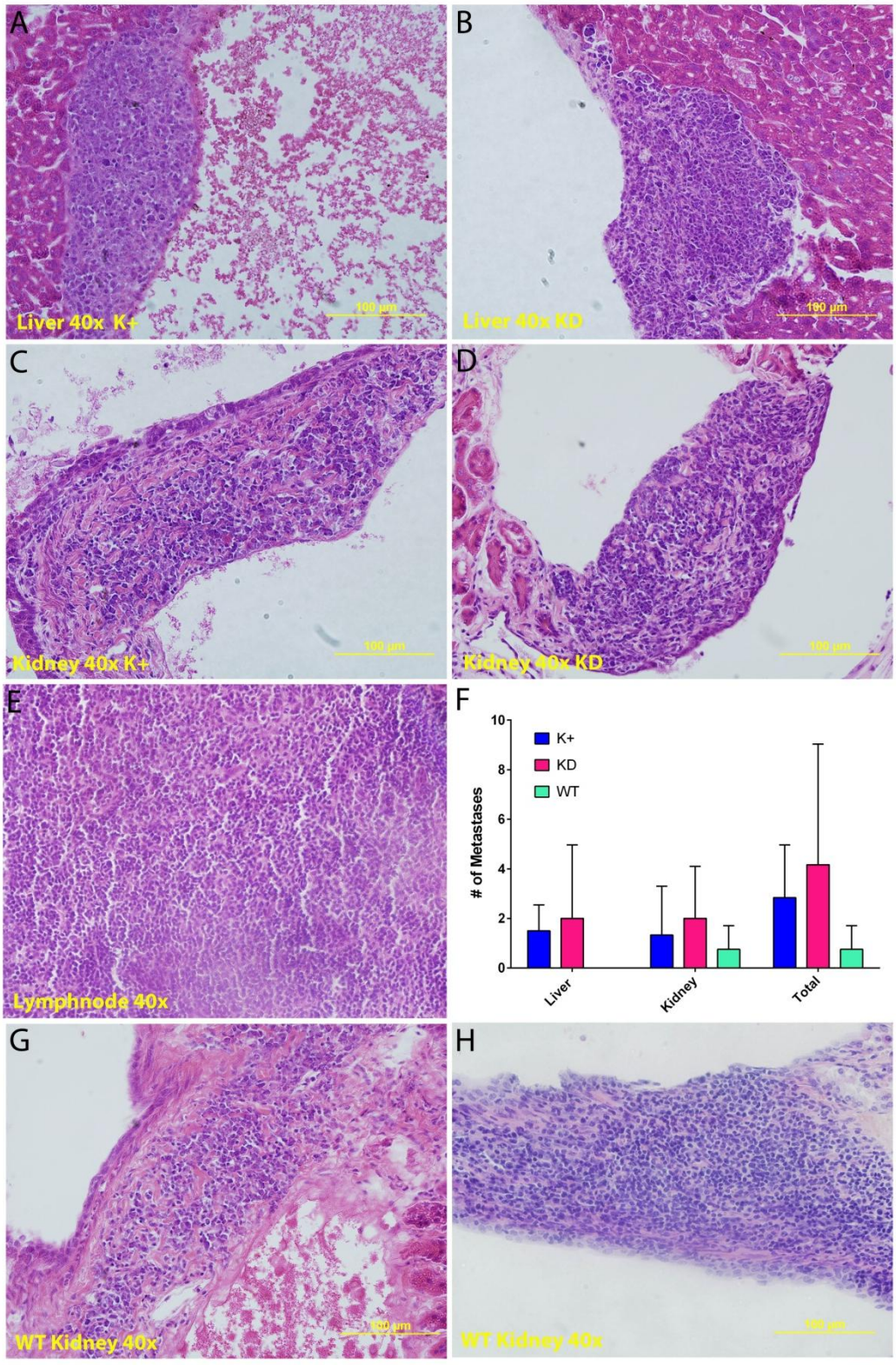

Figure 3.9: Metastases in IN injected mice

Histological analysis revealed abnormal growth in the liver (A), kidney (B) and lymph nodes (E). Compared to the mostly well differentiated adenocarcinomas in the lung, these lesions were more poorly differentiated. Similar lesions could be found in the non-injected wild type control animals (kidney, C) but not the injected wild type controls. The injected wild type controls only showed an increase in lymphocyte aggregation (kidney, D). Panel F shows the mean number of metastases in liver, kidney and total with the standard deviation as error bars (n=6).

3.5 $Kras^{G12D}$ activation

3.5.1 Determination of Kras activation by RT-PCR

To confirm the activation of the conditional $Kras^{G12D}$ allele, RT-PCR was performed. In Figure 3.10 it can be seen that Kras activation is almost exclusively found in the organs in which the tumors developed. This is true for the IP injections with the HNC peptide (A) as well as for the IN injections using Adeno-Cre (B).

Panel C) shows that Kras is activated in the lungs of mice that were injected with $5x\ 10^7$ PFU. No mutant band is seen in the first four mice, a finding that is consistent with the very low to almost non-existent tumor burden in these animals (see paragraph 3.4 of this chapter). The RNA samples were taken from the whole lung. Since the first four tumors had a very low to almost non-existent tumor burden, the normal tissue is predominant, thus we don't readily see a mutant band. In all other samples the amount of tumor was still enough to be detected. All figures also show that Kras is activated, although not completely. Visual determination suggests that the lower band (mutant) is approximately one fourth as intense as the upper (wild type) band. Considering the heterozygosity and the fact that equal band intensity would indicate 100% activation, this would equal a 25 % activation in my samples. Quantification of the bands with ImageJ results in Kras activation rates between 40 % and 80 %.

3.5.2 Determination of Kras activation by pyrosequencing

In order to more sensitively quantitate the amount of Kras activation Pyrosequencing was performed.

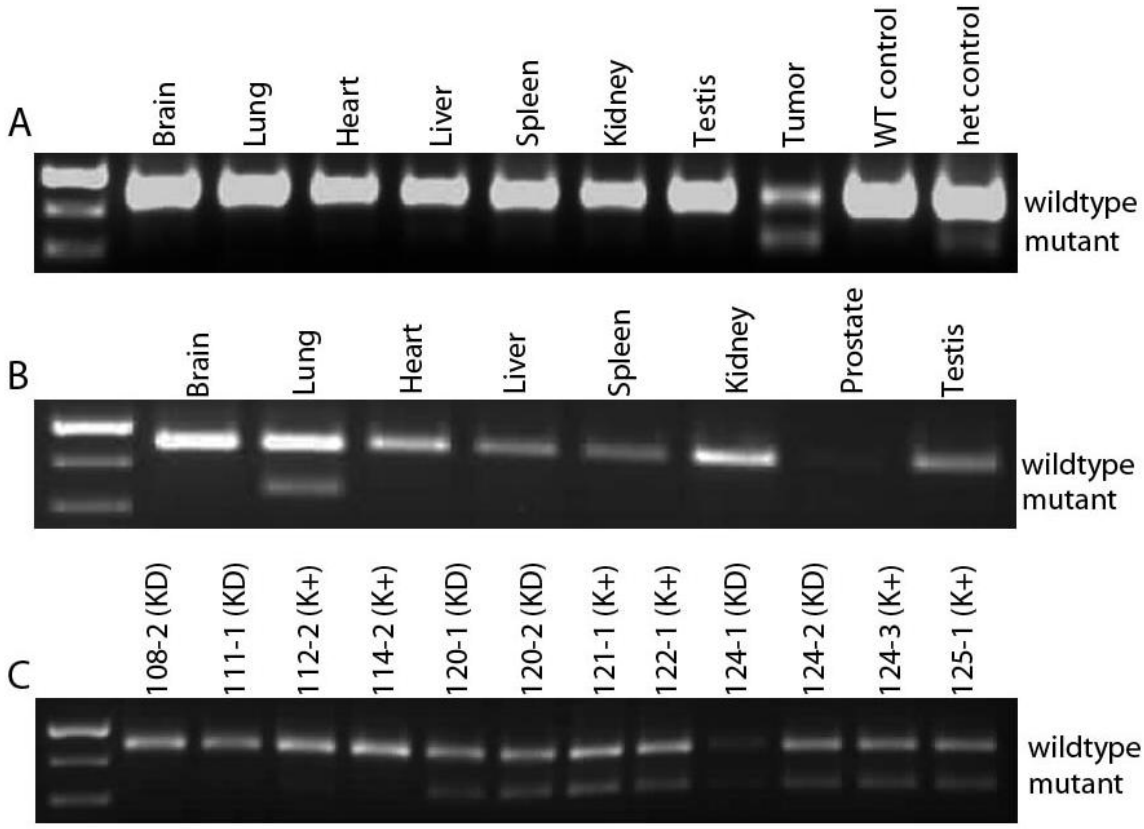

Figure 3.10: Kras^{G12D} activation in abdominal and lung tumors

This figure shows the Kras^{G12D} activation by RT-PCR. Panel (A) shows activation of Kras in various organs of a mouse injected intraperetoneally (IP) with the HNC protein. Panel (B) shows activation in various organs of a mouse injected intranasally (IN) with Adeno-Cre precipitate in the pilot study. Panel (C) compares the Kras activation in whole lungs from the IN injected mice in the final cohort. The first 4 mice of this cohort were excluded from further analysis, due to their low amount of tumor and therefore extensive predomination of the normal tissue.

Pyrosequencing can be used for mutation analysis or determination of the methylation status of any given sequence. In principle the single stranded DNA is immobilized on streptavidin-sepharose beads through a biotin residue that was added to one of the PCR primers. During the sequencing step, the nucleotides are then dispensed into the reaction according to the pre-determined order of the sequence itself. Each time a nucleotide is incorporated the liberated Phosphate stimulates luciferase to emit light, which can then be measured by intensity. All the non-incorporated nucleotides are then degraded by Apyrase. At the end the user obtains a pyrogram, which is essentially a plot of the light emission over time. From the ratio in intensity (peak heights) between the non-mutated peak and the mutated peak can then be used to determine the percentage of mutation in the whole sample.

Figure 3.11 shows a representative result. Panel A) shows the histogram and dispensation order of the nucleotides. The yellow bars indicate the mutation sites. The height of the red bars in the histogram indicates the amount of bases to be incorporated. Panel B) shows the actual pyrogram, with the mutation sites again highlighted in yellow. The computer calculated the heights for each peak, which can then be used to determine the percentage of mutation. Calculating the ratio of the two peaks at each mutation site indicates a Kras activation of 20 %. This is similar with the visual estimation from the previous paragraph.

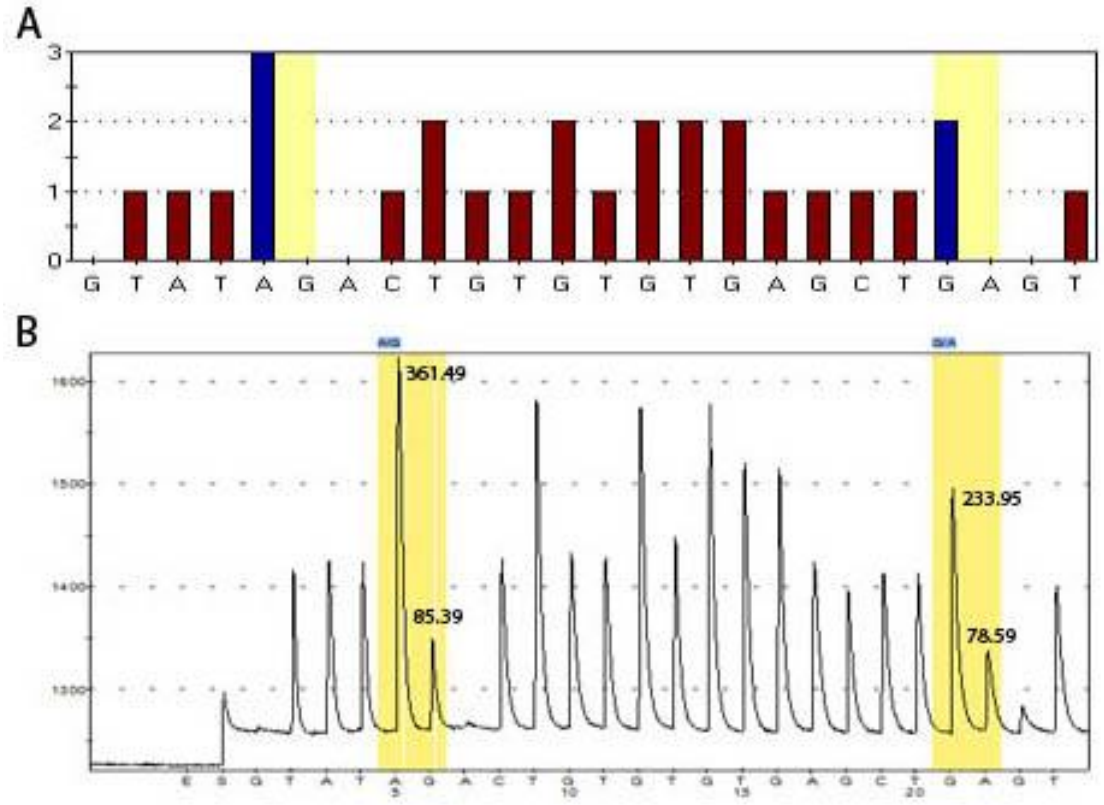

Figure 3.11: Kras activation lung tumors – Pyrosequencing

Panel A) shows the histogram and dispensation order of the nucleotides. The yellow bars indicate the mutation sites. The height of the red bars in the histogram indicates the amount of bases to be incorporated. Panel B) shows the actual pyrogram, with the mutation sites again highlighted in yellow. The computer calculated the heights for each peak, which can then be used to determine the percentage of mutation. Calculating the ratio of the peaks heights of the two possible peaks at each mutation site indicates a Kras activation of 20 %.

3.6 Dlc1 expression and methylation pattern in tumors

3.6.1 Dlc1 Antibody validation

Initially the Dlc1 expression was to be determined through immunohistochemistry experiments. Before using the Dlc1 antibodies however, their integrity needed to be validated. To validate the antibodies immunohistochemistry and immunofluorescence experiments were performed. However, the antibody validation of the two antibodies tested did not show any conclusive staining when compared on Dlc1 expressing and non-expressing cells.

These cell lines were derived from mouse breast cancer tissue and have been shown to be either expressing Dlc1 at a high level or at a very low level by western blot analysis (data not shown).

Figure 3.12 shows the antibody validation experiment by immunohistochemistry. Two antibodies from Santa Cruz and BioSource (please refer to Chapter 3) were tested at two different dilutions (1:50 and 1:400). It can be seen that there is no difference in the staining pattern for Dlc1 expressing and non-expressing cells.

Figure 3.13 shows the antibody validation experiment by immunofluorescence. The same two antibodies were used on the same cells at different concentrations. Again there is no difference in the staining pattern for Dlc1 expressing or non-expressing cells. Therefore the method of Dlc1 detection was changed to a PCR based approach.

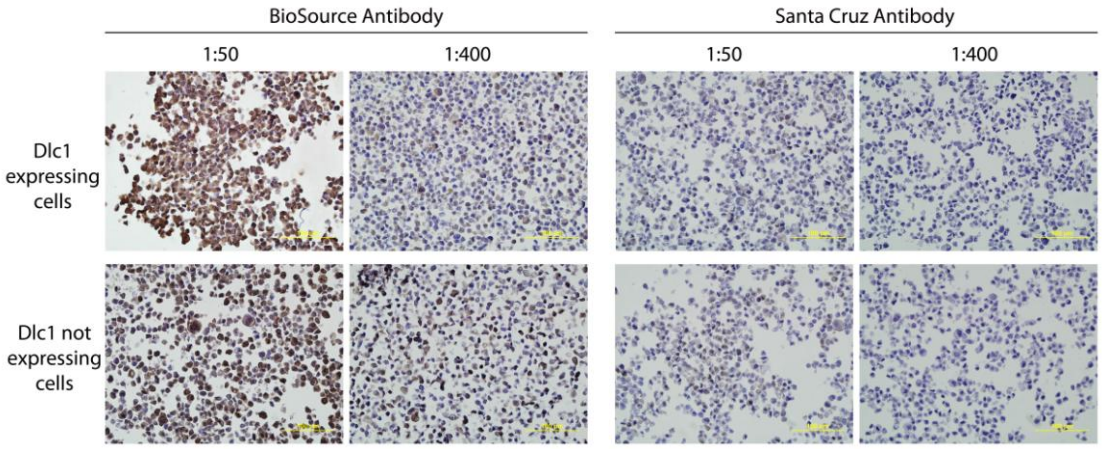

Figure 3.12: Dlc1 antibody validation – Immunohistochemistry

Two different antibodies (Santa Cruz and BioSource) were tested at two different concentrations (1:50 and 1:400) on breast cancer cells either expressing Dlc1 or not expressing it. Pictures shown above were taken at a magnification of 20x and show no observable difference in the staining pattern between the Dlc1 expressing and not expressing cells.

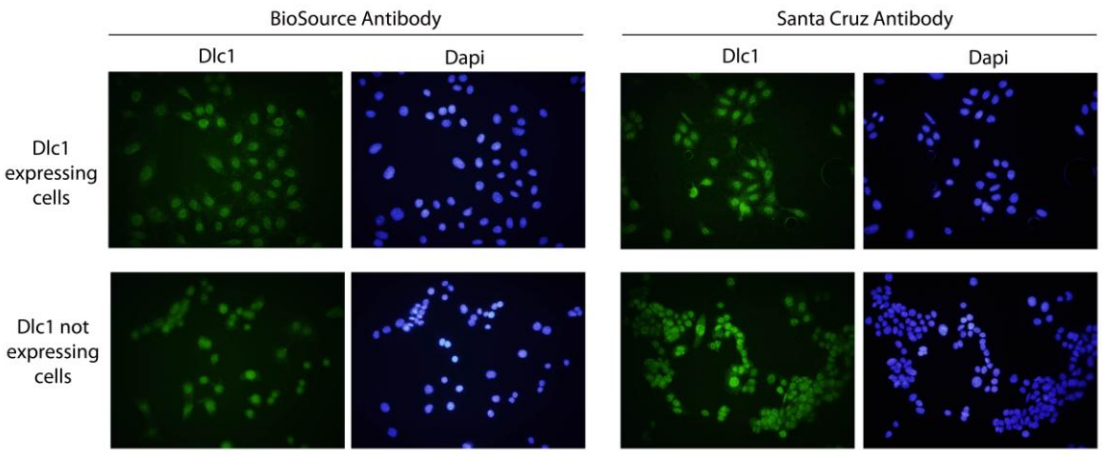

Figure 3.13: Dlc1 antibody validation – Immunofluorescence

The two different antibodies were also tested in immunofluorescence experiments. Again they were used at different concentrations on the breast cancer cells either expressing Dlc1 or not expressing it. Pictures shown above were taken at a magnification of 20x. They show no observable difference in staining pattern between the Dlc1 expressing and not expressing cells and are representative for all experiments done.

3.6.2 Dlc1 Isoform PCR

Since both antibodies were not suitable to detect Dcl1 expression, an RT-PCR based approach was taken. Primers specific for isoform 2 and isoform 3 were used to amplify the Dlc1 cDNA. GAPDH was amplified as control.

Figure 3.14 shows representative results of these reactions. The first four samples (#121-1 to #124-3) are whole lung samples from intranasally injected mice. These mice (and samples) were also used in other experiments throughout this thesis. Samples #149-0 to #150-2 are micro dissected lung tumors also from intranasally injected mice, but outside the main cohort. #082-0 and #097-0 are abdominal tumors from intraperitoneal injections and the last sample is whole wild type lung. It can be seen, that GAPDH is expressed evenly in all samples, confirming the quality of the cDNA (C). The isoforms 2 (A) and 3 (B) are expressed in all the lung tissues, but expression is reduced in the abdominal tumors. The moon shaped smear at the bottom of the gels indicates primer dimers, as suggested by the size.

For quantification, experiments were done in triplicate and the band intensities of the GAPDH gels as well as the isoform gels were then used to calculate the expression of the isoforms relative to the GAPDH expression (Figure 3.15). There is no statistical significant difference in expression of isoform 2 in the lung tumors compared to the wild type lung. In the abdominal tumors however, expression is significantly lower. Expression of isoform 3 is reduced in the abdominal tumors as well as in one of the microdissected lung tumors. However, we could not perform statistical analysis, because we only completed one experiment with isoform 3.

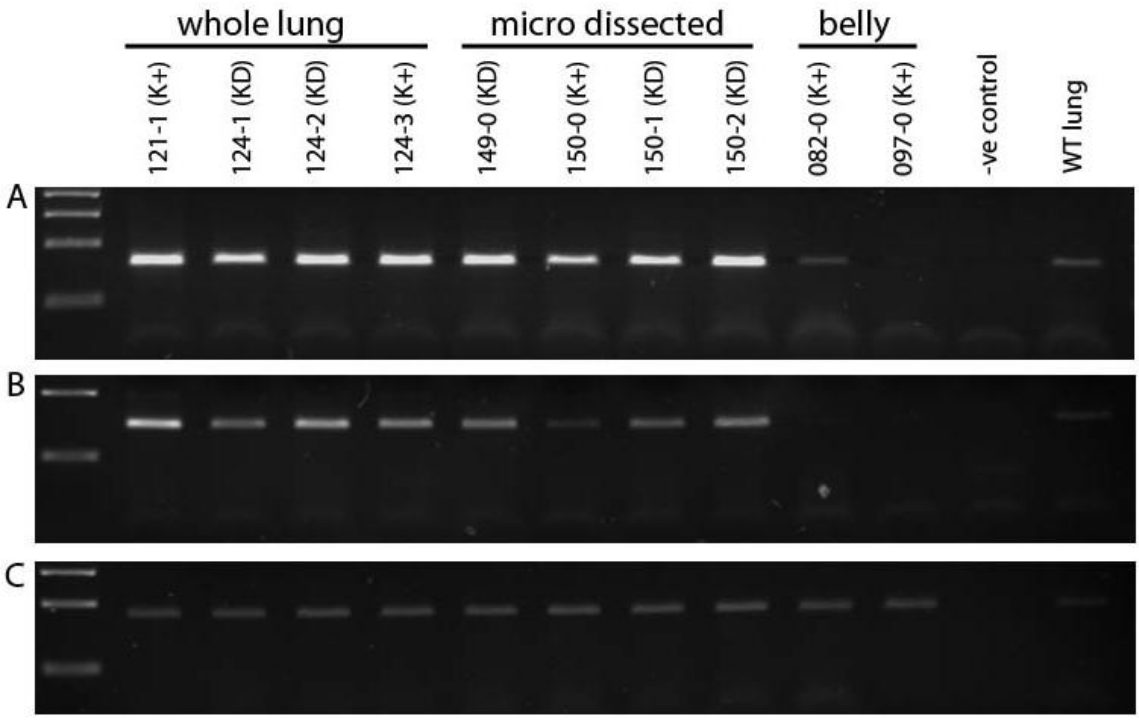

Figure 3.14: Dlc1 Isoform RT-PCR

Isoform specific RT-PCR using primers specific for isoform 2 (A), isoform 3(B) and GAPDH (C). The first four samples (#121-1 to #124-3) are whole lung samples from IN injected mice. Samples #149-0 to #150-2 are micro dissected lung tumors also from IN injected mice, but outside the main cohort. #082-0 and #097-0 are abdominal tumors and the last sample is whole wild type lung as control.

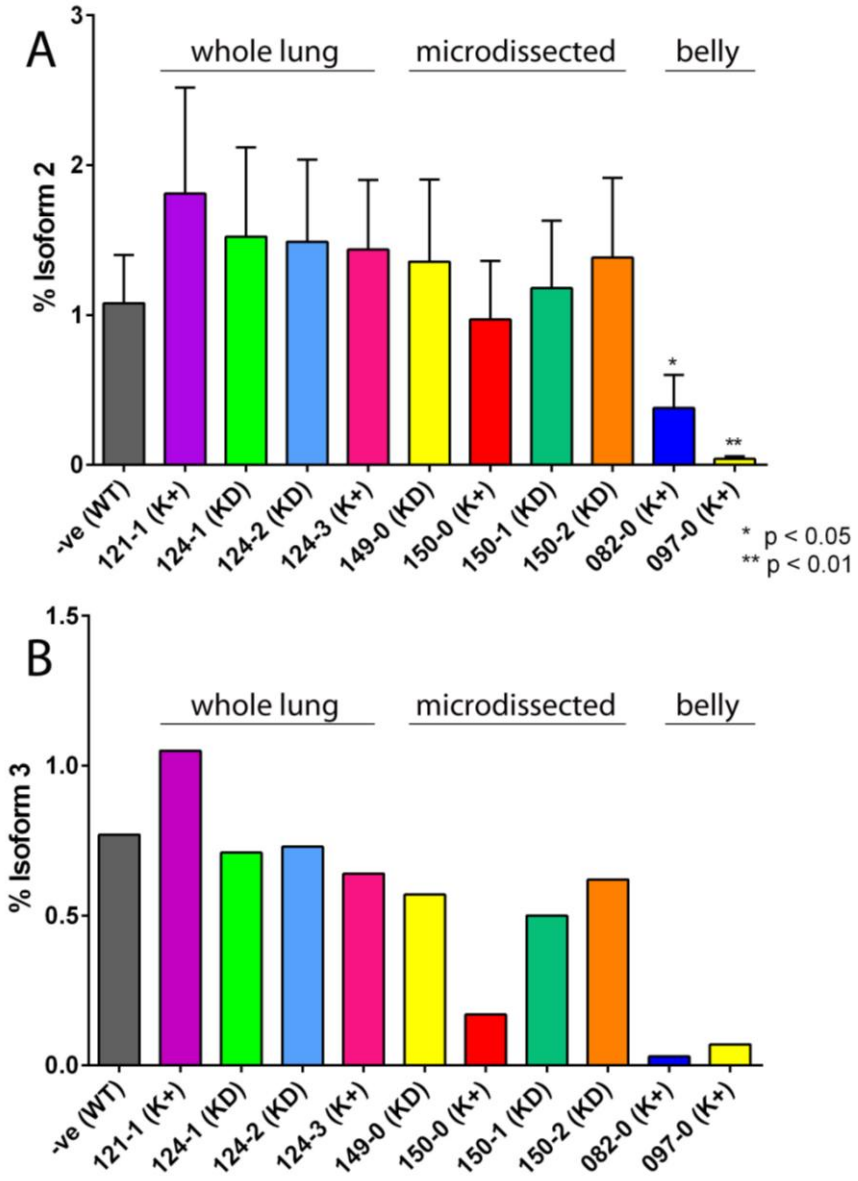

Figure 3.15: Semi-quantification Isoform PCR

For quantification, the band intensities from Figure 3.14 were measured and normalized to GAPDH. Samples #121-1 to #124-3 are whole lung samples from IN injected mice, samples #149-0 to #150-2 are micro dissected lung tumors also from IN injected mice and samples #082-0 and #097-0 are abdominal tumors. Panel A shows the expression of isoform 2 with the standard deviation as error bars (n=3), whereas panel B shows expression of isoform 3 (n=1).

3.7 Dcl1 methylation status

3.7.1 Methylation sensitive PCR

To determine the methylation status of the promoter of Dlc1 isoform 2, DNA was prepared from the tumors. Since it was impossible to cut the tumors right out of the lung, the tumors were micro dissected out of cryosections of the lung tumors.

The DNA prepared from these micro dissections was then treated with sodium bisulfite. The bisulfite converts all unmethylated cytosine bases into deoxyuridine, which can then pair with adenosine, while the methylated CpG islands remain unchanged. We used primers that are either specific for the methylated sequence of Dlc1 and for the unmethylated sequence in two separate PCR assays so that the ratio between the two could be determined.

Due to the very small amounts of DNA extracted from the tumors and the loss of DNA during bisulphite treatment, one round of PCR was not enough to amplify a visible amount of DNA. A second round of PCR was therefore needed. However, the experiments turned out to be not reproducible when done with different samples. Therefore, Pyrosequencing was used as alternative technique.

3.7.2 Pyrosequencing

Pyrosequencing was used to determine the methylation status of the promoter of Dlc1 isoform 2. Since the DNA was prepared from micro dissected tumors out of cryosections only two K+ and two KD samples could be used. To avoid contamination with normal cells the micro dissected tumor samples should be as “pure” as possible. In

the other samples, the tumors were too small and too dispersed to be dissected manually under the microscope.

Figure 3.16 shows a representative result. Panel A) shows the histogram and the dispensation order. The heights of the bars correlate with the amount of the same base incorporated. The grey highlights indicate the methylation sites, whereas the slight yellow bars indicate the bisulfite treatment controls. Panel B) shows the pyrogram for a more methylated promoter (positive control), in this case a sample from the abdominal tumors. Panel C) shows the program for an un-methylated promoter, in this case the lung tumor samples. Above the methylation sites are the calculated percentages of methylation. Although the computer automatically calculates these, one can work it out manually through determining the ratio of the peak heights at each CpG island. The amount of methylation in the lung tumor samples was then compared to the amount of methylation in a wild type sample (negative control) and a sample of the belly tumor (positive control). Statistical analysis was performed by ANOVA. Figure 3.17 shows the methylation status of the Dlc1 isoform 2 promoter for all samples. Panel A) shows the total methylation in each sample. There was no statistical significant difference between the lung tumor samples and the wild type control. Methylation in the abdominal tumor however was increased significantly. Since the methylation rates differ from site to site and statistical analysis was performed again, this time for each methylation site separately. Panel B) shows the different methylation rates at the separate CpG islands, however, there was no change in terms of significance.

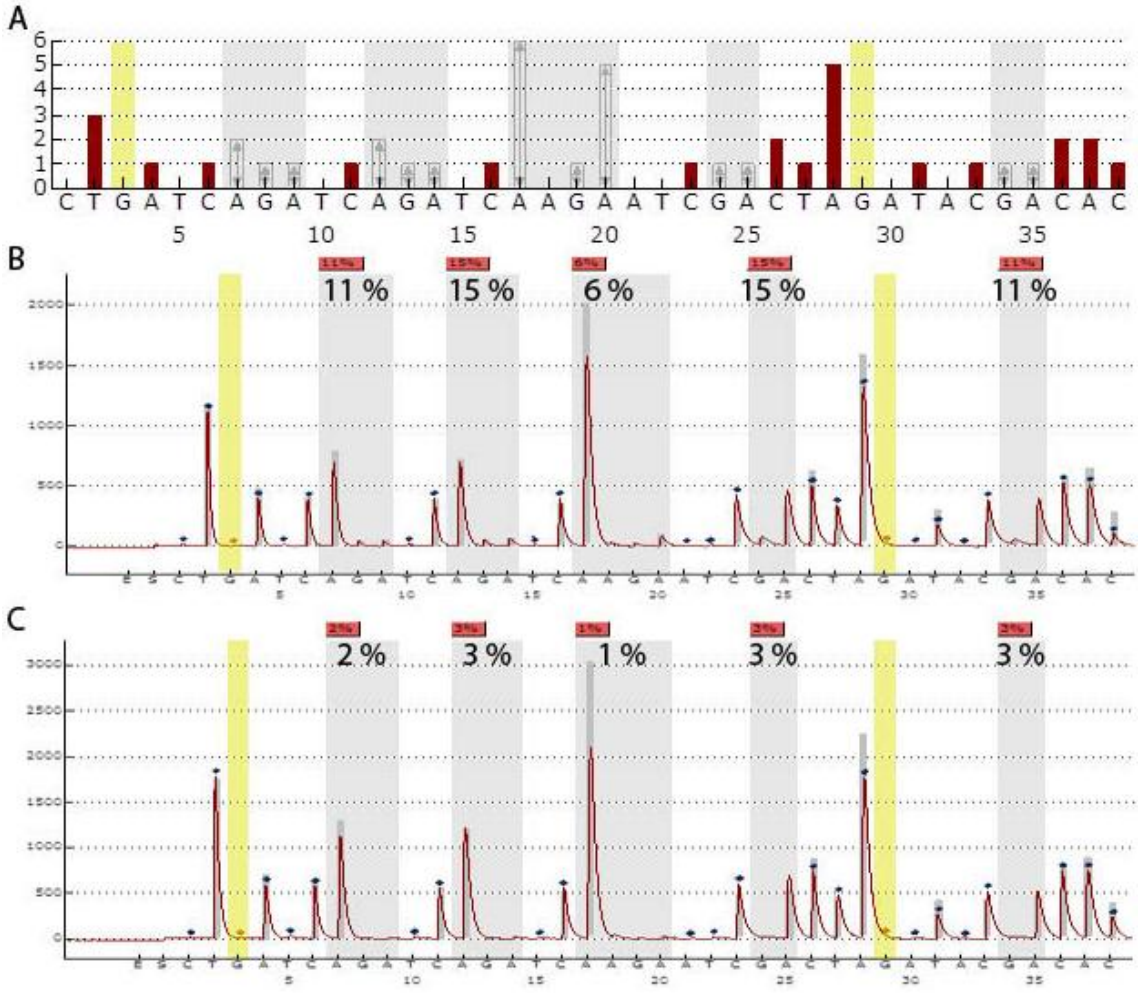

Figure 3.16: Dlc1 methylation studies - Pyrosequencing

Panel A) shows the histogram and the dispensation order of the nucleotides with the grey bars highlighting the methylation sites and the yellow bars indicating the bisulfite treatment controls. Panel B) shows the actual pyrogram and percentages of methylation for a somewhat methylated sequence, in this case the positive control (abdominal tumor). Panel C) shows the acutal pyrogram and percentages methylation for a mostly un-methylated sequence (lung tumors).

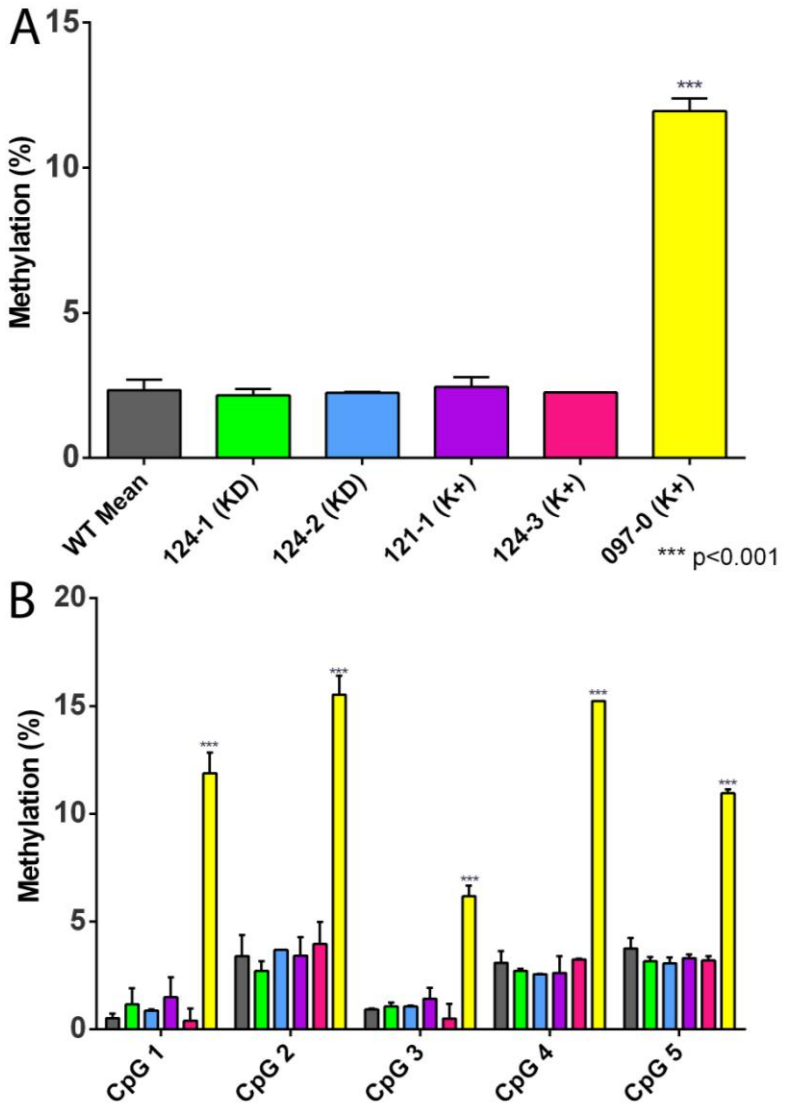

Figure 3.17: Methylation status of the Dlc1 Isoform2 promoter

Figure A) shows the mean methylation per sample. Statistical analysis by ANOVA revealed no statistical significant difference between the lung tumor samples and the wild type control lung. Methylation is increased significantly in the abdominal tumor (097-0). Figure B) shows the methylation on each CpG island, since the methylation rates differ from site to site. Error bars depict standard deviation (n=2).

3.8 Tumor burden comparison

After first scanning the histological samples of the lungs of IN injected mice it seemed that there might be a difference in tumor burden between mice carrying the Kras and the Dlc1 allele and mice that only carry the Kras allele. With the help of the Manitoba Tumor Bank the whole lungs were sectioned and every 10^{th} section was stained with H&E. These stained sections were then examined for tumor numbers, tumor sizes and tumor areas.

3.8.1 Tumor numbers

The first step was to investigate if there is a difference in tumor numbers between K+ and KD mice that were injected with Adeno-Cre. Going through the different sections all the tumors in the lungs were counted. Tumors already counted in one section were not counted again if they were still present in the adjunct section. If in one section two tumors were present and in the next section only one big tumor was visible, it was assumed that two tumors had merged into one bigger one. This assumption was based on the very common round and regular shape of the lung tumors. After obtaining the tumor numbers a Student t-test as well as a Mann-Whitney statistical test was performed to determine statistical significant differences. The results of the t-test are shown in Figure 3.18A. There was no statistically significant difference in the tumor numbers between K+ and KD mice with either test.

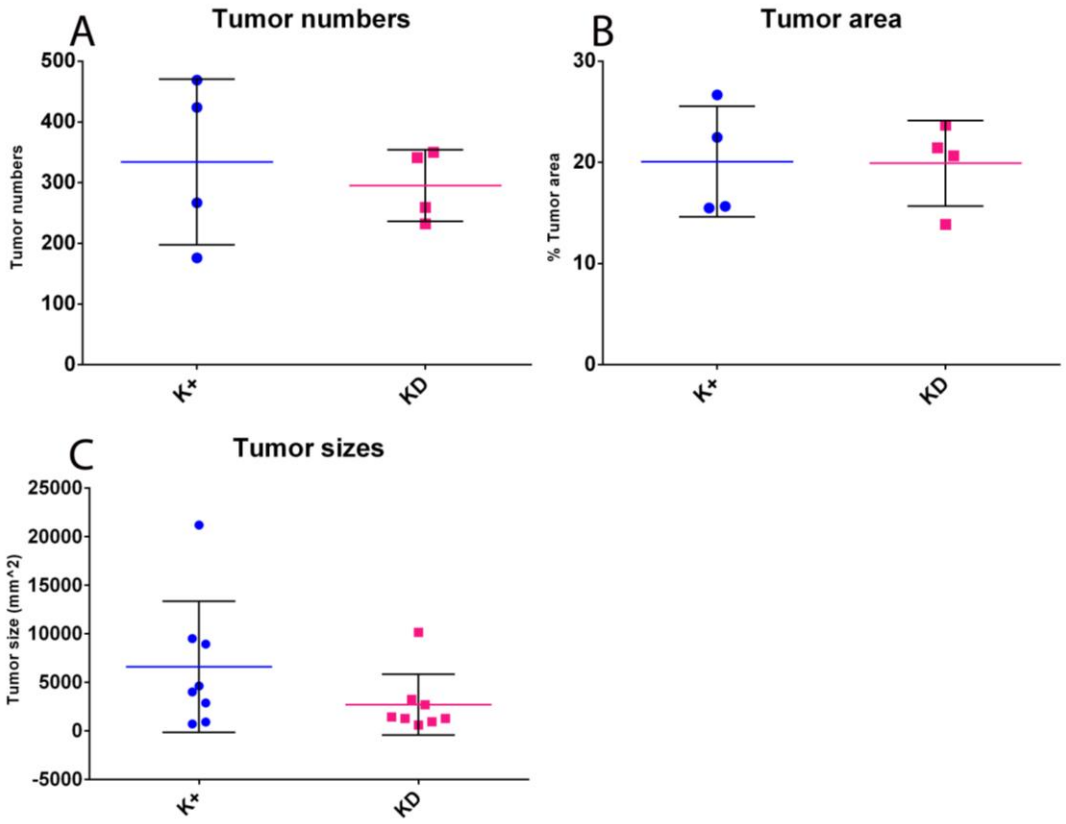

Figure 3.18: Tumor burden: Differences between K+ and KD

Comparison of the tumor numbers (A) and tumor area (B) and tumor sizes (C) between K+ (blue) and KD (pink) mice showed no statistical significant difference in either set. Graphs show the samples (dots), the mean (colored line) and the standard deviation (error bars).

3.8.2 Tumor sizes

Since the tumor numbers did not show any significant differences, we wanted to know, if there could possibly be a difference in the tumor size. The two biggest tumors in each mouse were identified and their area was measured using the freely available program Image J. After converting the pixel values into mm^2 areas, statistical analysis (Student t-test & Mann-Whitney test) was performed. As can be seen in Figure 3.18C the values in the K+ group cover a greater area than those in the KD group. However, there was still no statistical significant difference with either test.

3.8.3 Tumor area

Since measuring all tumors manually would have been too time consuming, the total tumor burden was instead determined with Laser Scanning Cytometry. This technique scans the already existent H&E sections with laser light which will then be absorbed depending on the density of the tissue. These differences in absorption/intensity can then be visualized and converted into tumor area through the use of virtual phantoms overlaying the scan.

The three biggest adjacent section of each mouse were chosen by visual examination. With the fact that all sections were cut with a 5 µm thickness and only every 10^{th} section was stained with H&E, those final three sections chosen for scanning were 50 µm apart and should be able to representative an exemplary and comparable view. For each section scanned the gain and offset were optimized, so the brightest spots as well as the background fall within the recommended borders and would therefore allow an appropriate mapping of the tumor areas. After defining the tumor regions (and

normal tissue) through the histogram, the amounts of phantoms in each region were summed up and converted into mm^2 values. From those values the percentage of tumor compared to total tissue (tumor plus normal tissue) was calculated and analyzed by Student t-test and Mann-Whitney test. In concordance with the previous approaches to determine the tumor burden, there was no statistical significant difference between the K+ and the KD mice with either test (Figure 3.18B).

Chapter 4: Discussion

4.1 Introduction

Previously our lab has developed a heterozygous gene trapped mouse model for Dlc1. It has been shown though, that downregulation of Dlc1 alone is not enough to induce tumor development. This suggested that another factor was needed, such as the cooperation with an oncogene. Due to the pathway interaction of Ras and Rho we hypothesized that Dlc1 and Kras would work together in tumor formation through the Rho signalling pathway.

We studied the cooperation of the two genes with the help of a mouse model containing a heterozygous gene trapped Dlc1 allele as well as a heterozygous conditional Kras oncogene. We hypothesized that mice containing both modified alleles would develop cancer faster and more aggressively compared to mice with only the conditional Kras oncogene. If the two genes cooperate then there should also be a more metastases.

As indicated by the results, we did not observe any significant difference between KD and K+ mice. Since this trend is visible throughout the various experiments, the initial hypothesis was thereby not supported.

4.2 Tumor development

In the first approach I took to activate the conditional Kras allele, mice were injected intraperitoneally (IP) with a cell permeable Cre protein (HNC). Injections occurred at a very young age (10-15 days), because we assumed that the higher cell turn over would multiply the Kras activated cells faster throughout the organs. This way the

tumor development should have happened within a shorter period of time. However, it took over one year before the animals showed first signs of sickness and were subsequently euthanized. Even so, only two animals showed excisable tumors that could be used in further studies.

Reverse transcriptase PCR revealed that Kras is activated mostly in organs of the peritoneal cavity, but not in more distant organs. This is consistent with the delivery of the protein to the peritoneal cavity, but it also suggests that the protein does not travel very well throughout the body. This result was in contrast to the previous report from the Ruley lab, showing that after IP injection of the HNC protein, Cre recombination occurs in organs throughout the body of the mouse (*Jo et al. 2001*). Another difference between our experiments and the original paper was the age of the animals at the time of injection and the time point of testing for recombination activity. In their study, Jo et al. injected adult mice and sacrificed them three days later (*Jo et al. 2001*). We injected very young mice and sacrificed them only after a year, or when signs of tumor development emerged.

In order to examine if our delivery method was somehow faulty or if the young age of our mice was a problem, we repeated the experiment on adult mice and analysed Kras activation three days post-injection. In their study, Jo et al. tested the protein on ROSA26 mice (*Jo et al. 2001*), whereas we used our conditional Kras strain. We observed that IP injection of HNC protein is capable of activating Kras in organs throughout the body, but highest rates were observed in the intraperitoneal cavity. A possible explanation is that the RT-PCR is a more sensitive approach to detect differences in the Kras activation than the uniform blue colouring of the X-Gal staining.

The fact that HNC protein is able to activate Kras throughout the whole body of adult mice, but not when injected into young mice, suggests that the higher cell turnover which we wanted to use to our advantage in reality worked against us. Several studies using chemically inducible conditional Kras mouse models have shown that a continuous activation of Kras is necessary for tumor maintenance and that removal of the trigger results in apoptosis and decrease of tumor volume (*Fisher et al. 2001, Wang et al. 2012*). It seems that the body is selecting against the cells with activated Kras in further cell proliferation. It could be that the Kras activation poses a growth disadvantage. This is consistent with literature reports that Ras activation can lead to growth arrest (*Jaffe & Hall 2002, Mitomi et al. 2007*). It is also consistent with the theory that in order to overcome this growth arrest, Ras transformed cells need higher levels of Rho (*Olson et al. 1998, Sahai et al. 2001*). Higher levels of Rho can be achieved by either up regulating guanine nucleotide exchange factors, which activate GTPases, or by downregulating GTPase activating proteins, such as Dlc1 (*Ellenbroek & Collard 2007*). Since we didn't find any significant downregulation of Dlc1 this suggests that there is no up regulation of Rho, which could have, in theory, overcome the growth arrest.

Another factor contributing to failure of HNC protein to cause tumorigenesis could be the volume we used in the intraperitoneal injections. In the original paper it was suggested to use 1 ml when injected into adult mice (*Jo et al. 2001*). It also determines that the distribution of the protein is via the blood stream and therefore reaches all organs. For the younger mice, we scaled down the volume and injected 200 µl. This amount may have been too small to provide sufficient osmotic pressure to promote effective dispersion of HNC protein throughout the peritoneal cavity and into the blood stream,

therefore failing to activate Kras in a sustained manner in different organs. The mice used in our experiments were bred on a C57BL/6 background, which has been reported to have low cancer susceptibility (*Blake et al. 1997, Li & Randerath 1990*). Together with the less than optimal injection protocol this could have been the reason why we did not see more tumors.

Despite all the downfalls, two mice did developed tumors in the abdominal cavity after HNC injections. Both tumors arose from the surrounding connective tissue rather than a specific organ. Upon histological examination both tumors showed spindle shaped cells, which suggests that they are some sort of spindle cell carcinoma or sarcoma. Reports in the literature indicate, that the most common age-related tumor in C57Bl/6 mice is fibrosarcoma, which would support our findings (*Li et al. 2007*). However, to determine the exact nature of the tumors, immunostaining that we did not perform is necessary. In the clinical setting a variety of markers are used on a regular basis to identify carcinomas, including a variety of different cytokeratine markers (*Moll et al. 1982*). To determine the origin from muscle cells (smooth and skeletal), actin or desmin can be used (*Turner & Goldsmith 2009*). Tumors arising from the blood vessels can be stained with endothelial markers CD31 or CD34 (*Pusztaszeri et al. 2006*).

In contrast to the IP injections of HNC protein, intranasal injections of Cre expressing adenovirus yielded lung tumors fairly quickly, likely due to high infection efficiency (*Fasbender et al. 1998*). As reported previously, Kras activation was limited to the lung using this approach (*Jackson et al. 2001*). Histological examination together with a pathologist identified lung tumors as adenocarcinomas because they showed

characteristic glandular structure, together with membrane irregularities and enlarged nuclei.

4.3 Metastasis in IN injected mice

All organs of the IN injected mice were carefully examined for metastases. Most animals showed metastases to the kidney and the liver, but when statistically analysed, there was no difference in numbers between mice carrying both the Kras oncogene and the Dlc1 gene trapped allele, compared to mice carrying only the conditional Kras oncogene. This suggests that partial downregulation of Dlc1 is not enough to increase the metastatic potential. This is in contrast to previous reports, which showed that Dlc1 is a metastasis suppressor and that loss of Dlc1 leads to increased metastasis (*Goodison et al. 2005, Ullmannova-Benson et al. 2008*). However, those studies were done in cell lines, whereas *in vivo* the environment is much more complex. On the other hand, Scott Lowe and his team have showed that the impact of Dlc1 as a tumor suppressor is much more prominent *in vivo* than *in vitro*, where it accelerates tumor onset significantly (*Xue et al. 2008*).

Of note, we also observed lesions in the kidneys of non-injected wild type controls. The fact, that no lesions were observed in injected wild type controls suggests that they are not a result of the injection protocol, but rather spontaneous formation. Although C57BL/6 mice have low cancer susceptibility some people have also reported spontaneous tumor formation in older mice, carrying spontaneous mutations such as the tumor suppressor p53 (*Adkison & Sundberg 1991, Heston & Vlahakis 1971, Li et al. 2007*). Since our mice were 9 months old by the time they were euthanized, spontaneous mutations could account for the lesions observed. It has also been reported that with

increased age chromosomal instability (CIN) increases and that it happens before tumors are visible (*Lushnikova et al. 2011*). This suggests that age-related chromosomal instability might contribute to tumor formation as well.

4.4 Lung tumor burden

Lung tumor formation was compared in mice carrying both the conditional Kras allele as well as the gene trapped Dlc1 allele (KD) and in mice carrying only the conditional Kras allele but were wild type for Dlc1 (K+). To determine tumor burden the number of the individual tumors was first counted and then total tumor area was measured by laser scanning cytometry (LSC). Statistical comparison between the two groups has revealed no significant difference in tumor burden between KD and K+ mice.

Four mice from the cohort were excluded from further studies, since they only exhibited very minimal tumor development and skewed the calculations. The most probable reason that those mice did not show the same amount of cancer as other mice is because they were the first to be injected and we did not have much experience with the technique. Spilling of the virus solution might have prevented the full dose to reach the lungs. Alternatively it could be that the solution was ingested rather than inhaled when not properly injected into the nose.

Tumor numbers were counted on sections spanning the whole lung in 50 µm intervals and this represented a good view through the whole organ. The determination of what was a tumor or not was based on histochemical staining (H&E) and pathological landmarks characteristic for adenocarcinomas, such as glandular structure seen in Figure 3.8. If at tumor appeared as one single lesion in one section but as two separate lesions in the next, it was always assumed that two tumors merged into one, rather than one tumor

branched into two. This assumption was based on the usually very round and compact structure of the tumors, especially at bigger sizes.

Since measuring tumor area on all the sections we prepared was technically unfeasible, only three representative sections of each mouse were chosen. Those sections were chosen subjectively by determining the biggest available section through visual examination and then adding the two adjacent ones on each side. In general the biggest downfalls of laser scanning cytometry are the subjective choices made along the way. After choosing the sections, the settings of the gain/offset were adjusted manually to optimize the signal to background ratio. The size of the phantoms was determined by trial and error. Different sizes were tested for their ability to cover the tumor as complete as possible without picking up too much background. And finally, the regions in the histogram were decided upon by the observer. If someone else would have done the same experiment he/she might have come to different calculations. However, it is expected, if there were a statistical significant difference in the tumor area values between K+ and KD mice they would have been big enough, so they would have been picked up either way.

Another downfall of LSC is that the measurement is purely about absorption intensity. There is no other way of determining the tumor areas in an H&E stained tissue. This does not take into account that fibrotic areas or airway epithelial and blood vessels might have similar density and would therefore present as tumors. We believe this artifact was eliminated, however, due to the threshold values we used to identify tumors. Similarly, if the sectioning process ripped a big tumor apart, those areas of tumor are automatically lost, since they would be counted as background.

When excising lungs from the animals and preparing them for paraffin embedding no special emphasis was given to anatomical structures nor were the lungs inflated to their normal size in the chest cavity. The latter issue likely contributed to “collapse” of some lung areas and these may have obscured tumor margins. Whole lungs were sliced in smaller parts and randomly taken for histology, RNA and DNA. Since Cre expressing adenovirus enters the lungs through the airways from the nose it might have been useful to always take the same part (i.e. lobe) from each lung for comparison. If the delivery system was performed correctly it can be assumed that the same areas of the lung were in contact with approximately the same amount of adenovirus in each mouse. That might have shown the infection rate (and therefore tumor development) in the upper lobes to be higher than in the lower parts due to contact with more adenovirus. The tumor formation could then directly be correlated to the amount of virus taken up by the cells.

In our studies, intranasally injected mice were left to the point where they started to exhibit signs of sickness, such as short breathing and lowered activity. Histological analysis of the lungs showed similarly high amounts of tumor load in both groups. There was also no difference in the time those tumors needed to develop. But at the endpoint all the tumors were already big enough to cause distress for the animal. Samples taken at different time points before the final stages might show a difference in the earlier stages of tumor development.

The lack of difference in tumor formation between KD and K+ as well as the development of so few metastasis shows that heterozygous downregulation of Dlc1 is not enough to induce any changes compared to Kras alone and might need the cooperation of yet another gene. While Kras is enough to induce tumors it also leads to an increase in

tumor suppressor gene response, such as p53 and $p16^{Ink4A}$ (*Parikh et al. 2012*). Although loss of p53 is not enough to initiate lung tumor development by itself it is certainly important for the progression of the lung cancer (*Jackson et al. 2005*). Tumor growth and metastasis formation can be greatly enhanced by loss of p53 or the Ink4A/Arf locus (*Fisher et al. 2001, Gibbons et al. 2009*). Several groups have combined Kras models with p53 models and found that tumor formation is increased by their cooperation, leading to bigger tumors and more metastatic disease (*DuPage et al. 2009, Jackson et al. 2005, Ji et al. 2007, Wang et al. 2006, Zheng et al. 2007*). Among other pathways, this could be due to the increase in NF-κB signalling induced by the expression of oncogenic Kras which enhances oncogenic transformation (*Basseres et al. 2010*) . Since NF-κB acts in an anti-apoptotic manner, inhibition of the pathway leads to reduced tumor development (*Meylan et al. 2009*). It should therefore be considered in the future to combine our Kras/Dlc1 model with a p53 or NF-κB component to increase tumor and metastasis development.

4.5 Dlc1 expression & methylation in IN injected mice

Since there was no detectable difference in tumor burden between KD and K+ mice we wanted to investigate if the status of the Dlc1 gene was changed at all in comparison to wild type. It has previously been reported that in a variety of tumors Dlc1 is downregulated (*Ng et al. 2000, Ullmannova & Popescu 2006*). This could be through deletion or promoter hypermethylation (*Wong et al. 2003*). We wanted to know if there is a change in Dlc1 expression in the tumors and if that change could be due to methylation of the Dlc1 promoter. We examined Dlc1 isoform 2 expression in tumor samples through reverse transcriptase PCR, since that was the location of the gene trapping cassette.

Simultaneously we determined the methylation status of the Dlc1 isoform 2 promoter by pyrosequencing.

RNA samples for the expression studies were taken from whole lungs, micro dissected lungs, abdominal tumors and wild type lungs. The band intensities were then quantified and normalized to GAPDH in the same samples. The experiments revealed no significant downregulation of Dlc1 in the lung tumors compared to wild type samples. This was true for the whole lung samples as well as for microdissected lung tumors. In the whole lung samples one could argue, that the normal tissue surrounding the tumor obscured the relatively small amount of tumor tissue, meaning even if there was a downregulation of Dlc1 in those tumors, it may not be detectable. That argument however was nullified because micro dissected tumors also did not show any decrease in Dlc1 expression.

We found that Dlc1 expression in KD mice, which carry one gene trapped Dlc1 allele, is not significantly lower than in the wild type. This is in contrast to previous reports from our lab that had reported lower Dlc1 expression in gene trapped cell lines (*Sabbir et al. 2010*). Also, previous experiments in our lab have looked at thymic tumors that were obtained through tail vein injection of Adeno-Cre. In those tumors Dlc1 expression was downregulated significantly (*Sabbir et al. 2012*). It has to be taken into account, however, that both experiments were done on cell lines whereas I examined tissue samples. Also of note is that the experiments were done on protein and mRNA samples, whereas my expression studies were performed on mRNA only. We could not study the protein, because our tumor samples were too small. To obtain better insight concerning the Dlc1 downregulation, protein levels need to be checked as well. If the

mRNA is expressed at almost normal levels, but the protein is abolished that could suggest that there is a currently unknown mechanism by which the protein production is inhibited.

My colleague Golam Sabbir has performed immunohistochemistry studies with a β-galactosidase gene connected to the Dlc1 and has shown that Dlc1 expression is not downregulated evenly throughout the tumors, but follows a more gradient pattern (data not shown). That way the part of the tumor expressing Dlc1 at a normal level could dominate over the part with Dlc1 downregulated and it would be impossible for me to detect it.

Consistent with no change in Dlc1 expression, we did not find a significant change in promoter methylation. Neither K+ nor KD mice showed increased methylation compared to the wild type lung. As positive control we used a DNA sample from abdominal tumors that developed after IP injection of HNC protein. This sample showed a significant increase in methylation compared to the wild type. As (*Sabbir et al. 2010*) have shown, the Dlc1 isoforms are expressed in different levels in different organs. Since the positive tumor control arose from abdominal tissue and the wild type control is lung tissue, we cannot directly compare them to each other.

One might think that different isoforms or even different members of the Dlc family compensate for each other. Indeed it has been suggested that Dlc1 (or Dlc3) might compensate for Dlc2 in embryonic development, but not the other way around (*Durkin et al. 2005, Yau et al. 2009*). However, the primers used in the expression studies were specific for Dlc1 isoform 2 and did not show any cross reaction with other isoforms.

4.6 Future Directions

Since there is no difference in tumor development between mice expressing the Kras oncogene as well as the Dlc1 gene trapped allele compared to mice only carrying the Kras oncogene, it is clear that the heterozygous downregulation of Dlc1 is not enough to increase the malignant and metastatic potential. Future studies related to this project should therefore work with a more rigorous downregulation of Dlc1 or introduce other cancer related genes, such as p53.

On the very top of the list stands a conditional mouse model for Dlc1. That would allow the knockout of both alleles in the adult mouse without having to worry about embryonic lethality. A knock out of both alleles might also have a greater impact on tumor development than silencing only one allele. Additionally, in the current gene trapped mouse model for Dlc1 only one isoform is targeted. A new model that would target all isoforms would prevent the isoforms from compensating for each other. When the mouse model is established, bigger numbers of mice included in the study are needed, to allow for all the outliers and still provide enough numbers for a better comparison and statistical analysis of the results.

To date more studies are underway with mice intranasally injected with Adeno-Cre. They were subjected to an even lower dose of Adeno-Cre in the hope that the lung tumors develop over a more prolonged timeframe, which allows metastases to develop before the animal succumbs to the primary tumor. It would also allow for the formation of only a few tumors, which then get the chance to grow bigger without interfering with the animal's life as much. Bigger tumors are an advantage in further experiments, because they are easier to handle, easier to excise and yield more tissue.

In the future all experiments should be done on micro dissected tumors, to assure as pure as possible tissue samples. That again would call for the formation of bigger tumors, as mentioned above. For further studies it would also be a great asset to develop cell lines from the tumors. Cell lines are easier to handle than the tumors and yield a lot of material which can then be used in a variety of experiments, such as protein, RNA and DNA isolation.

Since we have determined, that the Dlc1 promoter is not significantly methylated in the lung tumors, it would be interesting to study if there are deletions or other chromosomal rearrangements. This could be determined by FISH (fluorescent in situ hybridization), SKY (spectral karyotyping) and M-banding (multicolored banding) (*Benedek et al. 2004*). It has also been shown previously that telomere dysfunction is preventing tumor formation in the presence of p53. However, it also leads to chromosomal instability resulting in loss of p53 which eventually increases tumor formation again (*Perera et al. 2008*).

To study the involvement of the Rho component in more detail, future studies could also look at the expression and localization of active Rho protein by staining cells with GST-Rhotekin, an active Rho-GTP binding protein (*Ren & Schwartz 2000*). The formation of stress fibers, indicative of active Rho activity, can be detected by fluorescent phalloidin staining (*Wulf et al. 1979*).

In order to determine Dlc1 expression in paraffin embedded tissue sections, it would be helpful to obtain an antibody which could be reliably used in immunohistochemistry experiments. That way it would be possible to visualize changing Dlc1 expression throughout the tumor.

And finally, to better characterize the development of metastases immunohistochemistry experiments could determine if lesions outside the primary site are indeed metastases of that tumor or primary tumors themselves. In clinical settings, patients with lung cancer are routinely tested with TTF1 (Thyroid Transcription Factor 1). This marker is very specific for thyroid tissue and lung adenocarcinomas in adults (*Kaufmann & Dietel 2000, Ordonez 2000, Sheppard 2000*). Antibodies against surface protein C (SP-C) or Clara cell antigen (CC10), can aid in determining if the lung tumors arose from alveolar type II or Clara cells, respectively (*Jackson et al. 2001*).

4.7 Conclusion

This thesis started with the hypothesis that Kras and Dlc1 will cooperate in tumor development and that mice with Dlc1 loss show more aggressive tumors and increased metastases. At the end of this thesis we can say that on no account has there been a difference between mice carrying the oncogenic Kras allele as well as the Dlc1 gene trapped allele compared to mice carrying only the Kras oncogene.

But since studying the Dlc1 expression in the tumor samples did not show a significant downregulation of Dlc1 in any of them compared to wild type samples we were never able to ascertain if loss of Dlc1 really leads to more aggressive cancer. All we can say for sure is that heterozygous downregulation of Dlc1 in an experimental setup like ours is not enough to increase tumor formation and metastasis development in Kras lung tumors.

Chapter 5: References

Abremski, K., and Hoess, R. (1984) "Bacteriophage P1 site-specific recombination. Purification and properties of the Cre recombinase protein", *J Biol Chem* 259, 1509-1514.

Adkison, D. L., and Sundberg, J. P. (1991) ""Lipomatous" hamartomas and choristomas in inbred laboratory mice", *Vet Pathol* 28, 305-312.

Ahmed, B. Y., Chakravarthy, S., Eggers, R., Hermens, W. T., Zhang, J. Y., Niclou, S. P., Levelt, C., Sablitzky, F., Anderson, P. N., Lieberman, A. R., and Verhaagen, J. (2004) "Efficient delivery of Cre-recombinase to neurons in vivo and stable transduction of neurons using adeno-associated and lentiviral vectors", *BMC neuroscience* 5, 4.

Akagi, K., Sandig, V., Vooijs, M., Van der Valk, M., Giovannini, M., Strauss, M., and Berns, A. (1997) "Cre-mediated somatic site-specific recombination in mice", *Nucleic acids research* 25, 1766.

American Cancer Society, A. (2011) "Cancer Facts & Figures 2011", American Cancer Society.

Aznar, S., Fernandez-Valeron, P., Espina, C., and Lacal, J. C. (2004) "Rho GTPases: potential candidates for anticancer therapy", *Cancer Lett* 206, 181-191.

Baba, A. I., and Catoi, C. (2007) *"Comparative Oncology"*, Vol., 2010/09/01 ed.

Barbacid, M. (1987) "ras genes", *Annu Rev Biochem* 56, 779-827.

Basseres, D. S., Ebbs, A., Levantini, E., and Baldwin, A. S. (2010) "Requirement of the NF-kappaB subunit p65/RelA for K-Ras-induced lung tumorigenesis", *Cancer Res* 70, 3537-3546.

Beasley, M. B., Brambilla, E., and Travis, W. D. (2005) "The 2004 World Health Organization classification of lung tumors", *Semin Roentgenol* 40, 90-97.

Benedek, K., Chudoba, I., Klein, G., Wiener, F., and Mai, S. (2004) "Rearrangements of the telomeric region of mouse chromosome 11 in Pre-B ABL/MYC cells

revealed by mBANDing, spectral karyotyping, and fluorescence in-situ hybridization with a subtelomeric probe", *Chromosome Res* 12, 777-785.

Benitah, S. A., Valeron, P. F., van Aelst, L., Marshall, C. J., and Lacal, J. C. (2004) "Rho GTPases in human cancer: an unresolved link to upstream and downstream transcriptional regulation", *Biochim Biophys Acta* 1705, 121-132.

Bernards, A. (2003) "GAPs galore! A survey of putative Ras superfamily GTPase activating proteins in man and Drosophila", *Biochim Biophys Acta* 1603, 47-82.

Birnboim, H. C., and Doly, J. (1979) "A rapid alkaline extraction procedure for screening recombinant plasmid DNA", *Nucleic Acids Res* 7, 1513-1523.

Bishop, A. L., and Hall, A. (2000) "Rho GTPases and their effector proteins", *The Biochemical journal* 348 Pt 2, 241.

Blake, J. A., Richardson, J. E., Davisson, M. T., and Eppig, J. T. (1997) "The Mouse Genome Database (MGD). A comprehensive public resource of genetic, phenotypic and genomic data. The Mouse Genome Informatics Group", *Nucleic Acids Res* 25, 85-91.

Borczuk, A. C., Toonkel, R. L., and Powell, C. A. (2009) "Genomics of lung cancer", *Proc Am Thorac Soc* 6, 152-158.

Bos, J. L. (1989) "ras oncogenes in human cancer: a review", *Cancer Res* 49, 4682-4689.

Bos, J. L., Rehmann, H., and Wittinghofer, A. (2007) "GEFs and GAPs: critical elements in the control of small G proteins", *Cell* 129, 865.

Buchsbaum, R. J. (2007) "Rho activation at a glance", *J Cell Sci* 120, 1149-1152.

Canadian Cancer Society, C. (2011) "Canadian Cancer Statistics 2011", Canadian Cancer Society.

Cerami, E., Gao, J., Dogrusoz, U., Gross, B. E., Sumer, S. O., Aksoy, B. A., Jacobsen, A., Byrne, C. J., Heuer, M. L., Larsson, E., Antipin, Y., Reva, B., Goldberg, A. P., Sander, C., and Schultz, N. (2012) "The cBio Cancer Genomics Portal: An Open Platform for Exploring Multidimensional Cancer Genomics Data", *Cancer Discov* 2, 401-404.

Chang, E. H., Gonda, M. A., Ellis, R. W., Scolnick, E. M., and Lowy, D. R. (1982) "Human genome contains four genes homologous to transforming genes of

Harvey and Kirsten murine sarcoma viruses", *Proc Natl Acad Sci U S A* 79, 4848-4852.

Chen, J. C., Zhuang, S., Nguyen, T. H., Boss, G. R., and Pilz, R. B. (2003) "Oncogenic Ras leads to Rho activation by activating the mitogen-activated protein kinase pathway and decreasing Rho-GTPase-activating protein activity", *J Biol Chem* 278, 2807-2818.

Clark, E. A., Golub, T. R., Lander, E. S., and Hynes, R. O. (2000) "Genomic analysis of metastasis reveals an essential role for RhoC", *Nature* 406, 532-535.

Dhillon, A. S., Hagan, S., Rath, O., and Kolch, W. (2007) "MAP kinase signalling pathways in cancer", *Oncogene* 26, 3279-3290.

DuPage, M., Dooley, A. L., and Jacks, T. (2009) "Conditional mouse lung cancer models using adenoviral or lentiviral delivery of Cre recombinase", *Nat Protoc* 4, 1064-1072.

Durkin, M. E., Avner, M. R., Huh, C. G., Yuan, B. Z., Thorgeirsson, S. S., and Popescu, N. C. (2005) "DLC-1, a Rho GTPase-activating protein with tumor suppressor function, is essential for embryonic development", *FEBS letters* 579, 1191.

Durkin, M. E., Yuan, B. Z., Zhou, X., Zimonjic, D. B., Lowy, D. R., Thorgeirsson, S. S., and Popescu, N. C. (2007) "DLC-1:a Rho GTPase-activating protein and tumour suppressor", *Journal of Cellular and Molecular Medicine* 11, 1185.

Editor, A. p. "A plasmid Editor".

Ellenbroek, S. I., and Collard, J. G. (2007) "Rho GTPases: functions and association with cancer", *Clin Exp Metastasis* 24, 657-672.

Ellis, C. A., and Clark, G. (2000) "The importance of being K-Ras", *Cell Signal* 12, 425-434.

Ellis, J. (2012) "The impact of lung cancer on patients and carers", *Chron Respir Dis* 9, 39-47.

Etienne-Manneville, S., and Hall, A. (2002) "Rho GTPases in cell biology", *Nature* 420, 629-635.

Fasbender, A., Lee, J. H., Walters, R. W., Moninger, T. O., Zabner, J., and Welsh, M. J. (1998) "Incorporation of adenovirus in calcium phosphate precipitates

enhances gene transfer to airway epithelia in vitro and in vivo", *J Clin Invest* 102, 184-193.

Feil, R. (2007) "Conditional somatic mutagenesis in the mouse using site-specific recombinases", *Handb Exp Pharmacol* 3-28.

Fisher, G. H., Wellen, S. L., Klimstra, D., Lenczowski, J. M., Tichelaar, J. W., Lizak, M. J., Whitsett, J. A., Koretsky, A., and Varmus, H. E. (2001) "Induction and apoptotic regression of lung adenocarcinomas by regulation of a K-Ras transgene in the presence and absence of tumor suppressor genes", *Genes Dev* 15, 3249-3262.

Freed-Pastor, W. A., and Prives, C. (2012) "Mutant p53: one name, many proteins", *Genes Dev* 26, 1268-1286.

Friday, B. B., and Adjei, A. A. (2005) "K-ras as a target for cancer therapy", In *Biochim.Biophys.Acta*, p 127.

Fritz, G., Brachetti, C., Bahlmann, F., Schmidt, M., and Kaina, B. (2002) "Rho GTPases in human breast tumours: expression and mutation analyses and correlation with clinical parameters", *Br J Cancer* 87, 635-644.

Fritz, G., Just, I., and Kaina, B. (1999) "Rho GTPases are over-expressed in human tumors", *Int J Cancer* 81, 682-687.

Gamblin, S. J., and Smerdon, S. J. (1998) "GTPase-activating proteins and their complexes", *Curr Opin Struct Biol* 8, 195-201.

Ghoshal, K., Majumder, S., and Jacob, S. T. (2002) "Analysis of promoter methylation and its role in silencing metallothionein I gene expression in tumor cells", *Methods Enzymol* 353, 476-486.

Gibbons, D. L., Lin, W., Creighton, C. J., Zheng, S., Berel, D., Yang, Y., Raso, M. G., Liu, D. D., Wistuba, II, Lozano, G., and Kurie, J. M. (2009) "Expression signatures of metastatic capacity in a genetic mouse model of lung adenocarcinoma", *PLoS One* 4, e5401.

Glushkov, S. A., Bragin, A. G., and Dymshits, G. M. (2009) "Decontamination of polymerase chain reaction reagents using DEAE-cellulose", *Anal Biochem* 393, 135-137.

Gomez del Pulgar, T., Benitah, S. A., Valeron, P. F., Espina, C., and Lacal, J. C. (2005) "Rho GTPase expression in tumourigenesis: evidence for a significant link", *Bioessays* 27, 602-613.

Goodison, S., Yuan, J., Sloan, D., Kim, R., Li, C., Popescu, N. C., and Urquidi, V. (2005) "The RhoGAP protein DLC-1 functions as a metastasis suppressor in breast cancer cells", *Cancer Res* 65, 6042-6053.

Hakem, A., Sanchez-Sweatman, O., You-Ten, A., Duncan, G., Wakeham, A., Khokha, R., and Mak, T. W. (2005) "RhoC is dispensable for embryogenesis and tumor initiation but essential for metastasis", *Genes Dev* 19, 1974-1979.

Hall, A. (1998) "Rho GTPases and the actin cytoskeleton", *Science* 279, 509-514.

Hall, A. (2005) "Rho GTPases and the control of cell behaviour", *Biochem Soc Trans* 33, 891-895.

Harlow, E., and Lane, D. (1999) *"Using Antibodies - A laboratory manual"*, Vol., Cold Spring Harbor Laboratory Press.

Healy, K. D., Hodgson, L., Kim, T. Y., Shutes, A., Maddileti, S., Juliano, R. L., Hahn, K. M., Harden, T. K., Bang, Y. J., and Der, C. J. (2008) "DLC-1 suppresses non-small cell lung cancer growth and invasion by RhoGAP-dependent and independent mechanisms", *Mol Carcinog* 47, 326-337.

Heckman-Stoddard, B. M., Vargo-Gogola, T., McHenry, P. R., Jiang, V., Herrick, M. P., Hilsenbeck, S. G., Settleman, J., and Rosen, J. M. (2009) "Haploinsufficiency for p190B RhoGAP inhibits MMTV-Neu tumor progression", *Breast Cancer Res* 11, R61.

Heston, W. E., and Vlahakis, G. (1971) "Mammary tumors, plaques, and hyperplastic alveolar nodules in various combinations of mouse inbred strains and the different lines of the mammary tumor virus", *International Journal of Cancer* 7, 141-148.

Hoess, R., Abremski, K., Irwin, S., Kendall, M., and Mack, A. (1990) "DNA specificity of the Cre recombinase resides in the 25 kDa carboxyl domain of the protein", *J Mol Biol* 216, 873-882.

Hoess, R. H., Ziese, M., and Sternberg, N. (1982) "P1 site-specific recombination: nucleotide sequence of the recombining sites", *Proc Natl Acad Sci U S A* 79, 3398-3402.

Homma, Y., and Emori, Y. (1995) "A dual functional signal mediator showing RhoGAP and phospholipase C-delta stimulating activities", *EMBO J* 14, 286-291.

Jackson, E. L., Olive, K. P., Tuveson, D. A., Bronson, R., Crowley, D., Brown, M., and Jacks, T. (2005) "The differential effects of mutant p53 alleles on advanced murine lung cancer", *Cancer Res* 65, 10280-10288.

Jackson, E. L., Willis, N., Mercer, K., Bronson, R. T., Crowley, D., Montoya, R., Jacks, T., and Tuveson, D. A. (2001) "Analysis of lung tumor initiation and progression using conditional expression of oncogenic K-ras", *Genes Dev* 15, 3243-3248.

Jaffe, A. B., and Hall, A. (2002) "Rho GTPases in transformation and metastasis", *Adv Cancer Res* 84, 57-80.

Jaffe, A. B., and Hall, A. (2005) "Rho GTPases: biochemistry and biology", *Annu Rev Cell Dev Biol* 21, 247-269.

Ji, H., Ramsey, M. R., Hayes, D. N., Fan, C., McNamara, K., Kozlowski, P., Torrice, C., Wu, M. C., Shimamura, T., Perera, S. A., Liang, M. C., Cai, D., Naumov, G. N., Bao, L., Contreras, C. M., Li, D., Chen, L., Krishnamurthy, J., Koivunen, J., Chirieac, L. R., Padera, R. F., Bronson, R. T., Lindeman, N. I., Christiani, D. C., Lin, X., Shapiro, G. I., Janne, P. A., Johnson, B. E., Meyerson, M., Kwiatkowski, D. J., Castrillon, D. H., Bardeesy, N., Sharpless, N. E., and Wong, K. K. (2007) "LKB1 modulates lung cancer differentiation and metastasis", *Nature* 448, 807-810.

Jo, D., Nashabi, A., Doxsee, C., Lin, Q., Unutmaz, D., Chen, J., and Ruley, H. E. (2001) "Epigenetic regulation of gene structure and function with a cell-permeable Cre recombinase", In *Nat.Biotechnol.*, p 929.

Johnson, L., Greenbaum, D., Cichowski, K., Mercer, K., Murphy, E., Schmitt, E., Bronson, R. T., Umanoff, H., Edelmann, W., Kucherlapati, R., and Jacks, T. (1997) "K-ras is an essential gene in the mouse with partial functional overlap with N-ras", *Genes Dev* 11, 2468-2481.

Johnson, L., Mercer, K., Greenbaum, D., Bronson, R. T., Crowley, D., Tuveson, D. A., and Jacks, T. (2001) "Somatic activation of the K-ras oncogene causes early onset lung cancer in mice", *Nature* 410, 1111-1116.

Kamai, T., Arai, K., Tsujii, T., Honda, M., and Yoshida, K. (2001) "Overexpression of RhoA mRNA is associated with advanced stage in testicular germ cell tumour", *BJU Int* 87, 227-231.

Karnoub, A. E., Chenette, E. J., and Der, C. J. (2006) "Rho proteins in Ras signaling and transformation", In *Ras Family GTPases* (Der, C. J., Ed.), pp 143-167, Springer.

Kaufmann, O., and Dietel, M. (2000) "Thyroid transcription factor-1 is the superior immunohistochemical marker for pulmonary adenocarcinomas and large cell carcinomas compared to surfactant proteins A and B", *Histopathology* 36, 8-16.

Khosravi-Far, R., and Der, C. J. (1994) "The Ras signal transduction pathway", *Cancer Metastasis Rev* 13, 67-89.

Khosravi-Far, R., Solski, P. A., Clark, G. J., Kinch, M. S., and Der, C. J. (1995) "Activation of Rac1, RhoA, and mitogen-activated protein kinases is required for Ras transformation", *Mol Cell Biol* 15, 6443-6453.

Kim, C. F., Jackson, E. L., Kirsch, D. G., Grimm, J., Shaw, A. T., Lane, K., Kissil, J., Olive, K. P., Sweet-Cordero, A., Weissleder, R., and Jacks, T. (2005) "Mouse models of human non-small-cell lung cancer: raising the bar", *Cold Spring Harb Symp Quant Biol* 70, 241-250.

Kim, T. Y., Healy, K. D., Der, C. J., Sciaky, N., Bang, Y. J., and Juliano, R. L. (2008) "Effects of structure of Rho GTPase-activating protein DLC-1 on cell morphology and migration", *J Biol Chem* 283, 32762-32770.

Kim, T. Y., Vigil, D., Der, C. J., and Juliano, R. L. (2009) "Role of DLC-1, a tumor suppressor protein with RhoGAP activity, in regulation of the cytoskeleton and cell motility", *Cancer Metastasis Rev* 28, 77-83.

Ko, F. C., Yeung, Y. S., Wong, C. M., Chan, L. K., Poon, R. T., Ng, I. O., and Yam, J. W. (2010) "Deleted in liver cancer 1 isoforms are distinctly expressed in human tissues, functionally different and under differential transcriptional regulation in hepatocellular carcinoma", *Liver Int* 30, 139-148.

Koera, K., Nakamura, K., Nakao, K., Miyoshi, J., Toyoshima, K., Hatta, T., Otani, H., Aiba, A., and Katsuki, M. (1997) "K-ras is essential for the development of the mouse embryo", *Oncogene* 15, 1151-1159.

Kozma, R., Ahmed, S., Best, A., and Lim, L. (1995) "The Ras-related protein Cdc42Hs and bradykinin promote formation of peripheral actin microspikes and filopodia in Swiss 3T3 fibroblasts", *Mol Cell Biol* 15, 1942-1952.

Lee, E. Y., and Muller, W. J. (2010) "Oncogenes and tumor suppressor genes", *Cold Spring Harb Perspect Biol* 2, a003236.

Li, D. H., and Randerath, K. (1990) "Strain differences of I-compounds in relation to organ sites of spontaneous tumorigenesis and non-neoplastic renal disease in mice", *Carcinogenesis* 11, 251-255.

Li, H., Fan, X., Kovi, R. C., Jo, Y., Moquin, B., Konz, R., Stoicov, C., Kurt-Jones, E., Grossman, S. R., Lyle, S., Rogers, A. B., Montrose, M., and Houghton, J. (2007) "Spontaneous expression of embryonic factors and p53 point mutations in aged mesenchymal stem cells: a model of age-related tumorigenesis in mice", *Cancer Res* 67, 10889-10898.

Liao, Y. C., and Lo, S. H. (2008) "Deleted in liver cancer-1 (DLC-1): a tumor suppressor not just for liver", *Int J Biochem Cell Biol* 40, 843-847.

Liao, Y. C., Shih, Y. P., and Lo, S. H. (2008) "Mutations in the focal adhesion targeting region of deleted in liver cancer-1 attenuate their expression and function", *Cancer Res* 68, 7718-7722.

Ligeti, E., and Settleman, J. (2006) "Regulation of RhoGAP specificity by phospholipids and prenylation", *Methods Enzymol* 406, 104-117.

Lin, Q., Jo, D., Gebre-Amlak, K. D., and Ruley, H. E. (2004) "Enhanced cell-permeant Cre protein for site-specific recombination in cultured cells", In *BMC.Biotechnol.*, p 25.

Lodish, H., Berk, A., Zipursky, S. L., Matsudaira, P., Baltimore, D., and Darnell, J. (2000) *"Molecular Cell Biology"*, Vol., W.H. Freeman, New York.

Low, J. S., Tao, Q., Ng, K. M., Goh, H. K., Shu, X. S., Woo, W. L., Ambinder, R. F., Srivastava, G., Shamay, M., Chan, A. T., Popescu, N. C., and Hsieh, W. S. (2011) "A novel isoform of the 8p22 tumor suppressor gene DLC1 suppresses tumor growth and is frequently silenced in multiple common tumors", *Oncogene* 30, 1923-1935.

Lushnikova, T., Bouska, A., Odvody, J., Dupont, W. D., and Eischen, C. M. (2011) "Aging mice have increased chromosome instability that is exacerbated by elevated Mdm2 expression", *Oncogene* 30, 4622-4631.

Mao, X., Fujiwara, Y., and Orkin, S. H. (1999) "Improved reporter strain for monitoring Cre recombinase-mediated DNA excisions in mice", *Proc Natl Acad Sci U S A* 96, 5037-5042.

McGrath, J. P., Capon, D. J., Smith, D. H., Chen, E. Y., Seeburg, P. H., Goeddel, D. V., and Levinson, A. D. (1983) "Structure and organization of the human Ki-ras proto-oncogene and a related processed pseudogene", *Nature* 304, 501-506.

Meuwissen, R., Linn, S. C., van der Valk, M., Mooi, W. J., and Berns, A. (2001) "Mouse model for lung tumorigenesis through Cre/lox controlled sporadic activation of the K-Ras oncogene", *Oncogene* 20, 6551-6558.

Meylan, E., Dooley, A. L., Feldser, D. M., Shen, L., Turk, E., Ouyang, C., and Jacks, T. (2009) "Requirement for NF-kappaB signalling in a mouse model of lung adenocarcinoma", *Nature* 462, 104-107.

Mitomi, H., Ohkura, Y., Fukui, N., Kanazawa, H., Kishimoto, I., Nakamura, T., Yokoyama, K., Sada, M., Kobayashi, K., Tanabe, S., and Saigenji, K. (2007) "P21WAF1/CIP1 expression in colorectal carcinomas is related to Kras mutations and prognosis", *Eur J Gastroenterol Hepatol* 19, 883-889.

Molina, J. R., and Adjei, A. A. (2006) "The Ras/Raf/MAPK pathway", *J Thorac Oncol* 1, 7-9.

Moll, R., Franke, W. W., Schiller, D. L., Geiger, B., and Krepler, R. (1982) "The catalog of human cytokeratins: patterns of expression in normal epithelia, tumors and cultured cells", *Cell* 31, 11-24.

Moon, S. Y., and Zheng, Y. (2003) "Rho GTPase-activating proteins in cell regulation", *Trends Cell Biol* 13, 13-22.

Ng, I. O., Liang, Z. D., Cao, L., and Lee, T. K. (2000) "DLC-1 is deleted in primary hepatocellular carcinoma and exerts inhibitory effects on the proliferation of hepatoma cell lines with deleted DLC-1", *Cancer Res* 60, 6581-6584.

Nobes, C. D., and Hall, A. (1995) "Rho, rac, and cdc42 GTPases regulate the assembly of multimolecular focal complexes associated with actin stress fibers, lamellipodia, and filopodia", *Cell* 81, 53-62.

Olivier, M., Hollstein, M., and Hainaut, P. (2010) "TP53 mutations in human cancers: origins, consequences, and clinical use", *Cold Spring Harb Perspect Biol* 2, a001008.

Olson, M. F., Paterson, H. F., and Marshall, C. J. (1998) "Signals from Ras and Rho GTPases interact to regulate expression of p21Waf1/Cip1", In *Nature*, p 295.

Ordonez, N. G. (2000) "Thyroid transcription factor-1 is a marker of lung and thyroid carcinomas", *Adv Anat Pathol* 7, 123-127.

Parikh, N., Shuck, R. L., Nguyen, T. A., Herron, A., and Donehower, L. A. (2012) "Mouse tissues that undergo neoplastic progression after K-Ras activation are distinguished by nuclear translocation of phospho-Erk1/2 and robust tumor suppressor responses", *Mol Cancer Res* 10, 845-855.

Peck, J., Douglas, G. t., Wu, C. H., and Burbelo, P. D. (2002) "Human RhoGAP domain-containing proteins: structure, function and evolutionary relationships", *FEBS Lett* 528, 27-34.

Perera, S. A., Maser, R. S., Xia, H., McNamara, K., Protopopov, A., Chen, L., Hezel, A. F., Kim, C. F., Bronson, R. T., Castrillon, D. H., Chin, L., Bardeesy, N., Depinho, R. A., and Wong, K. K. (2008) "Telomere dysfunction promotes genome instability and metastatic potential in a K-ras p53 mouse model of lung cancer", *Carcinogenesis* 29, 747-753.

Pfeifer, A., Brandon, E. P., Kootstra, N., Gage, F. H., and Verma, I. M. (2001) "Delivery of the Cre recombinase by a self-deleting lentiviral vector: efficient gene targeting in vivo", *Proc Natl Acad Sci U S A* 98, 11450-11455.

Preudhomme, C., Roumier, C., Hildebrand, M. P., Dallery-Prudhomme, E., Lantoine, D., Lai, J. L., Daudignon, A., Adenis, C., Bauters, F., Fenaux, P., Kerckaert, J. P., and Galiegue-Zouitina, S. (2000) "Nonrandom 4p13 rearrangements of the RhoH/TTF gene, encoding a GTP-binding protein, in non-Hodgkin's lymphoma and multiple myeloma", *Oncogene* 19, 2023-2032.

Pruitt, K., and Der, C. J. (2001) "Ras and Rho regulation of the cell cycle and oncogenesis", *Cancer Lett* 171, 1-10.

Pusztaszeri, M. P., Seelentag, W., and Bosman, F. T. (2006) "Immunohistochemical expression of endothelial markers CD31, CD34, von Willebrand factor, and Fli-1 in normal human tissues", *J Histochem Cytochem* 54, 385-395.

Ray, K. C., Bell, K. M., Yan, J., Gu, G., Chung, C. H., Washington, M. K., and Means, A. L. (2011) "Epithelial tissues have varying degrees of susceptibility to Kras(G12D)-initiated tumorigenesis in a mouse model", *PLoS One* 6, e16786.

Ren, X. D., and Schwartz, M. A. (2000) "Determination of GTP loading on Rho", *Methods Enzymol* 325, 264-272.

Repository, N. M. "B6.129-Krastm4Tyj PCR Protocol", NCI Mouse Repository.

Ridley, A. J. (2004) "Rho proteins and cancer", In *Breast Cancer Res.Treat.*, p 13.

Ridley, A. J., and Hall, A. (1992) "The small GTP-binding protein rho regulates the assembly of focal adhesions and actin stress fibers in response to growth factors", *Cell* 70, 389-399.

Ridley, A. J., Paterson, H. F., Johnston, C. L., Diekmann, D., and Hall, A. (1992) "The small GTP-binding protein rac regulates growth factor-induced membrane ruffling", *Cell* 70, 401-410.

Sabbir, M. G., Prieditis, H., Ravinsky, E., and Mowat, M. R. (2012) "The Role of Dlc1 Isoform 2 in K-Ras2(G12D) Induced Thymic Cancer", *PLoS One* 7, e40302.

Sabbir, M. G., Wigle, N., Loewen, S., Gu, Y., Buse, C., Hicks, G. G., and Mowat, M. R. (2010) "Identification and characterization of Dlc1 isoforms in the mouse and study of the biological function of a single gene trapped isoform", *BMC Biol* 8, 17.

Sahai, E., and Marshall, C. J. (2002) "RHO-GTPases and cancer", *Nat Rev Cancer* 2, 133-142.

Sahai, E., Olson, M. F., and Marshall, C. J. (2001) "Cross-talk between Ras and Rho signalling pathways in transformation favours proliferation and increased motility", *EMBO J* 20, 755-766.

Sambrook, J., and Russell, D. W. (2001) *"Molecular cloning - A laboratory manual"*, Vol. 1, 3rd ed., Cold Spring Harbor Laboratory Press, New York.

Sheppard, M. N. (2000) "Specific markers for pulmonary tumours", *Histopathology* 36, 273-276.

Stanford, W. L., Cohn, J. B., and Cordes, S. P. (2001) "Gene-trap mutagenesis: past, present and beyond", *Nat Rev Genet* 2, 756-768.

Sternberg, N., and Hamilton, D. (1981) "Bacteriophage P1 site-specific recombination. I. Recombination between loxP sites", *J Mol Biol* 150, 467-486.

Suwa, H., Ohshio, G., Imamura, T., Watanabe, G., Arii, S., Imamura, M., Narumiya, S., Hiai, H., and Fukumoto, M. (1998) "Overexpression of the rhoC gene correlates with progression of ductal adenocarcinoma of the pancreas", *Br J Cancer* 77, 147-152.

Takai, Y., Sasaki, T., and Matozaki, T. (2001) "Small GTP-binding proteins", *Physiol Rev* 81, 153-208.

Tan, L. W., and Dobrovic, A. (2001) "Methylation analysis of formalin-fixed, paraffin-embedded sections using a nontoxic DNA extraction protocol", *Biotechniques* 31, 1354, 1356-1357.

Tcherkezian, J., and Lamarche-Vane, N. (2007) "Current knowledge of the large RhoGAP family of proteins", *Biol Cell* 99, 67-86.

Tichelaar, J. W., Lu, W., and Whitsett, J. A. (2000) "Conditional expression of fibroblast growth factor-7 in the developing and mature lung", *J Biol Chem* 275, 11858-11864.

Turner, M. S., and Goldsmith, J. D. (2009) "Best practices in diagnostic immunohistochemistry: spindle cell neoplasms of the gastrointestinal tract", *Arch Pathol Lab Med* 133, 1370-1374.

Tuveson, D. A., Shaw, A. T., Willis, N. A., Silver, D. P., Jackson, E. L., Chang, S., Mercer, K. L., Grochow, R., Hock, H., Crowley, D., Hingorani, S. R., Zaks, T., King, C., Jacobetz, M. A., Wang, L., Bronson, R. T., Orkin, S. H., DePinho, R. A., and Jacks, T. (2004) "Endogenous oncogenic K-ras(G12D) stimulates proliferation and widespread neoplastic and developmental defects", *Cancer Cell* 5, 375-387.

Ullmannova-Benson, V., Guan, M., Zhou, X., Tripathi, V., Yang, X. Y., Zimonjic, D. B., and Popescu, N. C. (2008) "DLC1 tumor suppressor gene inhibits migration and invasion of multiple myeloma cells through RhoA GTPase pathway", In *Leukemia*.

Ullmannova, V., and Popescu, N. C. (2006) "Expression profile of the tumor suppressor genes DLC-1 and DLC-2 in solid tumors", *Int J Oncol* 29, 1127-1132.

Wang, W., Wu, F., Fang, F., Tao, Y., and Yang, L. (2008) "Inhibition of invasion and metastasis of hepatocellular carcinoma cells via targeting RhoC in vitro and in vivo", *Clin Cancer Res* 14, 6804-6812.

Wang, Y., and You, M. (2001) "Alternative splicing of the K-ras gene in mouse tissues and cell lines", *Exp Lung Res* 27, 255-267.

Wang, Y., Zhang, Z., Lubet, R. A., and You, M. (2006) "A mouse model for tumor progression of lung cancer in ras and p53 transgenic mice", *Oncogene* 25, 1277-1280.

Wang, Z., Feng, Y., Bardessy, N., Wong, K. K., Liu, X. Y., and Ji, H. (2012) "Temporal dissection of K-ras(G12D) mutant in vitro and in vivo using a regulatable K-ras(G12D) mouse allele", *PLoS One* 7, e37308.

Wellcome. (2004) "X-Gal staining Protocol", Wellcome Trust Sanger Institute.

Wennerberg, K., and Der, C. J. (2004) "Rho-family GTPases: it's not only Rac and Rho (and I like it)", *J Cell Sci* 117, 1301-1312.

Wennerberg, K., Rossman, K. L., and Der, C. J. (2005) "The Ras superfamily at a glance", *J Cell Sci* 118, 843-846.

White, M. A., Nicolette, C., Minden, A., Polverino, A., Van Aelst, L., Karin, M., and Wigler, M. H. (1995) "Multiple Ras functions can contribute to mammalian cell transformation", *Cell* 80, 533-541.

Will, E., Klump, H., Heffner, N., Schwieger, M., Schiedlmeier, B., Ostertag, W., Baum, C., and Stocking, C. (2002) "Unmodified Cre recombinase crosses the membrane", *Nucleic acids research* 30, e59.

Wong, C. M., Lee, J. M., Ching, Y. P., Jin, D. Y., and Ng, I. O. (2003) "Genetic and epigenetic alterations of DLC-1 gene in hepatocellular carcinoma", *Cancer research* 63, 7646.

Wu, P. P., Jin, Y. L., Shang, Y. F., Jin, Z., Wu, P., and Huang, P. L. (2009) "Restoration of DLC1 gene inhibits proliferation and migration of human colon cancer HT29 cells", *Ann Clin Lab Sci* 39, 263-269.

Wulf, E., Deboben, A., Bautz, F. A., Faulstich, H., and Wieland, T. (1979) "Fluorescent phallotoxin, a tool for the visualization of cellular actin", *Proc Natl Acad Sci U S A* 76, 4498-4502.

Xue, W., Krasnitz, A., Lucito, R., Sordella, R., Vanaelst, L., Cordon-Cardo, C., Singer, S., Kuehnel, F., Wigler, M., Powers, S., Zender, L., and Lowe, S. W. (2008) "DLC1 is a chromosome 8p tumor suppressor whose loss promotes hepatocellular carcinoma", *Genes & development* 22, 1439.

Yang, L., Wang, L., Geiger, H., Cancelas, J. A., Mo, J., and Zheng, Y. (2007) "Rho GTPase Cdc42 coordinates hematopoietic stem cell quiescence and niche interaction in the bone marrow", *Proc Natl Acad Sci U S A* 104, 5091-5096.

Yau, T. O., Leung, T. H., Lam, S., Cheung, O. F., Tung, E. K., Khong, P. L., Lam, A., Chung, S., and Ng, I. O. (2009) "Deleted in liver cancer 2 (DLC2) was

dispensable for development and its deficiency did not aggravate hepatocarcinogenesis", *PLoS One* 4, e6566.

Yuan, B. Z., Durkin, M. E., and Popescu, N. C. (2003) "Promoter hypermethylation of DLC-1, a candidate tumor suppressor gene, in several common human cancers", *Cancer Genet Cytogenet* 140, 113-117.

Yuan, B. Z., Jefferson, A. M., Baldwin, K. T., Thorgeirsson, S. S., Popescu, N. C., and Reynolds, S. H. (2004) "DLC-1 operates as a tumor suppressor gene in human non-small cell lung carcinomas", *Oncogene* 23, 1405-1411.

Yuan, B. Z., Miller, M. J., Keck, C. L., Zimonjic, D. B., Thorgeirsson, S. S., and Popescu, N. C. (1998) "Cloning, characterization, and chromosomal localization of a gene frequently deleted in human liver cancer (DLC-1) homologous to rat RhoGAP", *Cancer research* 58, 2196.

Yuan, B. Z., Zhou, X., Durkin, M. E., Zimonjic, D. B., Gumundsdottir, K., Eyfjord, J. E., Thorgeirsson, S. S., and Popescu, N. C. (2003) "DLC-1 gene inhibits human breast cancer cell growth and in vivo tumorigenicity", *Oncogene* 22, 445-450.

Zheng, S., El-Naggar, A. K., Kim, E. S., Kurie, J. M., and Lozano, G. (2007) "A genetic mouse model for metastatic lung cancer with gender differences in survival", *Oncogene* 26, 6896-6904.

Zhou, X., Thorgeirsson, S. S., and Popescu, N. C. (2004) "Restoration of DLC-1 gene expression induces apoptosis and inhibits both cell growth and tumorigenicity in human hepatocellular carcinoma cells", In *Oncogene*, p 1308.